A zero dynamics based approach to actuator positioning controlling a beam with one-sided spring

Sanders, L.T.A.

Award date:
1997

Controlling a beam with one-sided spring

A zero dynamics based approach to actuator positioning

L.T.A. Sanders

WFW report 97.022

Professor: Prof.dr.ir. J.J. Kok
Supervisors: Ir. M.F. Heertjes
Dr.ir. M.J.G. van de Molengraft

Eindhoven University of Technology

Faculty: Mechanical engineering
Department: Fundamental mechanical engineering, WFW
Section: Systems & control engineering

Graduation report, March 1997

Abstract

In many mechanical systems dynamic loads cause vibrations. Especially vibrations with large amplitudes are undesirable, because they can cause stretching, stresses, excessive sound production, etcetera. These vibrations might cause damage to the system, thus justifying research into methods to eliminate or suppress them.

The results described in this report are part of a research into vibration reduction in non-linear multi-DOF[1] systems, using active control. The considered system is an under-actuated beam with a local non-linearity, i.e. a one-sided spring. In certain frequency ranges, the behaviour of the non-linear system makes it possible to *efficiently* suppress the amplitude of vibrations in the system, i.e. using coexisting solutions. The suppression can be realized with relatively little effort of one or more actuators, resulting in a long life of the actuator(s). In this project, one actuator has been used. In order to accomplish the vibration reduction in the system, only one DOF, i.e. the actuator DOF, is actually controlled. However, the efficiency of the vibration reduction is also determined by the behaviour of the uncontrolled DOFs.

This report describes the results of a research into the determination of an optimal actuator position with regard to the behaviour of the *un*controlled DOFs. The optimization problem has been addressed by means of an analysis of the zero dynamics of the beam system. The stability of the zero dynamics provides an interesting basis for an actuator positioning criterion, defining optimality of the actuator position with regard to the uncontrolled DOFs. Yet, it has proved to be difficult to adequately quantify this stability for the non-linear beam system. During the research, bifurcations in the behaviour of the zero dynamics have emerged as a research inviting property of the non-linear zero dynamics.

Besides an optimal actuator position, the quality of the transfer between the calculated control effort u and the control force F_{act} that is actually applied (by means of a shaker), is also very important for the optimal functioning of the controller in an experimental environment. As there was room for improvement of the quality of this transfer, a combined amplifier/actuator model has also been given some attention in this report. Its parameters have been estimated and the performance has been evaluated by means of two tests, one of which is a control experiment, showing the active control based vibration reduction in practice.

[1] DOF = degree of freedom

A reality, completely independent of the spirit
that conceives it, sees it or feels it,
is an impossibility.
A world so external as that, even if it existed,
would be forever inaccessible to us.

- Henri Poincaré -

Preface

This report describes the results of the research I've done for my graduation, performed in the WFW laboratory near the experimental set-up of the beam with one-sided spring. Both theoretical and practical wanderings that are irrelevant to the results of this research, have been omitted.

Furthermore, I'd like to use this opportunity to thank not only my supervisors, but also J. Banens, R. Kodde, K. Koekkoek and - last but not least - my parents for their indispensable support for this research in general and my graduation in particular.

It has been a pleasure to participate in the acquisition of knowledge about the dynamics of non-linear systems such as the vibrating beam with one-sided spring.

Borre Sanders,

Eindhoven, March 1997.

List of symbols

scalar	unit	description
f_e	[Hz]	excitation frequency
F_{act}	[N]	actuator force, actually applied control effort
F_{ex}	[N]	excitation force
f_s	[Hz]	sample frequency
k	[N/m]	stiffness of the one-sided linear spring
k_{nl}	[N/m]	non-linear stiffness of the one-sided spring
m_e	[kg]	effective mass of the mass unbalance
n	[-]	number of degrees of freedom (DOFs)
r_e	[m]	distance from shaft center to effective mass of mass unbalance
s	[m/s]	switch variable for the sliding computed torque controller
u	[N]	desired control effort
x_a	[m]	actuator position, application point of the actuator force F_{act}
y_a	[m]	1^{st} DOF, application point of the actuator force F_{act}
y_m	[m]	2^{nd} DOF, application point of the excitation force F_{ex}
η	[m/s^2]	parameter for the (sliding) computed torque controller
λ	[Hz]	parameter for the (sliding) computed torque controller
σ	[m/s]	parameter for the sliding computed torque controller
ξ	[m]	3^{rd} DOF, virtual degree of freedom

vector	size	description
$\underset{\sim}{e}$	$(n \times 1)$	column with the tracking errors for all DOFs
$\underset{\sim}{\hat{e}}$	$(n \times 1)$	column with the estimated tracking errors
$\underset{\sim}{H}_m$	$(n \times 1)$	distribution column for application to DOF 2
$\underset{\sim}{H}_a$	$(n \times 1)$	distribution column for the control effort u
$\underset{\sim}{q}$	$(n \times 1)$	column with the degrees of freedom
$\underset{\sim}{q}_d$	$(n \times 1)$	column with desired trajectories for all DOFs
$\underset{\sim}{\hat{q}}_d$	$(n \times 1)$	column with approximated desired trajectories for all DOFs

matrix	size	description
$\underline{B}$	$(n \times n)$	damping matrix
$\underline{C}$	$(21 \times n)$	matrix with Fourier coefficients
$\underline{M}$	$(n \times n)$	mass matrix
$\underline{K}$	$(n \times n)$	stiffness matrix

notation	description
$\overline{x}$	complex conjugate of x
$\Im[x]$	imaginary part of x
$\Re[x]$	real part of x

Contents

Chapter 1

Introduction

In many mechanical systems dynamic loads cause vibrations. Especially vibrations with large amplitudes are undesirable, because they can cause stretching, stresses, excessive sound production, etcetera. Our objective is to reduce these undesired vibrations using active control. More specifically, we will try to reduce the vibration amplitude of such systems by actuating at a suitable position.

In this report vibration reduction of a beam system with a local non-linearity is studied. The word 'local' expresses that the non-linearity occurs at a discrete position on the system. Figure 1.1 shows an overview of the experimental set-up that represents the system of our interest.

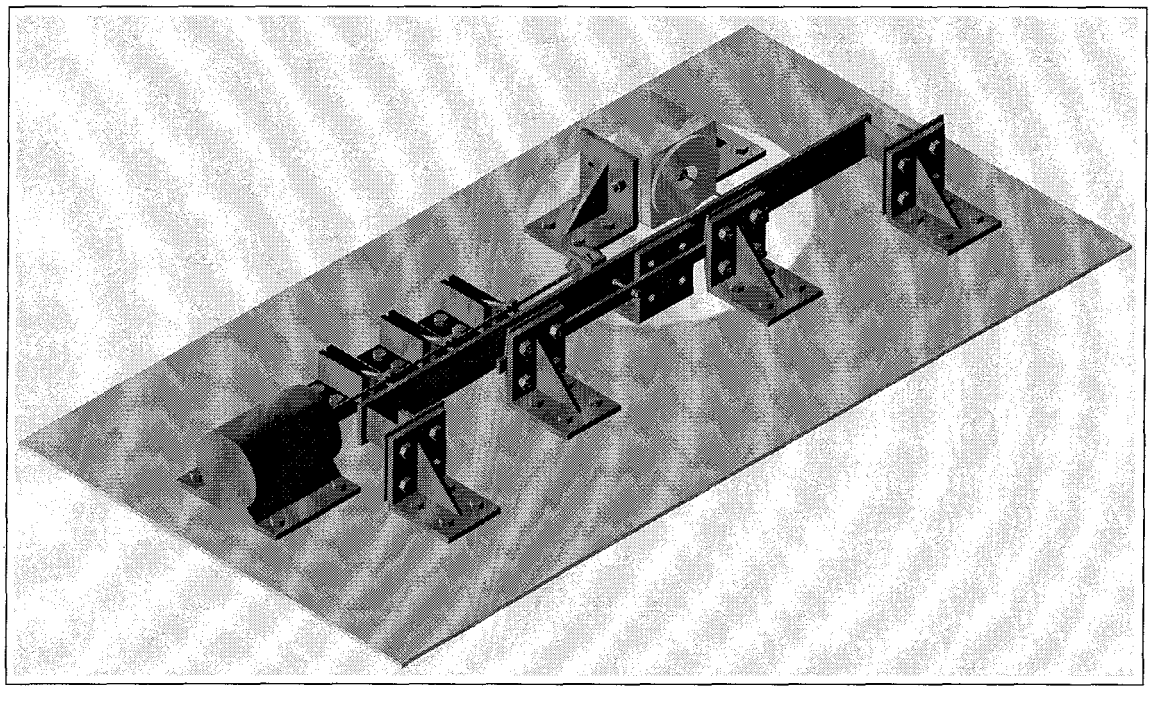

Figure 1.1: AutoCAD model of the experimental set-up of the non-linear beam system.

Due to its local non-linearity, i.e. the one-sided spring, the vibrating beam with one-sided spring shown in figure 1.1 provides us with a convenient non-linear system that incorporates possibilities for very *efficient* vibration reduction. It's a convenient system as it can be modelled relatively easily and yet is expected to provide insight into ways to achieve efficient vibration reduction for more complex systems like complete drive lines, satellite

solar panels, traffic bridges, etcetera.

In order to allow both effective and efficient reduction of vibrations, the system is to be controlled using an actuator force F_{act}, supplied by an actuator. This actuator has been implemented by means of a shaker. The actuator force F_{act} should resemble a desired control effort u, calculated with a PC. It can be applied to the beam system at several positions. In figure 1.1 the actuator has been placed in the spotlight, as this report describes the results of a research focussed on the following problems related to the actuator:

1. Finding the best position to apply the actuator force to the beam.
2. Obtaining an adequate description of the transfer between the desired control effort u calculated by the PC and the actually applied actuator force F_{act}.

In the next section both the system itself and its dynamic behaviour will be described, hopefully providing the reader with sufficient information to understand both the relevance of the research itself and its objectives described at the end of this chapter.

1.1 System description

In this report only those aspects about the system description will be mentioned that are considered relevant for the modelling of the system and/or for the understanding of the experimental set-up.

1.1.1 Orientations and origin location

Figure 1.2 shows two pictures of the beam in the case that one actuator is used at position x_a. For the sake of clarity, a top view of the experimental set-up is shown in figure 1.2(a). In figure 1.2(b), the same view is shown in a schematic equivalent. Also, some important dimensions and the used definitions for positive directions of the positions and forces are indicated there. The $z = 0$ coordinate of the origin O of the coordinate system is located at the z coordinate of the middle of a cross-section of the beam.

1.1.2 System components

The beam system consists of the following components:

- *Beam.* To provide the reader with a notion of the dimensions of the experimental set-up, the dimensions of the beam are mentioned here: $l \times w \times h = 1330 \times 10 \times 90$ [mm^3]. Due to its small width, the beam is quite flexible in the y-direction. As shown in figure 1.2, the beam is attached to the world by means of 2 leaf springs near each end of the beam. These leaf springs possess great stiffness in the y-direction but are not very resistant to z-axis rotations. Thus, they provide maximum freedom of movement for the beam whilst still properly connecting it to the world. Both the beam and the leaf springs are made of steel.
- *Mass unbalance.* As is shown in figure 1.2 and in more detail in figure 1.3, the mass unbalance provides the excitation force F_{ex}, applied to the middle of the beam in order to cause vibrations in the beam system. The horizontal component of the centrifugal force, caused by rotation of the eccentrically placed masses, is useful to generate a sine-shaped force F_{ex}, provided that little or no energy is absorbed by the bearings and that the rotation speed of the shaft is constant. In order to achieve this,

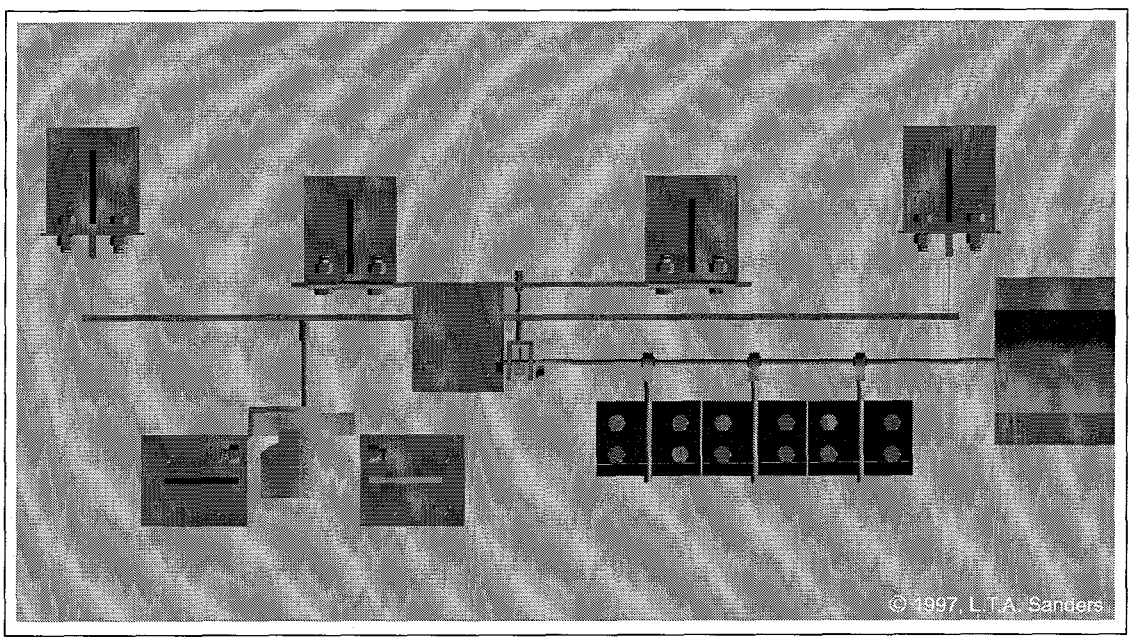

(a) top view of the experimental beam system.

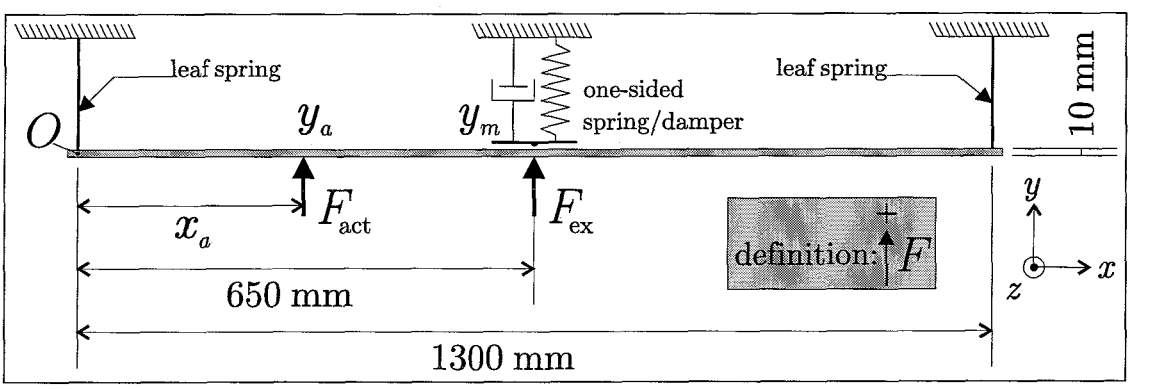

(b) schematic top view of the beam with one actuator.

Figure 1.2: top views of the beam with one actuator, including some definitions.

the shaft is connected to the mass unbalance by means of a flexible coupling. The constant speed is guaranteed by a tacho-controlled motor. The excitation frequency f_e can be chosen freely within a certain frequency range (with steps of 0.5 [Hz]). The result is a sine-shaped excitation force, represented by the following equation:

$$F_{ex} = m_e r_e \omega^2 \cos(\omega t) \text{ with } \omega = 2\pi f_e. \tag{1.1}$$

In this equation m_e is the effective mass of the total eccentrically placed mass, regarded as concentrated at effective radius r_e. In the models $m_e r_e = 0.984 \cdot 10^{-3}$ [kgm] has been used.
The long shaft, connecting the motor with the mass unbalance, has foam bearings at three points as can be seen in figures 1.2(a) and 1.3. These bearings are used to suppress vibrations in the shaft which can reduce the quality of the generated excitation force.

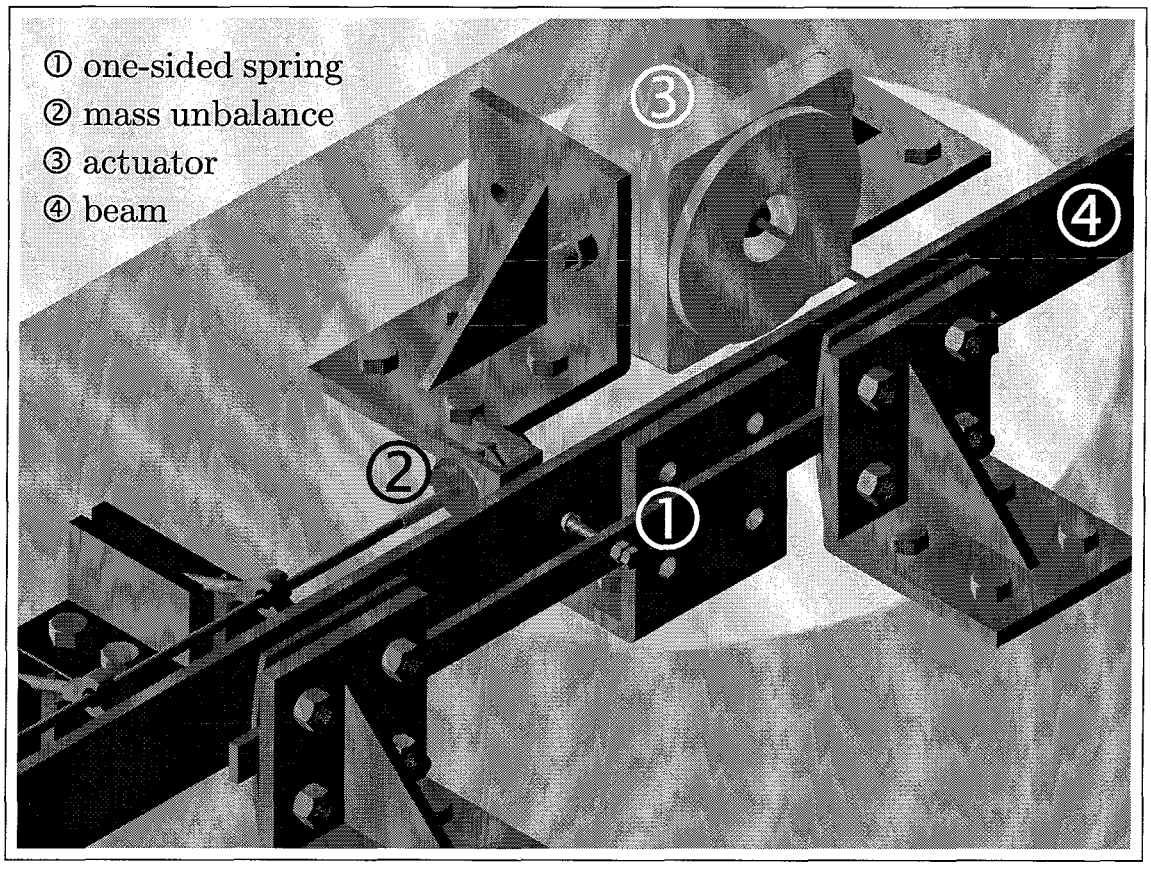

Figure 1.3: more detailed view of the shaker, mass-unbalance and one-sided spring.

- *One-sided spring.* Figure 1.3 shows the one-sided spring/damper, also located at the middle of the beam. The one-sided spring has been implemented using a steel butt-strip, clenched between a profile and a steel strip on both ends. Contact with the beam is provided by a bolt of which the position can be adjusted. In the models, the one-sided spring is presumed to have a linear characteristic, represented by stiffness k. The behaviour of the one-sided spring can be denoted as a non-linear stiffness k_{nl}, resulting in:

$$k_{nl} = k \operatorname{int}\left(\frac{1 + \operatorname{sign}(y_m)}{2}\right) = \begin{cases} k & \text{if } y_m > 0, \\ 0 & \text{if } y_m \leq 0. \end{cases} \tag{1.2}$$

The one-sided damper has been implemented by means of some damping material attached to an additional steel profile. This material (not visible in figure 1.3) effectively suppresses undesired vibrations of the one-sided spring between collisions with the beam.

- *Actuator.* The calculated desired control effort u, required to reduce the vibration amplitude of the beam, is applied to the beam by means of an actuator, i.e. a shaker. This actuator, shown in detail in figure 1.3, provides a force F_{act} which under ideal circumstances equals the desired control effort u. In control *simulations*, this presumption applies. However, in experiments this presumption has turned out not to apply. It has therefore been given some attention in this report.

- *Sensors and amplifiers.* During experiments, 6 measurements are carried out at each sample moment: two LVDTs[1], two piezoelectric accelerometers and two piezoelectric force transducers are used for measuring respectively displacements y_a and y_m, accelerations $\ddot{y}_a$ and $\ddot{y}_m$ and forces F_{ex} and F_{act} at the mass unbalance position and at the actuator position. An overview of these measurements is shown in table 1.1.

channel	measurement	unit
0	y_a	[m]
1	y_m	[m]
2	$\ddot{y}_a$	[m/s^2]
3	$\ddot{y}_m$	[m/s^2]
4	F_{ex}	[N]
5	F_{act}	[N]

Table 1.1: measured quantities and corresponding units.

- *Personal computer* (PC). The 133 [MHz] Intel Pentium based PC calculates the required control effort u. Calculations for both experiments and simulations have been performed using Borland C[2], GNU C^{++} (Unix) and the TCE[3]-toolbox V1.2β. The latter has been ported to ANSI for the occasion.

- *Connecting hardware.* This hardware links the PC to the measurements and the actuator. The latter link will be discussed in more detail in chapter 3. The hardware consists of:

  1. 12 bit IO-board, manufactured by Data Translation, type DT2831-G.
  2. Voltage divider for the output voltage (to prevent loss of resolution).
  3. Output amplifier.
  4. Wiring for the 6 input signals (AD) and the output signal (DA).

1.1.3 System behaviour

As the beam is a distributed-parameter system, a model of the beam requires an infinite number of DOFs[4] if it is to describe the beam perfectly. Compromising between accuracy and available calculation time, the model is reduced to a limited number of DOFs,

[1] LVDT = Linear Variable Differential Transformer
[2] V1.01 in DOS, V5.0 in Windows NT.
[3] TCE = Tools for Control Experiments, see [5, 6].
[4] DOF = Degree Of Freedom

accounting for the influence of all DOFs with limited, yet sufficient accuracy. This is achieved using the CMS[5] method implemented in the FEM[6] package `Diana`.

In simulations based on these models several interesting features have emerged, like subharmonic and chaotic behaviour (see [8, 23]). As it's desirable to verify whether these numerical results can also be reproduced in experiments, the experimental beam system has been constructed. After several experiments and design changes, much of the simulated stable behaviour has been reproduced using the experimental set-up shown in figure 1.1 *without* the actuator (see [2, 12]). After these promising results had been achieved, the verification was taken one step further and it was decided that the existence of an unstable harmonic solution was to be verified.

As shown in figure 1.4, it had been found in simulations that, when the beam is excited (in the middle) with a sine-shaped excitation force with an excitation frequency f_e of 37 [Hz], an unstable harmonic solution coexists with a stable $\frac{1}{2}$ subharmonic solution (see [14]). This behaviour is caused by the local non-linearity and provides us with a possibility to *efficiently* suppress vibrations, as the amplitude of the unstable harmonic solution for each DOF is much smaller than the amplitude of the corresponding stable $\frac{1}{2}$ subharmonic solution, especially when the system is excited with a frequency f_e of 37 [Hz].

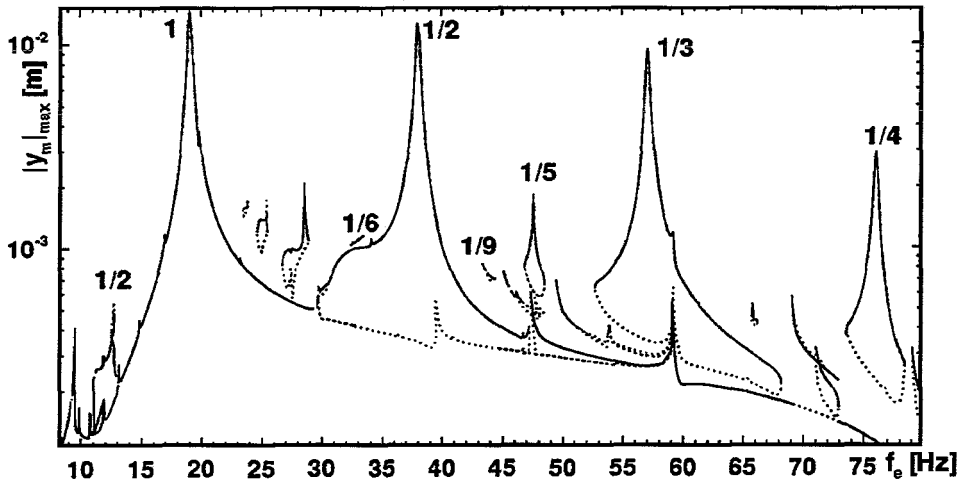

Figure 1.4: maxima of the absolute values of the steady-state response of the middle of the beam as a 'function' of the excitation frequency f_e (8 DOF model).

At least one actuator is required to force the system into the harmonic solution. However, due to the fact that the harmonic solution *is* a natural solution of the system when excited with a frequency f_e of 37 [Hz] (even though unstable), theoretically no control effort is required once all of the system's DOFs behave according to the stabilized unstable harmonic solution. Provided that the control effort required to force the system to the harmonic solution is relatively small, a relatively cheap and light actuator can be used.

As the beam system (even the reduced system) in general has a number of DOFs larger than the number of actuators, the system belongs to 'under-actuated' class of systems. Therefore, there's no way to force such a system to just any arbitrary state. However, since the state the system is to be driven to is a natural solution of the system, it was *presumed* that the uncontrolled DOFs will go to their corresponding harmonic solutions,

[5]CMS = Component Mode Synthesis
[6]FEM = Finite Element Method

once the controlled DOF has been brought into the harmonic solution.

Several controller concepts to stabilize the harmonic solution have been devised and tested in simulations, e.g. CRCTC[7] and SCTC[8] (see [23, 14]). Simulation results have shown that the other DOFs do indeed start to track their corresponding harmonic solutions, once the controlled DOF has reached the state corresponding to the harmonic solution. Continuing research has shown that, as far as the behaviour of the controlled DOF is concerned, the best position to control the system from a local[9] controllability point of view, is the middle of the beam (see [14]). A shaker has been added to the experimental set-up as an actuator, i.e. to apply the control force (see [24]). Eventually, continuing the work of De Vries [24], the existence of an unstable harmonic solution in the experimental set-up was shown using SCTC (see [19]).

1.2 Objectives

When this part of the research project was to begin, there were several problems and unanswered questions left as a result of prior research into the system behaviour, as described in subsection 1.1.3. To name two of them:

1. As local controllability had turned out *not* to be a real problem as long as the actuator was not placed too close to a leaf spring, there was no justification for the fact that the beam was controlled at position $x_a = 32$ [cm], other than that it had turned out to work satisfactorily so far. When the behaviour of the other DOFs is taken into account, it's interesting to find out if there are positions where the controller performs better and, if so, why it performs better.

2. In experiments it had been noticed that the applied actuator force F_{act} did not even nearly resemble the calculated desired control effort u. Apparently, there was room for improvement of the amplifier/actuator model and/or its parameters.

It was decided that research into these issues was to be considered the main objective of the research described in this report:

- Several criteria for optimal actuator *positioning* will briefly be discussed in chapter 2. Based on the behaviour of the so-called zero dynamics, a new criterion for the best actuator position for the vibrating beam with one-sided spring is proposed and evaluated.

- In chapter 3, a combined actuator/amplifier *model* is evaluated; its parameters are estimated and its overall performance is tested and evaluated.

- Finally, in chapter 4, conclusions will be drawn from the results and recommendations will be done for future research and/or enhancements.

[7] CRCTC = Computed Reference Computed Torque Control
[8] SCTC = Sliding Computed Torque Control
[9] i.e. in the neighbourhood of the unstable harmonic solution

Chapter 2

Zero dynamics based actuator positioning

In this research we are dealing with a locally non-linear multi-DOF beam system of which only one DOF y_a is controlled. As the total number of DOFs n in the system model is larger than the number of controlled DOFs, the beam system is so-called 'under-actuated'. The system is controlled by means of an actuator that can be placed at several positions x_a. Which position x_a is the best, is to be determined by means of a suitable criterion. In this report a quantitative measure for the stability of the so-called zero dynamics will be proposed as a new actuator positioning criterion for the considered beam system. The criterion is expected to be suitable for other under-actuated systems as well, provided that their zero dynamics is stable.

In order to be able to evaluate the merits of the zero dynamics based actuator positioning criterion for the beam with one-sided spring, first some aspects of the system model and the controller will have to be discussed, as will be done in sections 2.2 and 2.3. Then the concept of zero dynamics, the basis for the criterion, will be explained in section 2.4, resulting in the proposal of the stability of the zero dynamics as a new criterion for actuator positioning. Next, in section 2.5 a quantitative measure for the stability of the zero dynamics will be proposed. Using this measure, the criterion will be evaluated for the beam with one-sided spring. First it will be applied to the linear subsystem, i.e. the beam without the one-sided spring, because the powerful analysis techniques available for linear systems can then be applied and because the analysis of the linear subsystem provides us with a reference for the effects of the addition of the local non-linearity. Then the one-sided spring will be included, resulting in the complete non-linear beam system. This non-linear system will be evaluated as well. Finally, in section 2.6 conclusions will be drawn. First however, in the next section the actuator positioning issue will be introduced in more detail by discussing some commonly used criteria to determine an optimal actuator position in control experiments and comparing them to the new criterion.

2.1 Introduction to the actuator positioning issue

In control experiments a control effort is used to control the system to a defined objective. Such a control effort is applied to the system using at least one actuator. In multi-DOF systems, such as the beam with one-sided spring discussed in this report, there are usually several positions where the control effort can be applied to the system. In order to find an *optimal* position, it is essential to find an optimality criterion that expresses the suitability

of a certain actuator position x_a. The control objective itself provides a good basis for such a criterion. In servo problems, in general the following aspects are relevant for the elimination of some error, defined in the control objective:

1. Eliminate the tracking error(s) in as little time as possible (*speed*).
2. Achieve this with a control effort u as small as possible (*effort*).
3. Achieve this with maximum accuracy (*accuracy*).

In general these aspects lead to compromising criteria regarding the choice of controller type and controller parameters, resulting in an optimization problem. One of the parameters is the actuator position x_a.

2.1.1 Evaluation of some commonly used criteria

In relevant technical literature amongst others the following optimality criteria regarding optimal actuator positioning are described:

1. Maximize controllability and observability of the system (see [10, 11, 14]). The eigenvalues of the controllability gramians $\underline{W_c}$ and/or observability gramians $\underline{W_o}$ are used to quantify the required control effort (see [11, 14]), providing us with an actuator positioning criterion. In the case of an actuator that is collocated[1] with one or more sensors, in general the selected actuator position is a compromise between the position with the best controllability and the position with the best observability.
2. Minimize control and/or observation spillover, caused by the unjust attribution of unmodelled modes to (a combination of) modelled modes (see [3, 4, 10]). Spillover can be suppressed by placing the actuator at a position that is a zero or is close to being a zero, preferably in all, but at least in many of the mode shapes of the unmodelled modes. This provides us with an actuator positioning criterion. For further information on this criterion, the reader is referred to [3].
3. Minimize the total energy consumed by the controller or maximize the energy dissipated from the system by the controller (see [1]). For servo problems this criterion can be regarded as an error-energy criterion, as the objective need *not* be a state with a constant energy level.
4. Minimize the acceleration magnitude $|\ddot{y}|$ integrated over the beam span, i.e. $\int_0^l |\ddot{y}|^2 dx$, using decomposition in modes (see [17]).
5. Minimize a weighted combination of the time integrated square control effort u and the time integrated square error e of the controlled DOF (see [18]).

The usability of the controllability/observability criterion for the beam with one-sided spring system has already been investigated in the past, see [14]. The research has lead to the conclusion that, when one actuator is used to control the vibrating beam with one-sided spring towards the unstable harmonic solution, the controlled actuator DOF can be controlled towards the unstable harmonic solution with less effort when the actuator is placed closer to the middle of the beam. As the controllability/observability based criterion's focus is the behaviour of the controlled DOF y_a, the criterion is unsuitable to

[1] collocated = placed at the same position.

optimize the actuator position x_a with regard to the behaviour of the uncontrolled DOFs, whereas their behaviour is part of the control objective as well. Furthermore, the criterion's focus is the *effort* aspect of the control objective; the speed and accuracy aspects are not explicitly accounted for.

The spillover effect based criterion is unsuitable for two main reasons. The first is that the spillover effect has already been minimized for the linear subsystem, as the interface DOFs y_a and y_m are used to model residual flexibility modes of the linear subsystem. The second reason is that in general the mode concept does not apply for non-linear systems.

Problem with the criterion based on the minimization of the total energy consumed by the controller or on the maximization of the controller-induced dissipation energy is that in this non-linear system *no* obvious quantitative relation exists between this energy level and the stability of the so-called zero dynamics, defined by the uncontrolled DOFs.

The acceleration criterion is applicable only to linear systems, as mode decomposition can not be applied to non-linear systems.

The final criterion, discussed here, is the weighted combination of the time integrated square tracking error of the controlled DOF e_{y_a} and the time integrated square control effort u. In this criterion both the effort aspect and the accuracy aspect of the control objective are accounted for. Through the control effort, the influence of the uncontrolled DOFs can also be accounted for. However, in this case a new problem emerges, i.e. the necessity to find an appropriate choice for the weighting factors for the different parts of the criterion. Furthermore, the criterion does not explicitly account for the speed aspect of the control objective.

Except for the last criterion, none of the criteria discussed above can cope with the influence of the uncontrolled DOFs properly while being applicable to non-linear systems. And, although the last criterion can be used, it is interesting to have a criterion that can account for the behaviour of the uncontrolled DOFs only, as then the behaviour of the controlled DOF and the uncontrolled DOFs can be evaluated separately.

2.1.2 Merits and demerits of the new criterion

Therefore, at least one *additional* criterion is required to account for the behaviour of the uncontrolled DOFs. The zero dynamics stability based criterion proposed in this chapter can provide this criterion. In fact, the zero dynamics stability based criterion alone may be quite sufficient to determine an optimal actuator position x_a, as it has been shown in the past (see [14]) that the stabilization of the actuator DOF y_a is not a big issue as long as the actuator is not located too close to one of the leaf springs. Because much more time is required for the uncontrolled DOFs to damp out towards the harmonic solution than the time required to control the actuator DOF to the harmonic solution, the behaviour of the uncontrolled DOFs should receive much more attention than they have received so far. This happens in the next sections.

Using the zero dynamics stability based criterion, we can attempt to find an optimal actuator position x_a with regard to the damping behaviour of the uncontrolled DOFs. In general this position is different from the one found with a criterion based on the behaviour of the controlled DOF. We can then decide to use a combination of both criteria, resulting in a compromise between the optimal actuator positions x_a, or to just use the actuator position found using the zero dynamics stability based criterion.

2.2 System model for the beam with one-sided spring

In this section the mathematical model of the beam with one-sided spring is discussed very briefly for the case that a single actuator is used at position x_a. Compromising between accuracy and available calculation time, a FEM model of the beam with a large number of DOFs m is reduced to a model with a much smaller number of DOFs n, accounting for the (low frequency) influence of all m DOFs with limited, yet sufficient accuracy. This is achieved using the Component Mode Synthesis (CMS) method implementation of the FEM package `Diana`. For more details on the determination of such a model, the reader is referred to Fey [8].

The resulting n DOF model has interface DOFs y_a and y_m and $n-2$ virtual DOFs ξ_i, stored in a vector column $\underset{\sim}{q}$:

$$\underset{\sim}{q}^T = \begin{bmatrix} y_a & y_m & \xi_1 \dots \xi_{n-2} \end{bmatrix}. \tag{2.1}$$

- The interface DOFs y_a and y_m are used to describe residual flexibility modes of the linear beam system and can be used to apply external loads to the linear beam system. y_a represents the displacement of the beam at position x_a, i.e. the position where the calculated control effort u is applied to the beam by means of an actuator force F_{act}, generated by an actuator. y_m represents the displacement of the middle of the beam, i.e. the position where the excitation force F_{ex} and the force originating from the one-sided spring are applied to the beam.

- Other DOFs ξ_i are so-called virtual DOFs, representing virtual displacements. They describe eigenmodes of the linear beam system and can not directly be interpreted as a displacement at a certain position. In experiments the values of the virtual DOFs ξ_i are determined by means of state reconstruction, because their values can not be measured (see [19]).

In comparison to the model according to Kant [14], the following changes have been made (see also figure 2.1):

- 64 nodes (32 in the left half, 32 in the right half) have been inserted in the beam representation in order to allow the system dynamics to be evaluated for more different actuator positions x_a. As is shown in figure 2.1, the actuator can effectively be evaluated at 64 node positions[2]: nodes 3-66. Because of the symmetry in the beam system, it is not necessary to investigate actuator positions x_a on the other half of the beam.

- The linear damper in the middle of the beam has been removed from the model, as it suppresses the non-linear effects and is unrealistic: just like the one-sided spring, a realistic damper would be a one-sided damper, as shown in figure 2.1 (in gray). However, such a damper has *not* been implemented.

- Unless stated otherwise, the modal damping ratio for component mode synthesis has been chosen to be 0.001 for all modes, as non-linear effects become visible more clearly for low damping settings.

The resulting `Diana` data file can be found in appendix D.

[2] $x_a = 0.01 \times (\text{node} - 2)$ [m].

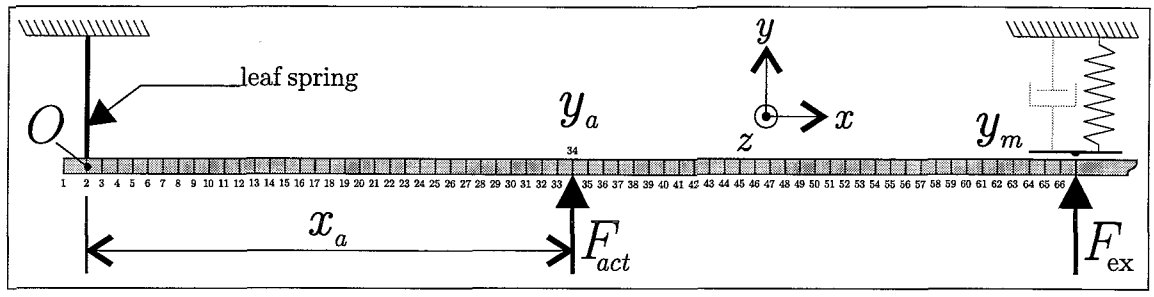

Figure 2.1: left half of the beam with one-sided spring and some essential node numbers.

The equations of motion of the model of the beam with one-sided spring are:

$$\underset{\sim}{M}\ddot{q} + \underset{\sim}{B}\dot{q} + \underset{\sim}{K}q + \underset{\sim}{H}_m k_{nl} y_m = \underset{\sim}{H}_m F_{ex} + \underset{\sim}{H}_a u. \tag{2.2}$$

- The $n \times n$ matrices $\underset{\sim}{M}$, $\underset{\sim}{B}$ and $\underset{\sim}{K}$ have been obtained using the CMS method implementation of the FEM package `Diana`.
- $\underset{\sim}{H}_m$ is a $n \times 1$ distribution vector column which is used to apply the influence of the one-sided spring and the excitation force F_{ex}. As these forces are applied to the beam at the 2^{nd} DOF y_m, we find:

$$\underset{\sim}{H}_m^T = [0\ 1\ 0 \ldots 0]. \tag{2.3}$$

- The term with k_{nl} accounts for the influence of the one-sided spring:

$$k_{nl} = k\,\mathrm{int}\left(\frac{1+\mathrm{sign}(y_m)}{2}\right) = \begin{cases} k & \text{if } y_m > 0, \\ 0 & \text{if } y_m \leq 0. \end{cases} \tag{2.4}$$

- The excitation force F_{ex} is applied to the beam at the 2^{nd} DOF:

$$F_{ex} = m_e r_e \omega^2 \cos(\omega t), \text{ with } \omega = 2\pi f_e. \tag{2.5}$$

  In this equation m_e is the effective mass of the total eccentric mass, regarded as concentrated at effective radius r_e. f_e represents the excitation frequency.

- $\underset{\sim}{H}_a$ is a $n \times 1$ distribution vector column for the scalar control effort u. This effort is applied to the beam at position x_a of the 1^{st} DOF y_a. Therefore:

$$\underset{\sim}{H}_a^T = [1\ 0\ 0 \ldots 0]. \tag{2.6}$$

2.3 The controller

2.3.1 Control objective

The control objective for this system is to bring the *entire system*, i.e. all DOFs, in the unstable harmonic solution. This objective has been translated to a desired trajectory $q_{d,i}$ for each defined DOF q_i, resulting in a servo problem. Each of these desired trajectories $q_{d,i}$ describes the trajectory that is followed by the corresponding DOF when the system behaves according to the unstable harmonic solution. They have been determined using the FEM package `Diana` and have each been approximated by means of a truncated Fourier series existing of 10 harmonics, because this facilitates continuous time evaluation of the

desired trajectory and its derivatives and requires less memory resources than for instance a time series. The Fourier coefficients have been stored in a matrix $\underline{C}$. The approximations will be indicated by $\hat{q}_{d,i}$:

$$\hat{q}_{d,i} = \underline{C}(i,1) + \sum_{j=1}^{10} \left(\underline{C}(i,j+1)\cos(j2\pi f_e t) + \underline{C}(i,j+11)\sin(j2\pi f_e t)\right). \tag{2.7}$$

For the i^{th} DOF we define the tracking error e_i as the difference between the actual displacement q_i and its desired displacement $q_{d,i}$. The actual tracking errors of the DOFs are stored together in a vector column $\underset{\sim}{e}$:

$$\underset{\sim}{e} = \underset{\sim}{q} - \underset{\sim}{q}_d. \tag{2.8}$$

Similarly, we define the estimated tracking error $\hat{e}_i$ as the difference between the actual displacement q_i and its approximated desired displacement $\hat{q}_{d,i}$. They are stored together in a vector column $\underset{\sim}{\hat{e}}$:

$$\underset{\sim}{\hat{e}} = \underset{\sim}{q} - \underset{\sim}{\hat{q}}_d. \tag{2.9}$$

As only one DOF, i.e. the actuator DOF y_a, actually is controlled in this research, it is convenient to think of the control objective as split up into two parts, each of which must eventually be satisfied:

- *Part 1*: Control the actuator DOF y_a towards the unstable harmonic solution.
- *Part 2*: Let other DOFs damp towards their corresponding harmonic solutions.

It has been presumed that the second part will be satisfied automatically, once the first part has been satisfied. After all, the harmonic solution *is* a natural solution of the system. This presumption will receive some attention in section 2.4.

2.3.2 The control algorithm

As explained before, only the actuator DOF y_a is controlled. A computed torque controller (CTC) with additional PD-term is used to satisfy the previously defined first part of the control objective. The controller will be based on a 3 DOF model, i.e. $n = 3$, because this model is used in the experiments. As the same method can be applied to n DOF models with $n > 3$, i.e. with more than just one virtual DOF ξ, this means no loss of generality.

To eliminate the tracking error e_1 of the first DOF y_a, a control effort u is required. From the system of equations 2.2, it follows that:

$$u \equiv \underline{M}_{1,1\ldots3} \begin{bmatrix} \ddot{q}_1 \\ \ddot{q}_2 \\ \ddot{q}_3 \end{bmatrix} + \underline{B}_{1,1\ldots3}\underset{\sim}{\dot{q}} + \underline{K}_{1,1\ldots3}\underset{\sim}{q}. \tag{2.10}$$

Therefore, if u is chosen to be

$$u = \underline{M}_{1,1\ldots3} \begin{bmatrix} v(t) \\ \ddot{q}_2 \\ \ddot{q}_3 \end{bmatrix} + \underline{B}_{1,1\ldots3}\underset{\sim}{\dot{q}} + \underline{K}_{1,1\ldots3}\underset{\sim}{q}, \tag{2.11}$$

it yields:

$$\ddot{q}_1 = v(t). \tag{2.12}$$

Provided that an appropriate choice for $v(t)$ is made, the first equation of the system of equations 2.2 has been linearized by feedback. This method is called partial feedback linearization (PFL). In robotics this method is often referred to as computed torque control (CTC). The reason it's called *partial* feedback linearization is that the *other* equations of 2.2 have *not* been linearized by this choice for the control effort u.
The choice has now been moved to $v(t)$. A sensible choice for $v(t)$ is the desired acceleration $\ddot{q}_{d,1}$ in combination with two terms proportional to respectively the tracking error e_1 and its derivative $\dot{e}_1$:

$$v(t) = \ddot{q}_{d,1} - K_P e_1 - K_D \dot{e}_1. \tag{2.13}$$

Substitution of equation 2.13 in 2.12 then results in the following error equation:

$$\ddot{e}_1 + K_D \dot{e}_1 + K_P e_1 = 0. \tag{2.14}$$

If we introduce control parameters η and λ and choose $K_P{=}\eta\lambda$ and $K_D{=}\eta + \lambda$, the poles of equation 2.14 are located at $-\eta$ and $-\lambda$ for $\{\lambda, \eta\} \in \mathbb{R}$. As long as $\{\lambda, \eta\} \in \mathbb{R}^+$, the tracking error e_1 will eventually disappear, as $e_1 = 0$ then is an asymptotically stable equilibrium point of equation 2.14. This results in the following control law:

$$u = \frac{\left(\underset{\sim}{M}^{-1}\left(\underset{\sim}{K}\underset{\sim}{q} + \underset{\sim}{B}\dot{\underset{\sim}{q}} + \underset{\sim}{H}_m(k_{nl}y_m - F_{ex})\right)\right)_1 + \overbrace{\ddot{q}_{d,1} - (\eta+\lambda)\dot{e}_1 - \eta\lambda e_1}^{v(t)}}{\left(\underset{\sim}{M}^{-1}\underset{\sim}{H}_a\right)_1}. \tag{2.15}$$

In the past, it has been shown both in simulations and in experiments that the first part of the control objective can indeed be satisfied using this control law. Like in the past (see [14]), values $\eta = 100$ and $\lambda = 100$ have been used for the controller parameters in the simulations described in this report.

2.4 Zero dynamics

In the previous subsection it has been shown how the first part of the control objective can be satisfied, i.e. the controlled DOF behaves as desired. In this section, it will be proved that the presumption that the second part of the control objective will be satisfied automatically once the first part has been satisfied, is theoretically allowed. To achieve this, it is necessary to investigate the dynamics of the uncontrolled DOFs y_m and ξ, past the point that the first part of the control objective has been satisfied.

If we look at the equations of motion, like stated in equation 2.2 and have a look again at the 3 DOF case, the system description can be written as follows:

$$\underset{\sim}{M}\ddot{\underset{\sim}{q}} + \underset{\sim}{B}\dot{\underset{\sim}{q}} + \underset{\sim}{K}\underset{\sim}{q} + \begin{bmatrix} 0 \\ k y_m \operatorname{int}\left(\frac{1+\operatorname{sign}(y_m)}{2}\right) \\ 0 \end{bmatrix} = \begin{bmatrix} u \\ F_{ex} \\ 0 \end{bmatrix}. \tag{2.16}$$

As the desired trajectories, stored in vector column $\underset{\sim}{q}_d$, are a solution of the system, no further control effort is required once both the first and the second part of the control objective have been satisfied, i.e. all DOFs behave according to their corresponding unstable harmonic solutions:

$$\underset{\sim}{M}\ddot{\underset{\sim}{q}}_d + \underset{\sim}{B}\dot{\underset{\sim}{q}}_d + \underset{\sim}{K}\underset{\sim}{q}_d + \begin{bmatrix} 0 \\ k y_{m,d} \operatorname{int}\left(\frac{1+\operatorname{sign}(y_{m,d})}{2}\right) \\ 0 \end{bmatrix} = \begin{bmatrix} 0 \\ F_{ex} \\ 0 \end{bmatrix}. \tag{2.17}$$

When we subtract equation 2.17 from equation 2.16, the following system of error equations is obtained, using the definition of the error vector column $\underset{\sim}{e}$ according to equation 2.8:

$$\underline{M}\ddot{\underset{\sim}{e}} + \underline{B}\dot{\underset{\sim}{e}} + \underline{K}\underset{\sim}{e} + \begin{bmatrix} ky_m \operatorname{int}\left(\frac{1+\operatorname{sign}(y_m)}{2}\right) \\ 0 \\ -ky_{m,d} \operatorname{int}\left(\frac{1+\operatorname{sign}(y_{m,d})}{2}\right) \end{bmatrix} = \begin{bmatrix} u \\ 0 \\ 0 \end{bmatrix}. \quad (2.18)$$

Now, let's take one step back: when only the first part of the control objective has been satisfied, so $e_{y_a} \to 0$, the damping of the control effort is determined by the following part of the first error equation of the system of equations defined by equation 2.18:

$$u = \begin{bmatrix} M_{12} & M_{13} \end{bmatrix} \begin{bmatrix} \ddot{e}_{y_m} \\ \ddot{e}_\xi \end{bmatrix} + \begin{bmatrix} B_{12} & B_{13} \end{bmatrix} \begin{bmatrix} \dot{e}_{y_m} \\ \dot{e}_\xi \end{bmatrix} + \begin{bmatrix} K_{12} & K_{13} \end{bmatrix} \begin{bmatrix} e_{y_m} \\ e_\xi \end{bmatrix}. \quad (2.19)$$

This means that, once the first part of the control objective has been satisfied, the control effort u only compensates for the influence of the internal dynamics of the system on the tracking error e_{y_a} of the controlled DOF. This internal dynamics is caused by the uncontrolled DOFs and is called *zero dynamics*: the zero dynamics describes the internal behaviour of the system when inputs are chosen in such a way that the output is kept at zero (see [21]). Here, the tracking error e_{y_a} of the actuator DOF is considered to be the output. The control effort u is the input of the system.

After the first part of the control objective has been satisfied, i.e. $e_{y_a} \to 0$, the course of the zero dynamics (and therefore the course of the control effort u) is determined by the tracking errors e_{y_m} and e_ξ, as is shown by equation 2.19. Only after these errors have damped out completely, the second part of the control objective has been satisfied. Then and only then, the control effort u has also become 0. The course of the tracking errors of the uncontrolled DOFs therefore depends on the following two factors:

1. Stability of the zero dynamics.
2. The spot in phase space of the zero dynamics (error space) where the DOFs are located at the moment the first part of the control objective is satisfied, i.e. $e_{y_a} \to 0$. By this spot the values of the errors of the uncontrolled DOFs are described at the moment the controller no longer influences the system other than to compensate for the disturbances in the controlled DOF y_a caused by the other DOFs. This moment will be referred to as the moment at which the zero dynamics have been 'reached'.

It is therefore essential to have a zero dynamics as stable as possible and to 'reach' the zero dynamics at a convenient spot in the error space. The first aspect is explicitly discussed in this report, the second aspect is the subject of other studies. Here, in particular is examined whether the stability of the zero dynamics can provide a useful criterion for the determination of the best actuator position x_a.

From equation 2.18 it follows that the zero dynamics of the system for a 3 DOF model is described by the following system of non-linear equations:

$$\overbrace{\begin{bmatrix} M_{22} & M_{23} \\ M_{32} & M_{33} \end{bmatrix}}^{\underline{M}_z} \begin{bmatrix} \ddot{e}_{y_m} \\ \ddot{e}_\xi \end{bmatrix} + \overbrace{\begin{bmatrix} B_{22} & B_{23} \\ B_{32} & B_{33} \end{bmatrix}}^{\underline{B}_z} \begin{bmatrix} \dot{e}_{y_m} \\ \dot{e}_\xi \end{bmatrix} + \overbrace{\begin{bmatrix} K_{22} & K_{23} \\ K_{32} & K_{33} \end{bmatrix}}^{\underline{K}_z} \begin{bmatrix} e_{y_m} \\ e_\xi \end{bmatrix} + \begin{bmatrix} \overbrace{ky_m \operatorname{int}\left(\frac{1+\operatorname{sign}(y_m)}{2}\right)}^{\phi(e_{y_m})} \\ 0 \\ -ky_{m,d} \operatorname{int}\left(\frac{1+\operatorname{sign}(y_{m,d})}{2}\right) \end{bmatrix} = \begin{bmatrix} 0 \\ 0 \end{bmatrix}. \quad (2.20)$$

In equation 2.20 the influence of the non-linearity is represented by the scalar $\phi(e_{y_m})$. The mass, damping and stiffness matrices, $\underline{M}_z$, $\underline{B}_z$ and $\underline{K}_z$ are a function of the actuator position x_a. Thus, the actuator position x_a can be used as a tool to influence the stability of the zero dynamics. Vice versa, a quantitative measure for the stability of the zero dynamics can be used as a criterion for actuator positioning.
Stability of the zero dynamics means that the two uncontrolled DOFs have an asymptotically stable equilibrium point in respectively $e_{y_m} = 0$ and $e_\xi = 0$. Proving that these points are asymptotically stable also proves that the second part of the control objective will automatically be satisfied, once the first part of the control objective has been satisfied. This proof can be given using Popov's criterion, which is based on the Kalman-Yacubovitch theorem (see appendix A).

2.4.1 Proof for asymptotic stability of the zero dynamics

In appendix A, it is shown that Popov's criterion may be used to test global asymptotic stability if the following necessary and sufficient (NAS) conditions are satisfied:

- system matrix $\underline{A}$ is Hurwitz,
- the pair $(\underline{A}, \underline{B})$ is controllable,
- the pair $(\underline{C}, \underline{A})$ is observable,
- the non-linearity ϕ belongs to the sector $(0, k)$.

Popov's criterion (see equation A.20) implies that global asymptotic stability of the zero dynamics is guaranteed if a straight line through the point $(-\frac{1}{k},0)$ with slope $\frac{1}{r} > 0$ can be found that satisfies the condition that the Popov plot stays to the right of this line $\forall\omega \in \mathbb{R}$. The matrix and the vector columns which define the (scalar) transfer function $F(j\omega)$, required to produce a Popov plot, are given by:

$$\underline{A} = \begin{bmatrix} \underline{O} & \underline{I} \\ -\underline{M}_z^{-1}\underline{K}_z & -\underline{M}_z^{-1}\underline{B}_z \end{bmatrix}, \quad \underline{b} = \begin{bmatrix} 0 \\ 0 \\ \underline{M}_z^{-1}\begin{bmatrix}1\\0\end{bmatrix} \end{bmatrix}, \quad \underline{c} = \begin{bmatrix}1\\0\\0\\0\end{bmatrix}. \tag{2.21}$$

The matrices $\underline{M}_z$, $\underline{B}_z$ and $\underline{K}_z$ are defined by the zero dynamics (see equation 2.20).

To illustrate that a line through point $(-\frac{1}{k}, 0)$ with such a slope $\frac{1}{r}$ exists for each actuator position for the system of the beam with one-sided spring, the values of r have been evaluated for the actuator, positioned at 64 different nodes $3 - 66$ as indicated in figure 2.1. For the one-sided spring, a stiffness of respectively $k = 82.5$, $k = 165$ and $k = 330$ [kN/m] has been used. The required system models have been determined using the FEM package `Diana` with a modal damping ratio of 0.001 for each mode.

Whether the NAS conditions, allowing the *use* of Popov's criterion, are satisfied, has been tested. The tests indicate that Popov's criterion may be applied, as all conditions are satisfied:

- The eigenvalues of $\underline{A}$ for the 64 different actuator positions x_a can be found in appendix C.2 for the case that $k = 165$ [kN/m]. As they all have negative real parts, $\underline{A}$ is Hurwitz for all 64 actuator positions x_a. The value of the stiffness k of the one-sided spring has no effect on the eigenvalues of $\underline{A}$. Therefore, the same holds for other values of the stiffness k.

- The pair $(\underline{A}, \underline{B})$ is controllable due to the fact that the 4×4 controllability matrix

$$\underline{P} = [\underline{b} \quad \underline{A}\underline{b} \quad \underline{A}^2\underline{b} \quad \underline{A}^3\underline{b}] \tag{2.22}$$

has rank 4 for all 64 actuator positions, for all values of k.

- The same holds for the observability matrix

$$\underline{Q} = [\underline{c} \quad (\underline{c}^T\underline{A})^T \quad (\underline{c}^T\underline{A}^2)^T \quad (\underline{c}^T\underline{A}^3)^T]^T. \tag{2.23}$$

Thus, the observability condition for the pair $(\underline{C}, \underline{A})$ is also satisfied.

- The non-linearity $\phi(e_{y_m})$, originating from the one-sided spring, is described in equation 2.20. Table 2.1 shows that it satisfies the sector condition.

sign e_{y_m}	case	value $\frac{\phi(e_{y_m})}{e_{y_m}}$
$e_{y_m} > 0$	$y_m > y_{m_d} \geq 0$	k
	$y_m > 0,\ y_{m_d} < 0$	$0 < \frac{k y_m}{y_m - y_{m_d}} < k$
	$y_{m_d} < y_m \leq 0$	0
$e_{y_m} = 0$	$y_m = y_{m_d}$	0
$e_{y_m} < 0$	$y_{m_d} > y_m \geq 0$	k
	$y_m < 0,\ y_{m_d} > 0$	$0 < \frac{-k y_{m_d}}{y_m - y_{m_d}} < k$
	$y_m < y_{m_d} \leq 0$	0

Table 2.1: proof that the sector condition is satisfied for the beam with one-sided spring.

In figure 2.2 some results are shown for different actuator positions. Figure 2.2(a) shows an example Popov plot for the case that the actuator is located at node 38, with $k = 165$ [kN/m] as stiffness of the one-sided spring. The point $(-\frac{1}{k}, 0)$ is marked with an asterisk. The transfer function $F(j\omega)$ remains right of a straight line through the point $(-\frac{1}{k}, 0)$ with slope $\frac{1}{r}$ for values of $r \geq 0.30$. The critical values of r for all examined actuator positions are visualized in figure 2.2(b) for the different stiffness cases. The numerical values for case $k = 165$ [kN/m] can be found in appendix C.3.

Thus, the zero dynamics has been proved to be globally asymptotically stable for the 64 examined positions and therefore it has also been proved for these positions that theoretically the second part of the control objective will be satisfied automatically once the first part of the control objective has been satisfied. When we look at the course of r as a function of the actuator position x_a shown in figure 2.2(b), there's *no* reason to suspect that actuator positions x_a exist where a valid value of r can *not* be found, except for the leaf spring positions. Therefore, this proof is assumed to apply for all possible actuator positions x_a except for the leaf spring positions.
An interesting point is the notion that the stiffness of the one-sided spring k can be chosen arbitrarily large. This can be seen in the Popov plot, figure 2.2(a). For increasing values of k, the point $(-\frac{1}{k}, 0)$ moves towards $(0, 0)$. It is, however, always possible to find a value for $r > 0$ which satisfies equation A.20.

2.4.2 Stability of the zero dynamics as an actuator positioning criterion

In the previous subsection it has been proved that the zero dynamics is stable for all examined actuator positions x_a. Therefore, a quantitative measure for the stability of the

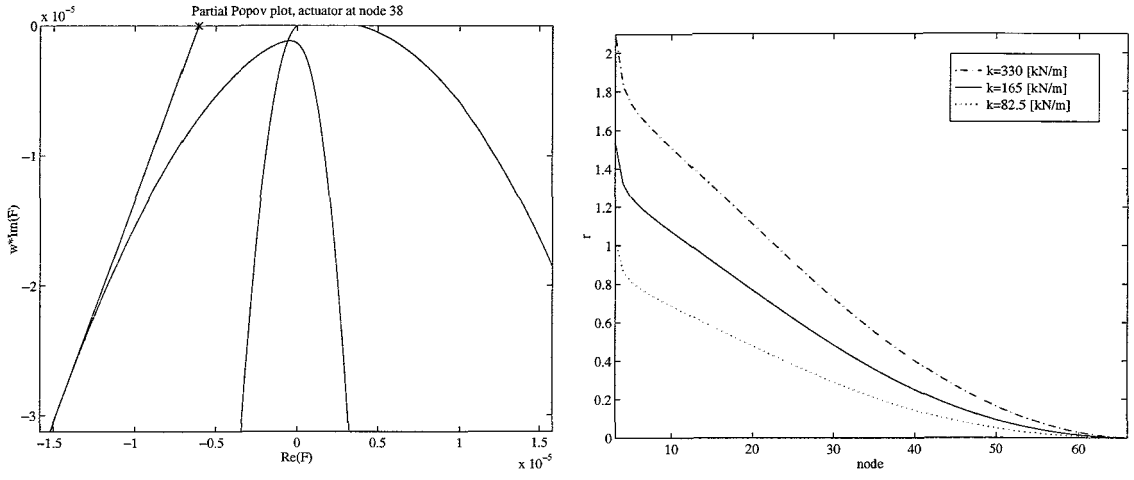

(a) Popov plot for node 38, $k = 165$ [kN/m].

(b) values of r. Actuator at nodes 3-66.

Figure 2.2: stability analysis using Popov's criterion.

zero dynamics is a sensible actuator positioning criterion with regard to the second part of the control objective. However, one needs to be aware that the first part of the objective can not be accounted for when using such a measure. The stability criterion, defining optimality with regard to the second part of the control objective, should therefore be used in conjunction with a criterion that defines optimality with regard to the first part of the control objective.

Unfortunately the value of $\frac{1}{r}$ itself is not suitable to be used as such a measure, as no clear relation exists between the value of r and the performance of the zero dynamics, i.e. the damping rate of the tracking errors of the uncontrolled DOFs. The fact that valid values $\frac{1}{r}$ exist, shows only *that* the zero dynamics is stable, but the values do not necessarily indicate *how* stable it is in a quantitative way, as Popov's criterion provides a sufficient but not essentially necessary condition.

In the next section, we will attempt to find an appropriate quantitative measure for the criterion.

2.5 Quantification of the stability of the zero dynamics

Because the control effort u for the zero dynamics depends on the tracking errors e_{y_m} and e_ξ only as can be seen in equation 2.19, it is sufficient to use only (the absolute value of) the control effort u to quantify the stability of the zero dynamics. In this section the stability of the zero dynamics will be quantified using a measure in which all control effort values are weighted evenly. The quantitative measure will first be evaluated for the linear subsystem of the beam with one-sided spring, i.e. the beam without the one-sided spring, because the powerful analysis techniques available for linear systems can then be applied and because the analysis of the linear subsystem provides us with a reference for the effects of the addition of the local non-linearity. Then the one-sided spring will be included, resulting in the non-linear beam system. The measure will be evaluated for the non-linear system as well and its results will be compared to the results for the linear

subsystem.

2.5.1 The linear subsystem

If the one-sided spring is removed from the system, i.e. $k = 0$ [kN/m], the resulting subsystem is linear. The system of error equations 2.20 describing the behaviour of the zero dynamics then simplifies to the following:

$$\overbrace{\begin{bmatrix} M_{22} & M_{23} \\ M_{32} & M_{33} \end{bmatrix}}^{\underline{M}_z} \begin{bmatrix} \ddot{e}_{y_m} \\ \ddot{e}_\xi \end{bmatrix} + \overbrace{\begin{bmatrix} B_{22} & B_{23} \\ B_{32} & B_{33} \end{bmatrix}}^{\underline{B}_z} \begin{bmatrix} \dot{e}_{y_m} \\ \dot{e}_\xi \end{bmatrix} + \overbrace{\begin{bmatrix} K_{22} & K_{23} \\ K_{32} & K_{33} \end{bmatrix}}^{\underline{K}_z} \begin{bmatrix} e_{y_m} \\ e_\xi \end{bmatrix} = \begin{bmatrix} 0 \\ 0 \end{bmatrix}. \tag{2.24}$$

Let λ_1 and λ_2 be the eigenvalues of equation 2.24 and let $\underset{\sim}{v}_1$ and $\underset{\sim}{v}_2$ be the corresponding eigenvectors. Then, past the point in time where the first part of the control objective has been satisfied, the course of the tracking errors of the uncontrolled DOFs can be described by a linear combination of the two eigenvectors, indicated by the complex coefficients α_i:

$$\begin{bmatrix} e_{y_m} \\ e_{\xi_1} \\ \vdots \\ e_{\xi_{n-2}} \end{bmatrix} = \sum_{i=1}^{n-1} \left(\alpha_i \mathrm{e}^{\lambda_i t} \underset{\sim}{v}_i + \overline{\alpha}_i \mathrm{e}^{\overline{\lambda}_i t} \overline{\underset{\sim}{v}}_i \right). \tag{2.25}$$

In this equation $n - 1$ represents the number of uncontrolled DOFs. The values of α_i, indicating which combination of the eigenvectors occurs, depend on the state of the system at the point in time where the first part of the control objective is satisfied, i.e. the 'initial conditions' of the zero dynamics.
For the linear subsystem, the quantitative stability of the zero dynamics is determined by the negativity of the real parts of the eigenvalues λ_1 and λ_2. These real parts represent the damping in the system which is caused by the internal damping of the beam, represented by the damping matrix $\underline{B}_z$. In figure 2.3 the negative real parts of the eigenvalues of the subsystem are shown (as positive values).
Now, suppose that the system can be controlled to any arbitrary state. In that case, the best damping of the tracking errors $\underset{\sim}{e}$ can be achieved at the position where either of the eigenvalues has *the* most negative value. Then, actuator position $x_a = 0.47$ [m] (node 49) would be the best choice for the actuator position x_a as far as the linear subsystem is concerned. Equation 2.25 and figure 2.3 show that this requires that the zero dynamics is reached in a state that matches the eigenvector $\underset{\sim}{v}_2$ corresponding to eigenvalue λ_2 with the largest negative real part, so that the other eigenvectors have coefficients $|\alpha_i| = 0$. Unfortunately, the current control algorithm can *not* force the system into such a state, as the system is under-actuated. As a result, the real parts of the eigenvalues alone can *not* be used to quantify the stability of the zero dynamics. However, they do indicate the following:

1. The linear subsystem theoretically *can* benefit from an actuator position other than that as close to the middle of the beam as possible, as suggested earlier with regard to the first part of the control objective (see [14]).

2. They show the limits with regard to the maximum damping rate that can theoretically be achieved for the linear subsystem.

As the real parts of the eigenvalues can not be used to quantitatively predict the stability of the zero dynamics that occurs during an experiment (especially for the non-linear system), a different approach has to be used.

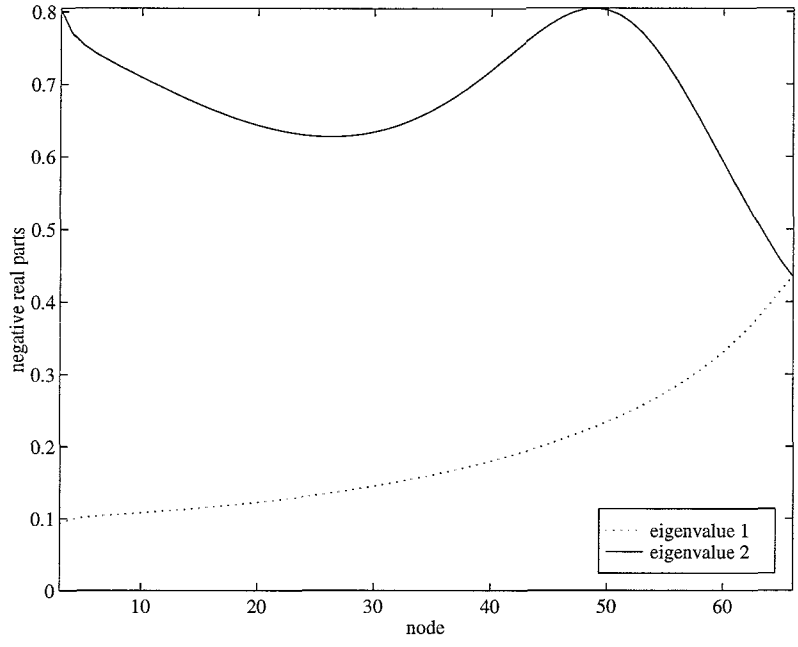

Figure 2.3: negative real parts of the eigenvalues of the linear subsystem versus the node at which the actuator is positioned.

Proposition for a quantitative measure

Using some of the new simulators described in appendix B, an exponential function u_{envelope} enveloping the control effort u has been determined using data from the moment when the first part of the control objective $\hat{e}_{y_a} \rightarrow 0$ has (approximately) been satisfied. This function can be regarded as a measure for the damping of the control effort u as a result of the internal dynamics. It is therefore a measure for the stability of the zero dynamics. One could suggest that a more appropriate description of the damping behaviour of the linear subsystem would be a linear combination of two exponential functions with $(\Re[\lambda_i]t)$ as exponents, as follows from equation 2.25. However, such a measure would not be useful for the non-linear system, because then the system's behaviour can not be decomposed into eigenmodes. The envelope is therefore described by a single exponential function with 2 parameters, c_1 and c_2:

$$u_{\text{envelope}} = c_1 \mathrm{e}^{-c_2 t}. \tag{2.26}$$

Equation 2.19 shows that the coefficient c_1 in equation 2.26 is both a measure for the control effort u and a measure for the combined tracking errors of the uncontrolled DOFs, at the point in time where the first part of the control objective is satisfied. Similarly, the coefficient c_2 is both a measure for the damping rate of the control effort u and a measure for the combined damping of the tracking errors of the uncontrolled DOFs. $\frac{1}{c_2}$ is a measure for the settling time: higher values of the damping coefficient c_2 imply a shorter settling time of the uncontrolled DOFs. Thus, using the measure defined by equation 2.26 we can account for all of the aspects of the (second part of the) control objective (speed, effort and accuracy), mentioned in section 2.1.

Simulation results

The behaviour of the beam has been simulated twice at the 64 actuator positions 3-66 shown in figure 2.1. The first series has been produced using the discrete time controller, running for 3 [s]. The second series has been produced using the continuous time controller, running for 25 [s]. For details on the operating conditions, the reader is referred to appendix B.1. The course of the control effort u and the course of the estimated tracking error of the actuator DOF $\hat{e}_{y_a}$ have been determined and stored for both series. With these results, the values of the parameters c_1 and c_2 have been determined in MATLAB using the procedure described in appendix E.2.2.

Figure 2.4 shows examples of the determination of this function for the case that the actuator is located at node 38, for both the continuous time controller simulator and the discrete time controller simulator. The upper graphs of both plots show the control effort u and the fitted envelope. As can be seen in figure 2.4, the fitted envelope is quite adequate in both cases. Both lower graphs show the estimated tracking error $\hat{e}_{y_a}$ of the actuator DOF. The point in time at which the first part of the control objective is found to be satisfied by the fit procedure, is indicated with an asterisk. The graphs also show that the first part of the control objective is satisfied very fast with the values for the control parameters that have been mentioned in section 2.3 and that much more time is required to satisfy the second part of the control objective than the time required to satisfy the first part, because some control effort still remains required a long time after the first part of the control objective has been satisfied.

The fit procedure has been used for all 64 actuator positions. The resulting numerical values of the coefficients c_1 and c_2 can be found in appendix C.1. Figure 2.5 shows the visualization of the coefficients c_1 and c_2 as a function of the actuator position x_a in respectively the upper and the lower graph. The lower graph of figure 2.5 and the relevant table in appendix C.1 show that good actuator positions would be respectively node 58 for the discrete time controller and node 64 for the continuous time controller. In the experimental set-up this leads to problems, as the dimensions of the mass unbalance prevent the usability of these positions. If this is taken into account, node 39 would be a good choice for the discrete time controller and as close to node 64 as possible would be a good choice for the continuous time controller.
Not only do the different controller types exhibit different optimal positions, but the damping behaviour of the control effort u is also quite different. Apparently the time discretization of the control effort u, which effectively filters it, has a positive influence on the stability of the zero dynamics. Time discretization has, however, little influence on the values of coefficient c_1, as can be seen in the upper graph of figure 2.5. The positive effect of filtering the control effort u on the stability of the zero dynamics has already been noticed in the past (see [14, 23]), but no clear explanation has been found so far. Such an explanation will not be pursued here either, as it seems to go beyond the objectives of this research.

Damping coefficients c_2 versus negative real parts of the eigenvalues

As expected, a comparison of the damping coefficients c_2 for the continuous time controller case, shown in the lower graph of figure 2.5 and the negative real parts of the eigenvalues of the zero dynamics, shown in figure 2.3, indicates that in the simulations a combination of the eigenvectors has occurred: the range of the damping coefficients c_2 corresponds to the range of the negative real parts of the eigenvalues. As a result of the previously explained

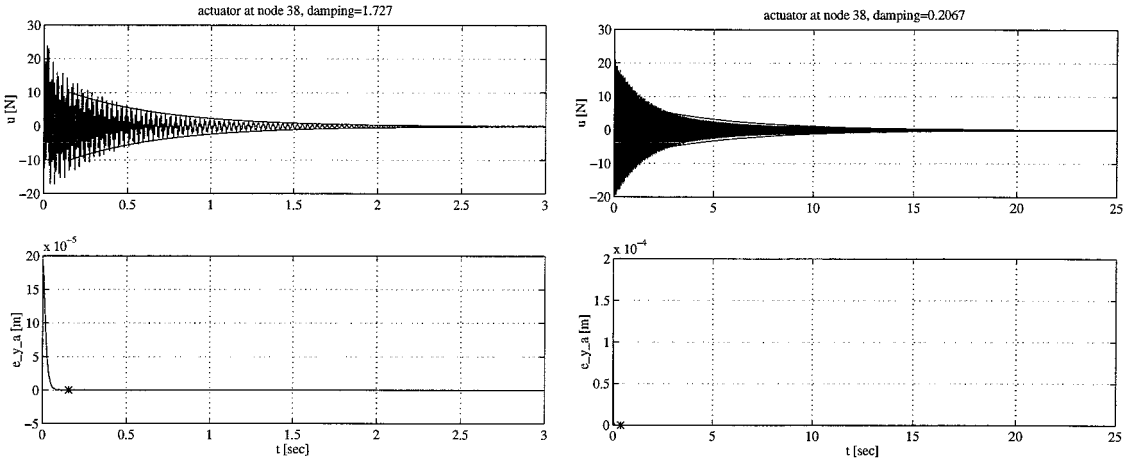

(a) discrete time, f_s=9990 [Hz].

(b) continuous time.

Figure 2.4: example envelopes for the control effort u for k=0 [kN/m]. Actuator at node 38.

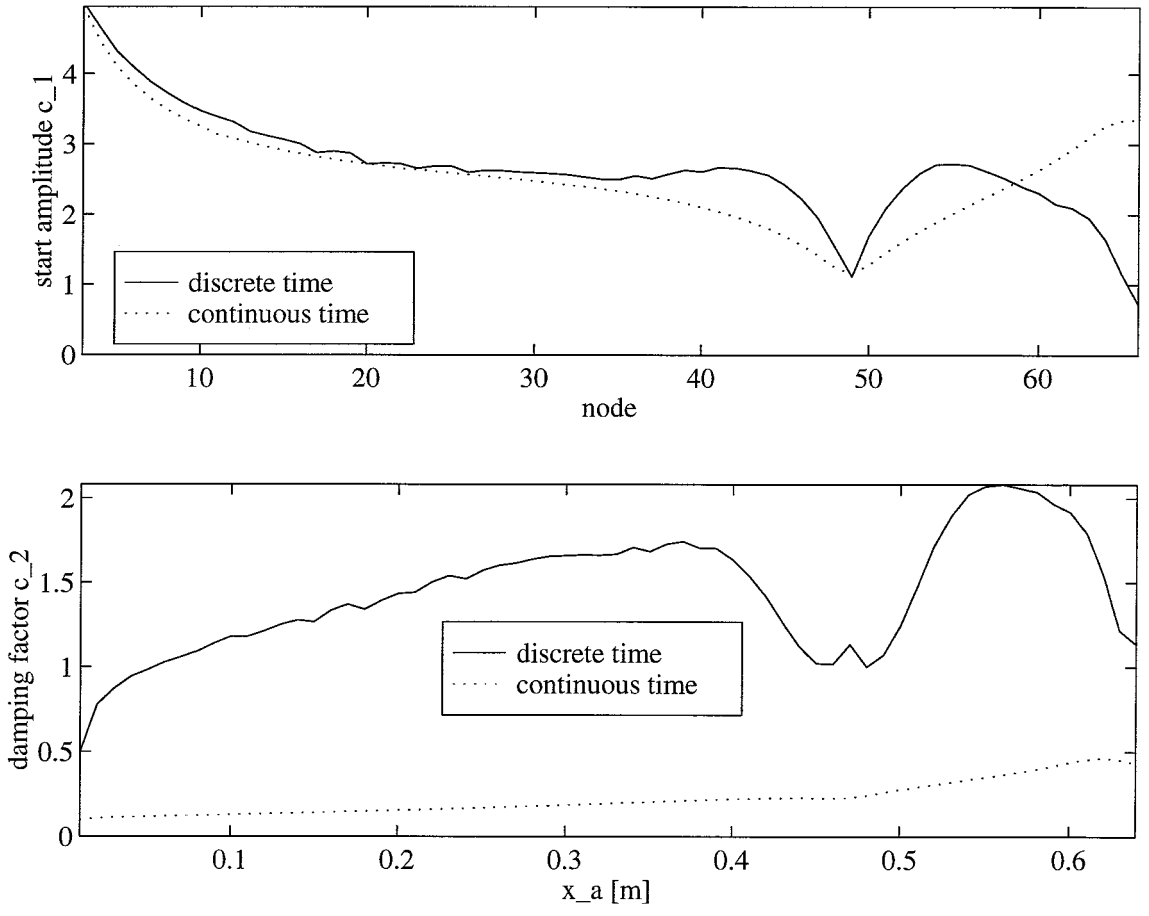

Figure 2.5: coefficients c_1 and c_2 for 64 actuator positions in case $k = 0$ [kN/m].

filter effect, the discrete time controller exhibits much higher damping rates.

2.5.2 The complete non-linear system

The two simulators have also been applied to the complete non-linear system, i.e. including the one-sided spring. As $k = 165$ [kN/m] corresponds to the value for the stiffness of the one-sided spring used in the experiments, this value has also been used in the simulations for the complete non-linear system.

Simulation results

The behaviour of the beam has been simulated for the 64 actuator positions 3-66, shown in figure 2.1. Again, the course of the control effort u and the course of the tracking error of the actuator DOF e_{y_a} were determined and stored. In the discrete time case the simulation has run for 2 [s]. In the continuous time case the simulation has run for 25 [s]. After finishing the simulations, an enveloping exponential function has been determined in the same way as for the linear subsystem. Figure 2.6 shows two examples of the determination of the envelope for the case that the actuator (again) is positioned at node 38 for both the discrete time controller and the continuous time controller. The upper graphs of both plots show the control effort u and the fitted envelope. Both lower graphs show the estimated tracking error $\hat{e}_{y_a}$ of the actuator DOF. The point in time at which the first part of the control objective is found to be satisfied by the fit procedure, is indicated by an asterisk. Obviously, the controller does *not* work properly for this actuator position:

- In the discrete time controller case the actuator DOF y_a itself is not even properly controlled towards the approximated harmonic solution $\hat{q}_{d,1}$ and kept there. This behaviour must be attributed to the time discretization of the control effort u. Considering the relatively high sample frequency f_s of 9990 [Hz], that is quite remarkable. As expected, the amplitude of the remaining estimated tracking error $\hat{e}_{y_a}$ becomes smaller in simulations with higher sample frequencies f_s (not shown).

- In the continuous time case the tracking error of the controlled DOF $\hat{e}_{y_a}$ rapidly disappears ($< 10^{-14}$!), but the other DOFs don't start to track the trajectories corresponding to the harmonic solution.

Also, the envelope fit procedure obviously fails for this actuator position, resulting in a very small (right graph) or even negative damping factor c_2 (left graph).

Figure 2.7 shows a graphical representation of the values of the coefficients c_1 and c_2 that have been found for each of the 64 actuator positions. The lower graph of figure 2.7 and the relevant table in appendix C.1 show that good actuator positions would be respectively node 58 for the discrete time controller and node 31 for the continuous time controller. The lower graphs of figure 2.8 show the damping behaviour for the continuous time controller for the case that the actuator is positioned at node 31. The upper graphs show that the estimated tracking errors of the uncontrolled DOFs damp out (which they are supposed to do).
However, several other actuator positions exhibit very small or even negative damping factors c_2, indicating that there's a problem with the stability there (as can best be noticed from tables C.3 and C.4 in appendix C.1). This would be in contradiction with the stability proof of subsection 2.4.1.

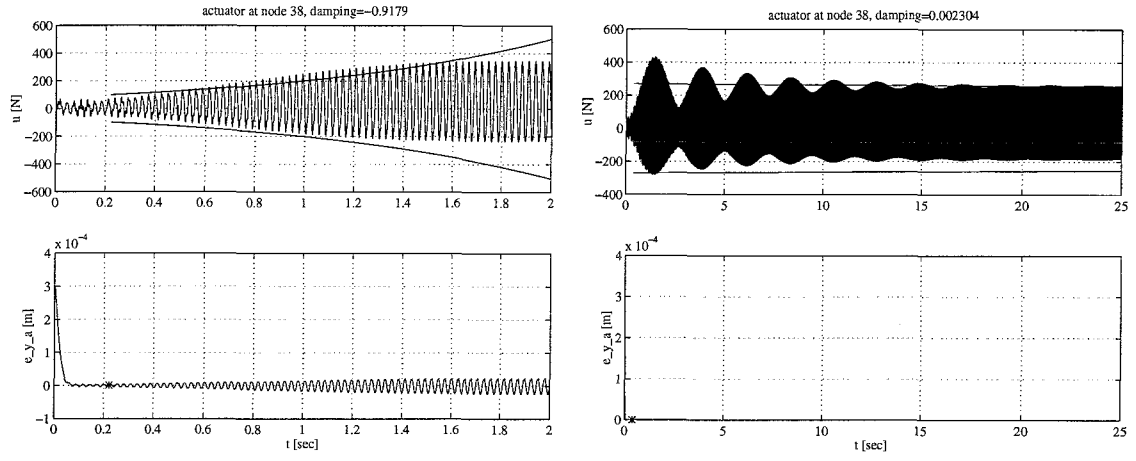

(a) discrete time, f_s=9990 [Hz].

(b) continuous time.

Figure 2.6: example envelopes for the control effort u for k=165 [kN/m]. Actuator at node 38.

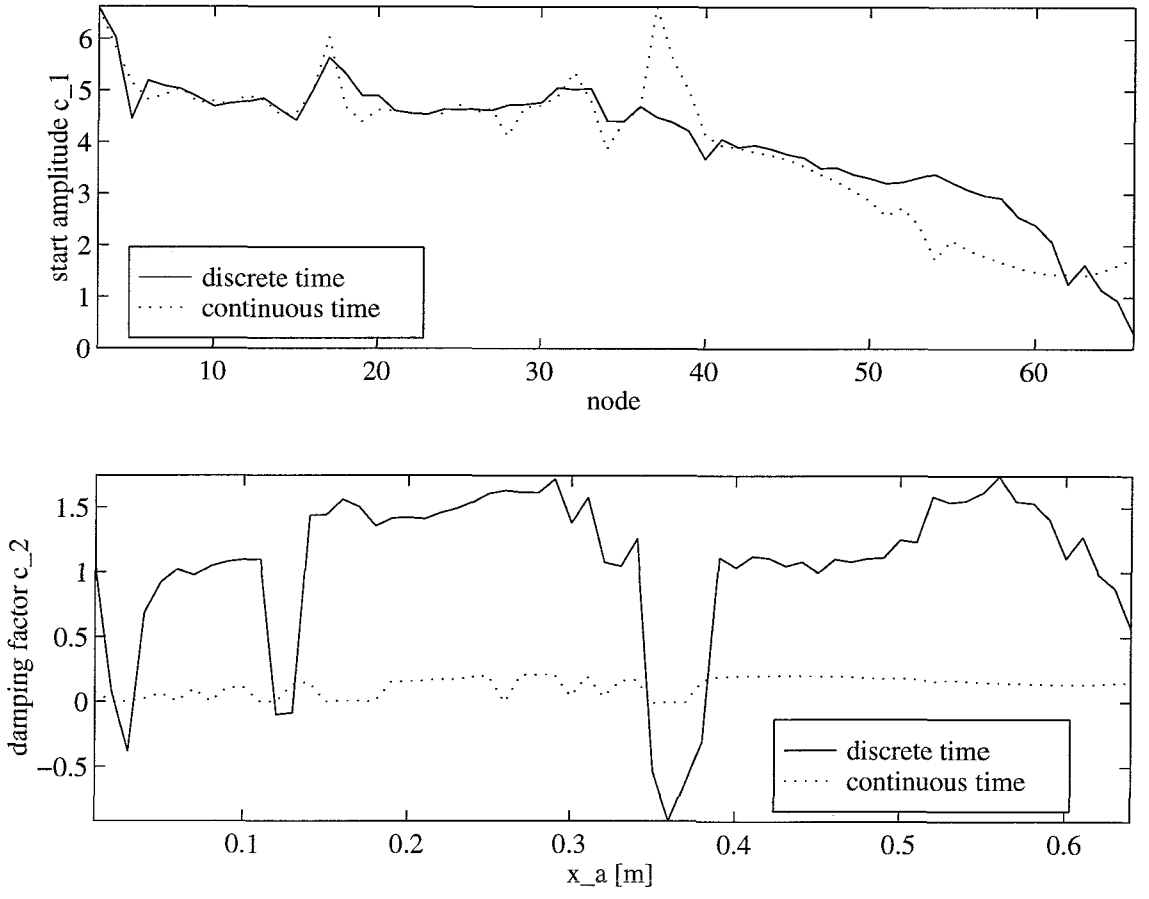

Figure 2.7: coefficients c_1 and c_2 for 64 actuator positions in case $k = 165$ [kN/m].

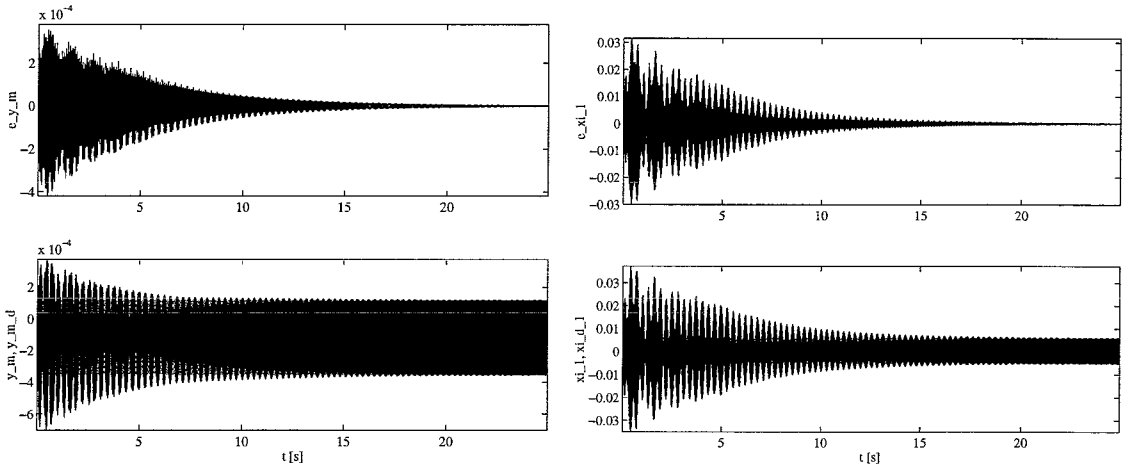

(a) $\hat{e}_{y_m}$ (upper), y_m and $\hat{y}_{m,d}$ (lower).

(b) $\hat{e}_\xi$ (upper), ξ and $\hat{\xi}_d$ (lower).

Figure 2.8: behaviour of the uncontrolled DOFs y_m and ξ, actuator positioned at node 31.

Analysis of the discordant behaviour

This behaviour of the non-linear system does not mean that the stability proof is incorrect. The problem is caused by the way the desired trajectories for the DOFs are described: as the desired trajectory for each DOF is approximated by a truncated Fourier series, the system is controlled to the approximated harmonic solution, represented by desired trajectories $\hat{q}_d$ instead of the real desired trajectories q_d.
The stability proof is based on the assumption that the first part of the control objective has been satisfied. Using the approximated desired trajectories $\hat{q}_d$, this is not exactly true, as is shown in figure 2.9 where the calculated desired trajectory is shown. The left hand side graphs show *both* the solution for the actuator DOF y_a, calculated in `Diana` (with a relative accuracy of 10^{-11}) and the corresponding approximations using the truncated Fourier series of 10 and 20 harmonics respectively. The right hand side graphs show the difference between the two values for both the 10 harmonics (solid) and the 20 harmonics (dotted) case. The absolute difference becomes relatively large for the higher time derivatives. The graphs also show that the benefit from the use of a larger number of harmonics in the approximation of the harmonic solution is rather limited. Despite the significant additional calculation effort that is required as a result of the increased number of harmonics that represent the approximation, there's only little improvement in the accuracy of the approximation. In control simulations the effect of the use of more (than 10) harmonics in the approximation of the desired trajectory has turned out to be negligible (not shown).

Using the equations of motion described by equation 2.17, the effects of the limited accuracy of the approximation can be translated to a vector column of disturbance forces $\underset{\sim}{F}_{res}$:

$$\underline{M}\ddot{\hat{q}}_d + \underline{B}\dot{\hat{q}}_d + \underline{K}\hat{q}_d + \begin{bmatrix} k\hat{y}_{m,d}\,\mathrm{int}\left(\frac{1+\mathrm{sign}(\hat{y}_{m,d})}{2}\right) - F_{ex} \\ 0 \end{bmatrix} = \underset{\sim}{F}_{res}. \tag{2.27}$$

Figure 2.10 shows the residues $F_{res,i}$ during one excitation period.
Figure 2.10(a) shows the residues for the 3 DOF case for approximations $\hat{q}_d$ based on 10

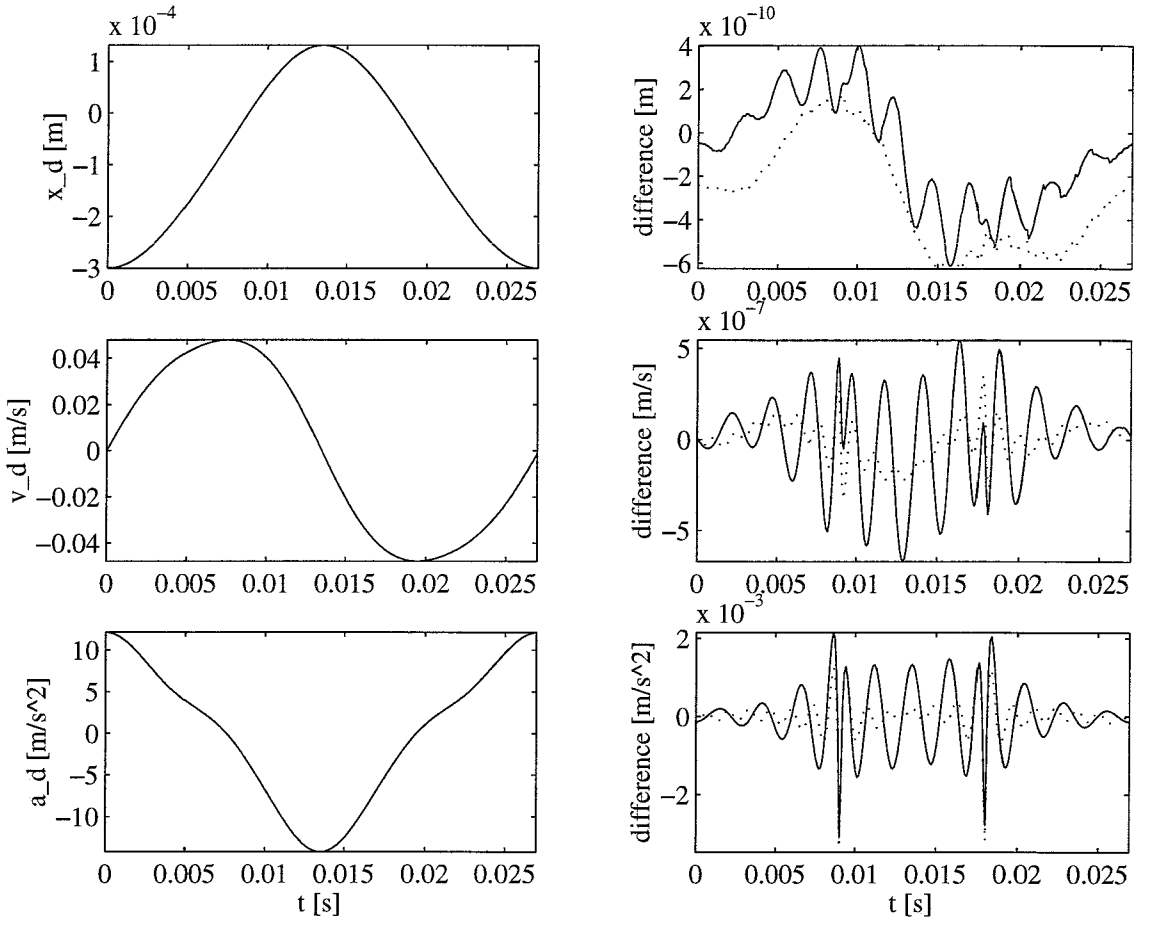

Figure 2.9: example desired trajectory and its approximation for actuator DOF y_a at node 38.

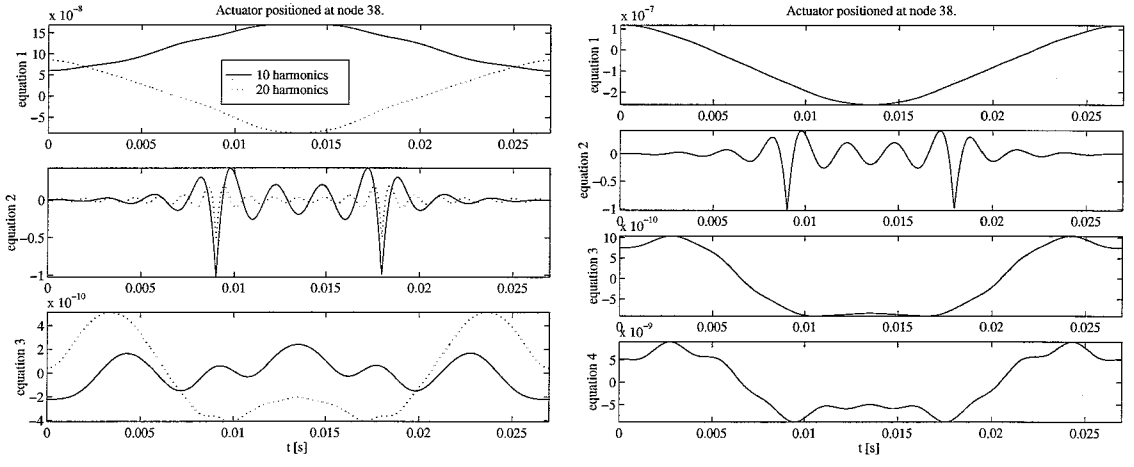

(a) 3 DOF model.

(b) 4 DOF model.

Figure 2.10: equation residues after $\hat{q}_{d,i}$ substitution. Actuator at node 38, $k = 165$ [kN/m].

and 20 harmonics. Figure 2.10(b) shows the residues for the 4 DOF case for approximations $\hat{q}_d$ based on 10 harmonics. The residue in the 2^{nd} equation is dominant in both cases. This must be attributed to the influence of the local non-linearity. When the left hand side plots and the right hand side plots are compared, it shows that the residue in the 2^{nd} equation appears to be insensitive to the number of DOFs in the model. Another interesting notion (not shown) is that the residue in the 2^{nd} equation appears to be very constant for the different models for the different actuator positions x_a. Apparently there's virtually no difference in the combined effects of the approximated solution for each DOF for the different models for the different actuator positions x_a.
The residues can be regarded as a disturbance source. This disturbance source can have a high impact on the system behaviour for some actuator positions x_a under certain conditions. As a result of this disturbance the control effort u will never become *exactly* zero and apparently the uncontrolled DOFs may even be prevented from tracking the harmonic solution $q_{d,i}$ under certain conditions. Instead of attracting the uncontrolled DOFs to the constant solution $\underset{\sim}{0}$ of the zero dynamics, the non-linear zero dynamics may exhibit bifurcations and other kinds of non-linear behaviour, when excited by the disturbance.

The occurrence of such behaviour will be illustrated by means of two examples. Figure 2.11 shows the steady-state course of the estimated tracking errors $\hat{e}_{y_m}$ and $\hat{e}_\xi$ during 6 excitation periods for the case that the actuator is located at node 38 and the continuous time controller is used. The tracking errors of the uncontrolled DOFs don't damp out towards 0, but behave harmonically, i.e. with the same period as the excitation force F_{ex} that causes the vibrations. Because the errors shown in figure 2.11 are a solution of the *approximated* zero dynamics, i.e. the zero dynamics based on $\hat{q}_d$, this illustrates that the disturbance, caused by the approximation of the desired trajectories, sometimes forces the zero dynamics to a solution other than the constant $\underset{\sim}{0}$. In fact, many other solutions may coexist.
A second example illustrates that other behaviour of the uncontrolled DOFs, like subharmonic and chaotic behaviour, is to be expected as well under some circumstances. Figure 2.12 shows the steady-state course of the estimated tracking errors $\hat{e}_{y_m}$ and $\hat{e}_\xi$ during 6 excitation periods for the case that the actuator is located at node 4 and the continuous time controller is used. The uncontrolled DOFs are attracted to a $\frac{1}{3}$ subharmonic solution: during 6 excitation periods the solution exhibits 2 periods.

Similar behaviour occurs for other positions where small or negative damping factors c_2 are found. When using different initial conditions, problems may occur at different positions. As such behaviour severely restricts the applicability of the proposed criterion, the background of this behaviour, i.e. the zero dynamics, must be studied in more detail. Therefore a sensitivity analysis has been performed.

Sensitivity analysis

The sensitivity of the system behaviour for these approximation errors depends on the initial state of the system when the controller is started and on the actuator position x_a, because problems occur for *some* actuator positions for *some* initial states $[\underset{\sim}{q}_0^T \ \dot{\underset{\sim}{q}}_0^T]^T$. System parameters also influence the sensitivity. Therefore the effects of variation of the following system parameters have been investigated:

- Internal (modal) damping in the system.
- Linear stiffness k of the one-sided spring.

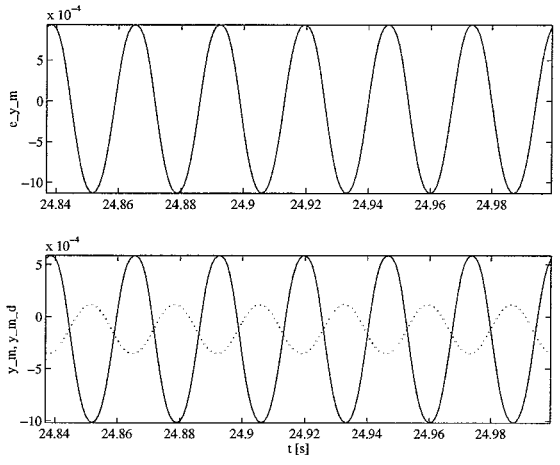

(a) $\hat{e}_{y_m}$ (upper), y_m and $\hat{y}_{m,d}$ (lower).

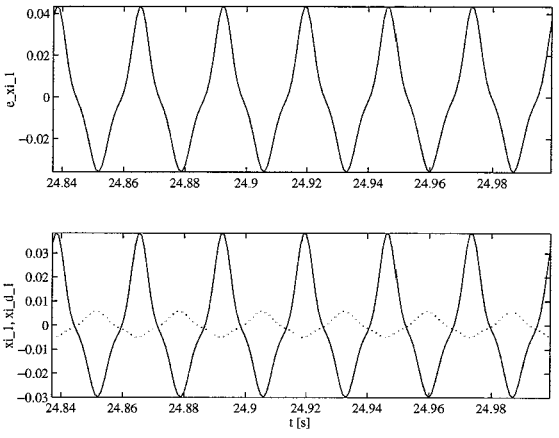

(b) $\hat{e}_\xi$ (upper), ξ and $\hat{\xi}_d$ (lower).

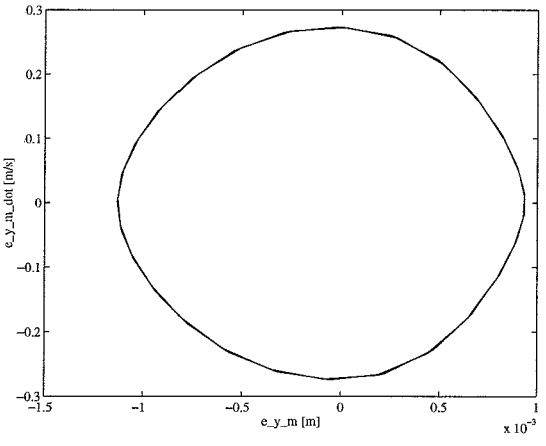

(c) phase plot for $\hat{e}_{y_m}$.

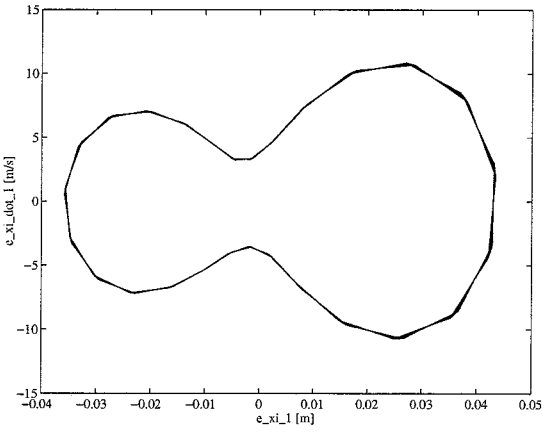

(d) phase plot for $\hat{e}_\xi$.

Figure 2.11: estimated errors $\hat{e}_{y_m}$ and $\hat{e}_\xi$ and corresponding phase plots. k=165 [kN/m], 6 excitation periods at the end of the data-set, actuator positioned at node 38.

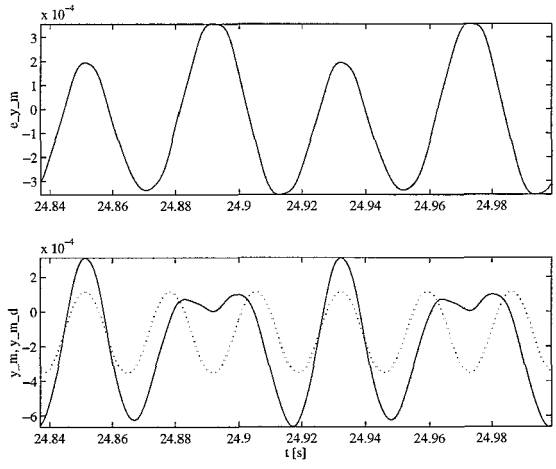

(a) $\hat{e}_{y_m}$ (upper), y_m and $\hat{y}_{m,d}$ (lower).

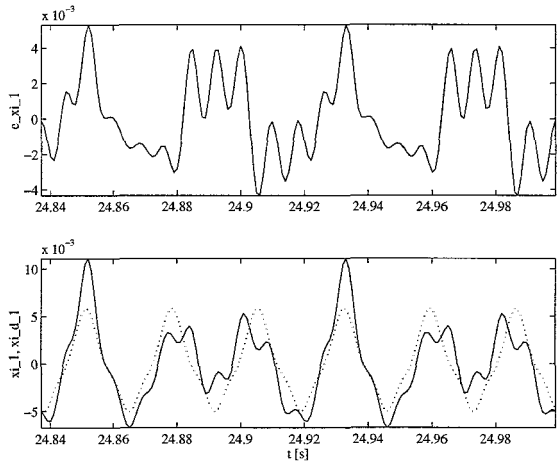

(b) $\hat{e}_\xi$ (upper), ξ and $\hat{\xi}_d$ (lower).

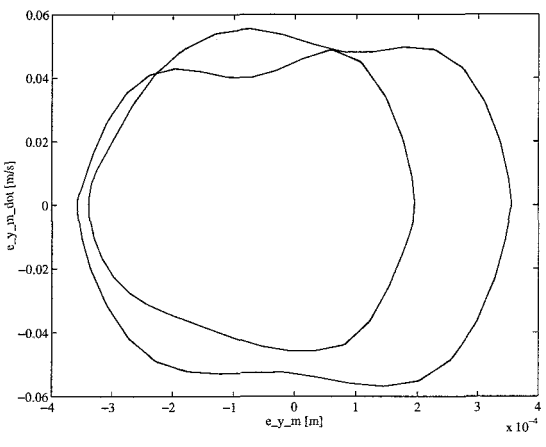

(c) phase plot for $\hat{e}_{y_m}$.

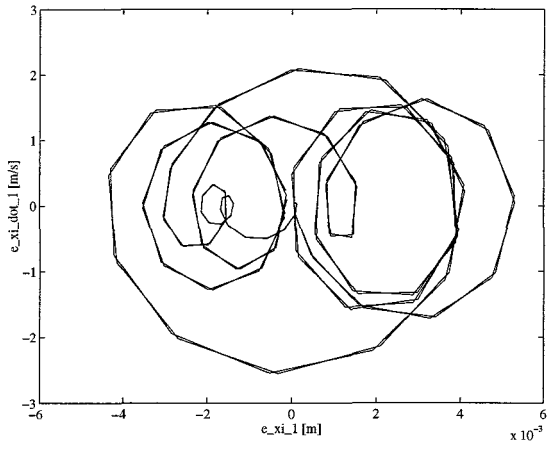

(d) phase plot for $\hat{e}_\xi$.

Figure 2.12: estimated errors $\hat{e}_{y_m}$ and $\hat{e}_\xi$ and corresponding phase plots. k=165 [kN/m], 6 excitation periods at the end of the data-set, actuator positioned at node 4.

- Model size, i.e. the number of (virtual) DOFs in the model.

Only the continuous time controller has been used for this analysis, as then there will not be any unpredictable influence of time discretization of the control effort u.

The internal damping of the system can be adjusted in the models by means of the modal damping. The modal damping ratio has been changed from 0.001 to respectively 0.01, 0.02, 0.03 and 0.04 (for all modes) and new models and corresponding desired trajectories have been determined. The values for the coefficients c_1 and c_2 have been determined with the results of simulations with these models. The envelope fit procedure has turned out to be unable to calculate accurate coefficients c_1 and c_2 for systems with high internal damping due to the fact that the (least squares) fit is unweighted. Therefore only a table that represents the stability problems in a qualitative way has been composed.

damping	**node**																																																															
								1										2										3										4										5										6						
	3	4	5	6	7	8	9	0	1	2	3	4	5	6	7	8	9	0	1	2	3	4	5	6	7	8	9	0	1	2	3	4	5	6	7	8	9	0	1	2	3	4	5	6	7	8	9	0	1	2	3	4	5	6	7	8	9	0	1	2	3	4	5	6
0.001		•	•	•	•	•		•			•	•			•	•	•	•								•				•		•			•	•	•																											
0.01		•	•	•								•																							•	•	•																											
0.02		•																																		•	•																											
0.03		•																																		•																												
0.04																																																																

Table 2.2: indication (•) of actuator positions with stability problems for different damping settings.

In table 2.2 the positions where problems with the stability of the zero dynamics occur, are marked with a bullet (•) (also applies to tables 2.3 and 2.4). Table 2.2 shows that stability problems are suppressed in systems with higher internal damping. This was to be expected, as higher damping settings suppress non-linear effects.

To test the influence of the stiffness k of the one-sided spring, the value of k has been varied. Using values of respectively $k = 0$, $k = 82.5$, $k = 165$ and $k = 330$ [kN/m], new models and corresponding desired trajectories have been determined. The values for the coefficients c_1 and c_2 that have been determined with the results of simulations with these models, are shown in figure 2.13. Figure 2.13 shows that more stability problems occur in systems with higher stiffnesses k of the one-sided spring. No problems occur in the linear case, i.e. $k = 0$ [kN/m]. This was to be expected, as the non-linear effects caused by the one-sided spring become more dominant for higher stiffness settings. Furthermore, in the linear case only one solution of the zero dynamics exists. In table 2.3 the same effects are shown in a qualitative way.

k [kN/m]	**node**																																																															
								1										2										3										4										5										6						
	3	4	5	6	7	8	9	0	1	2	3	4	5	6	7	8	9	0	1	2	3	4	5	6	7	8	9	0	1	2	3	4	5	6	7	8	9	0	1	2	3	4	5	6	7	8	9	0	1	2	3	4	5	6	7	8	9	0	1	2	3	4	5	6
0																																																																
82.5		•		•	•	•										•																						•																										
165		•	•	•	•	•		•			•	•			•	•	•	•								•				•		•			•	•	•																											
330	•		•	•	•	•	•	•			•	•			•	•	•	•	•	•	•			•	•	•	•		•	•	•	•	•	•	•	•	•											•																

Table 2.3: indication (•) of actuator positions with stability problems for different stiffnesses.

To test the influence of the model size, i.e. the total number of DOFs n, the number of virtual DOFs ξ_i in the model has been varied. Using respectively $n = 3$, $n = 4$, $n = 5$ and $n = 8$ DOFs, models and corresponding desired trajectories have been determined. The values for the coefficients c_1 and c_2 that have been determined with the results of

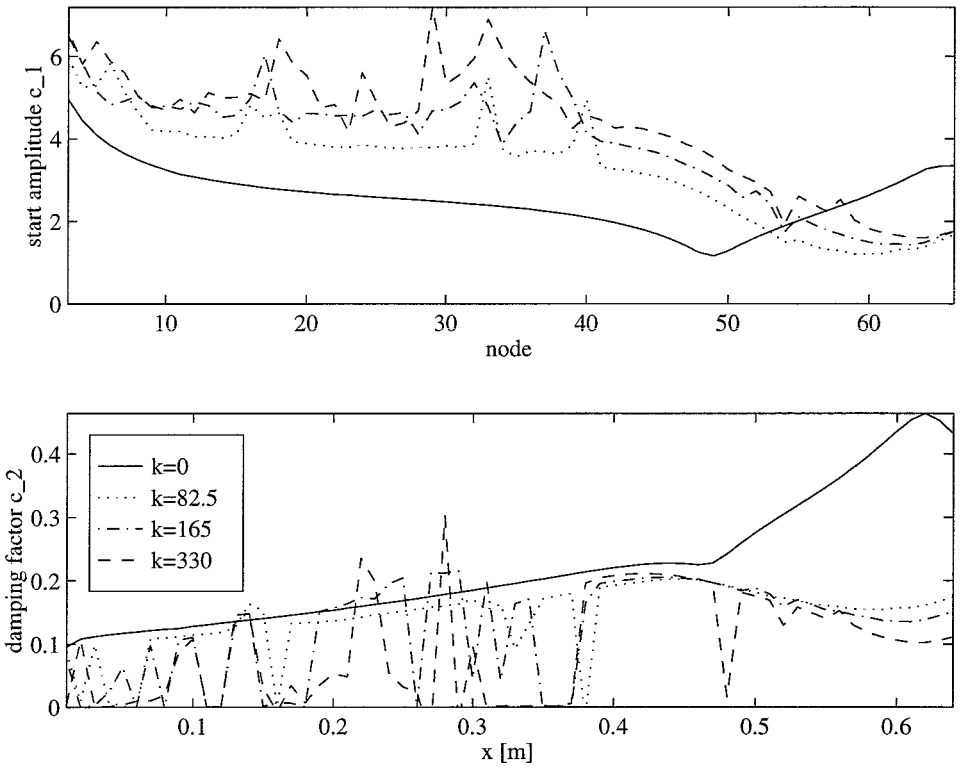

Figure 2.13: behaviour for different stiffness settings as a function of the actuator node (modal damping ratio set to 0.001 for all modes).

simulations with these models, are shown in figure 2.14.
Table 2.4 shows the stability problems in a qualitative way.

DOFs	node
	1 2 3 4 5 6
	3456789012345678901234567890123456789012345678901234567890123456
3	•••••• •• •••• • •• •••
4	•• • • •• • • •••••
5	• • • •• • • • ••••
8	•• • •• • • • • •• •••• • • •• •••

Table 2.4: indication (•) of actuator positions with stability problems for different model sizes.

Increasing the number of DOFs in the model, implies a better model representation of the physical properties of the beam system. However, there is no obvious relation between the quality of the model in terms of physical correctness and the sensitivity of the system for disturbances in the desired trajectories describing the harmonic solution. Such a relation is not expected to be found and is not expressed by figure 2.14 and table 2.4 either. The sensitivity for disturbances in the harmonic solution is determined by the region of attraction of the solution rather than by the correctness of the physical properties described by the model. An explanation for the damping behaviour displayed in figure 2.14 and table 2.4 would therefore require additional research into the behaviour of the zero dynamics. More specifically, (the region of attraction of) coexisting solutions of the zero dynamics should then be investigated. Equation 2.20 shows that the zero dynamics is described by a non-linear system of equations with two non-linearities. The evaluation of this system is therefore far from trivial and would require additional research beyond the scope of the actuator positioning issue alone.

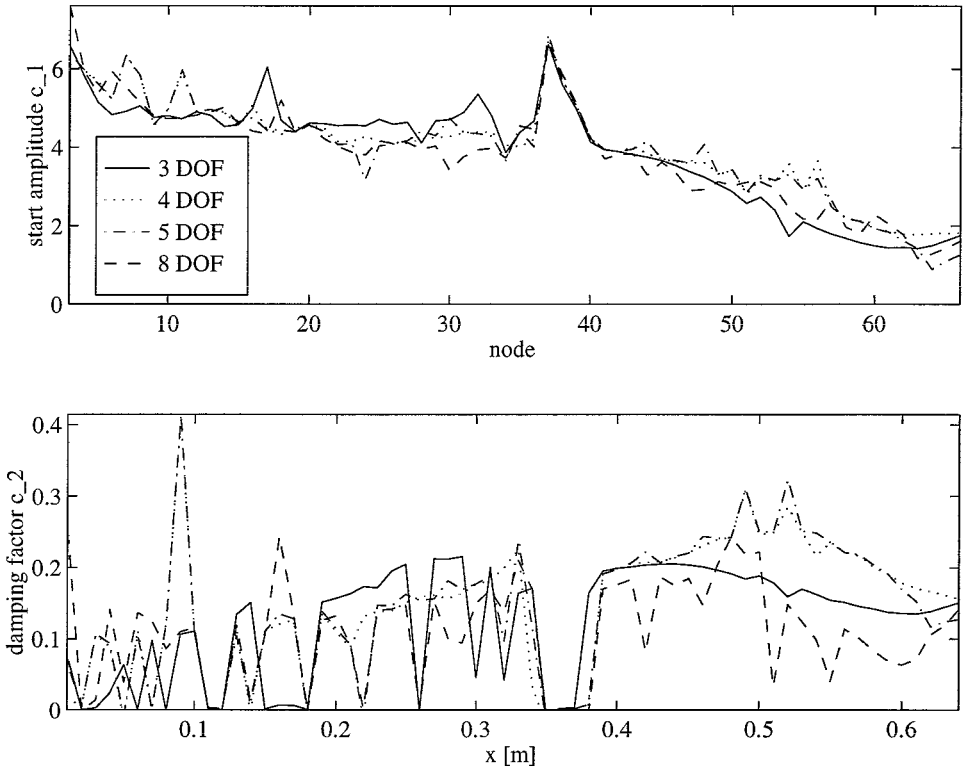

Figure 2.14: behaviour for different model sizes as a function of the actuator node (modal damping ratio set to 0.001 for all modes, stiffness k set to 165 [kN/m]).

2.5.3 Behaviour comparison

When the damping coefficients c_2 that have been found for the linear subsystem and for the complete non-linear beam system are compared, the following can be noticed:

- Node 58 is the best actuator position with regard to the second part of the control objective for the discrete time controllers in both cases.
- The continuous time controller yields no consistent best actuator position with regard to the second part of the control objective.
- The course of the damping behaviour as a function of the actuator position is quite different for the linear case and the non-linear case.

Another remarkable notion in a comparison between the linear subsystem and the complete non-linear beam system is the location of the damped 'eigenfrequencies'. Even though one can't speak of eigenfrequencies in the non-linear case, we can still look for similar peak resonances in the FFTs of the response of the non-linear system. Figure 2.15 shows the lower peak resonances that have been found using results obtained with the zero dynamics simulator.
There's relatively little shift in the peak response frequency as a result of an increased stiffness k of the one-sided spring. Near node 38 the system's lower peak resonance appears to be 'locked' at the excitation frequency $f_e = 37$ [Hz]. This must be attributed to the coexisting harmonic solution of the zero dynamics. The number of nodes where this 'locking' appears, becomes larger for larger values of the stiffness k of the one-sided spring.

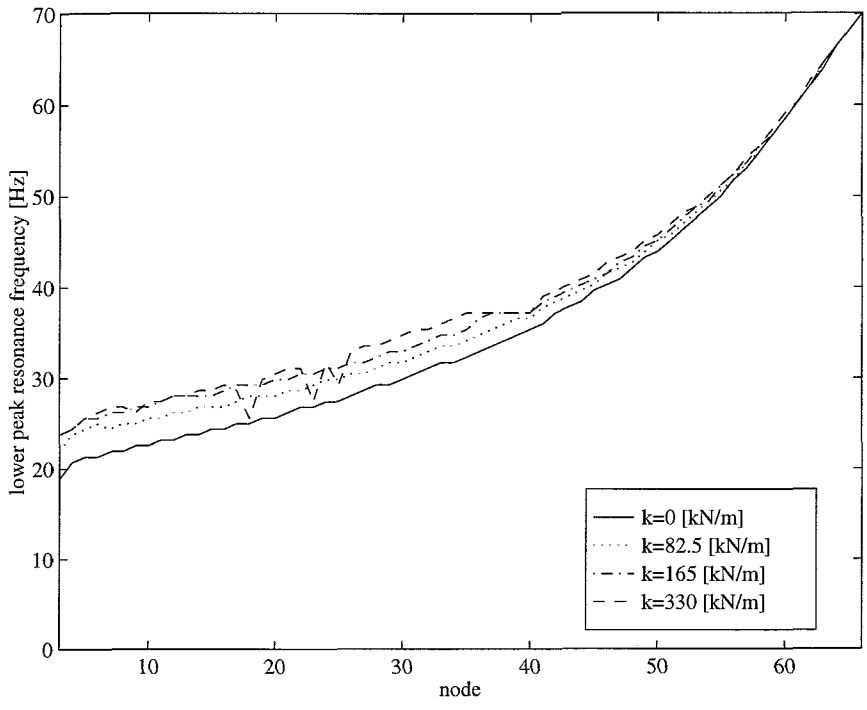

Figure 2.15: lower peak resonances in the zero dynamics of the non-linear system versus the actuator node, for different stiffnesses k.

2.6 Conclusions

From the results of the research into zero dynamics based actuator positioning, the following conclusions can be drawn:

- The stability of the zero dynamics is an interesting measure regarding the evaluation of actuator positions as it can be used to quantify the (damping) behaviour of the uncontrolled DOFs.
- It has, however, proved to be extremely difficult to find a good quantitative measure for the stability, especially for the non-linear system. The currently used measure is too dependent on operating conditions such as sample frequency and initial state of the system while their influence can not properly be accounted for.
- Based on the simulation results for the discrete time controller, which is used in practice, node 58 would be a good actuator position. As, considering the geometry of the experimental set-up, this position is difficult to use, the current position (node 34) is not all that bad after all. Simulations with the continuous time controller have not yielded a consistent good actuator position yet.
- As a result of several disturbance sources such as in the measurements, the generated excitation force F_{ex}, the generated actuator force F_{act}, in the description of the desired trajectories, etcetera, it is very unlikely that it will *ever* be possible to achieve that the system's control effort u will disappear completely.

Chapter 3

Amplifier and actuator dynamics

3.1 Introduction

Besides the choice of the best position of the actuator, the quality of the transfer between the computed control effort u and the actual actuator force F_{act} is also very important for the optimal functioning of the controller in an experimental environment. In the ideal case, the actuator force F_{act} provided by the actuator equals the computed control effort u. However, as mentioned in section 1.2, this transfer had appeared to be far from ideal in practice.

In the past, the actuator dynamics has been modelled with a second order model (see [24, 19]). The used mass-spring-damper actuator model with its current parameter values has turned out to be unsuitable to adequately describe the dynamics of the amplifier/actuator combination (both electronically and mechanically). This observation is the reason for the research into the dynamics of the components that convert the control effort u to an actual actuator force F_{act}. The results of this research are described in this chapter.

Figure 3.1 describes both the components that are used to generate the actuator force F_{act} and their connectivity.

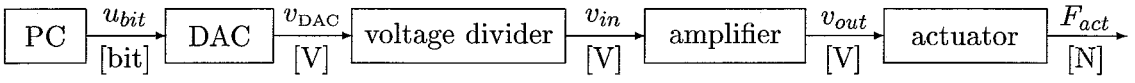

Figure 3.1: block-diagram of the generation of the actuator force F_{act}.

- The PC calculates the required control effort u [N] and presents it to the DA converter (DAC) as a bit value u_{bit} using a (chosen) resolution of 25/2048=0.012 [N/bit].
- The DAC converts the bit value u_{bit} to the voltage v_{DAC} using a fixed resolution of 10/2048 [V/bit].
- To prevent unnecessary loss of resolution in the total transfer as a result of the fixed resolution of the DAC, a voltage divider has been inserted. Thus, an amplification factor can be set through the voltage divider which is based on a potentiometer with maximum resistance $R_{max} = 10$ [kΩ].
- The amplifier, represented by the fourth block, allows a maximum input voltage of approximately 2.1 [V] only. The amplifier has a knob to set the amplification factor. As the only reproducible settings are 'off' and 'max', the setting 'max' is used.

- Finally, as represented by the fifth block, the output voltage v_{out} is translated to the actuator force F_{act} by the actuator, i.e. a shaker.

More details will be provided in the next section.

3.2 The experimental identification set-up

In order to determine the dynamics of the generation of the actuator force F_{act}, an experimental set-up was constructed with the components that are held responsible for the poor quality of the generated actuator force. These components and their signals are represented in figure 3.2. The left out components (see figure 3.1) are presumed to be linear and are not held responsible for the poor quality of the actuator force generation. This means that e.g. the possibility of a frequency dependency of the voltage divider could be investigated separately.

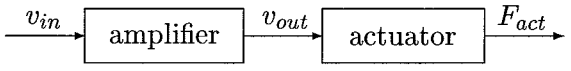

Figure 3.2: block-diagram of components that supposedly reduce the quality of the actuator force.

Thus, the set of components shown in figure 3.2 is presumed to determine the quality of the actuator force generation. It consists of the following interface signals and components:

1. *Input signal.* This is the voltage v_{in}, normally generated by the DA-converter of the IO-board. In the experiments described below the signal generated by the PC together with the 12 bit DA-converter and the voltage divider, has been replaced by a signal that is generated by the measuring system `DIFA` (see [7]).

2. *Amplifier.* The input voltage v_{in} is amplified to an output voltage v_{out}. For the reason explained in the introduction, the amplification factor has been set to 'max' during the experiments.

3. *Actuator.* By means of this device, in this case a shaker, the actuator force F_{act} is generated, based on the current i that runs through a coil as a result of the output voltage v_{out} of the amplifier. As a result of the coil being placed in a permanent magnetic field, a Lorentz force is produced, which is used to generate the actuator force F_{act}.

4. *Output signal.* This is the generated actuator force F_{act}.

A set-up was constructed by means of which the actuator and amplifier dynamics could be determined. This set-up is shown in figure 3.3(a). The set-up is supposed to provide a good approximation of a fixed connection to the world. For parts of the experiments, the connection between the force transducer and the 'world' has been replaced by a connection with a known mass m_{x_i}. Using the sensors indicated in figure 3.3(a), frame accelerations and the actual actuator force F_{act} are measured.

Besides the just mentioned mechanical quantities, the following electrical quantities are also measured: voltage v_{in}, voltage v_{out} and current i. Figure 3.3(b) shows the way these measurements have been carried out. The current i through the actuator has been measured on the grounded side of the actuator, using a 1 [Ω] resistor. The resistive part of the impedance of the actuator is approximately 6,4 [Ω]. This means that the voltage drop

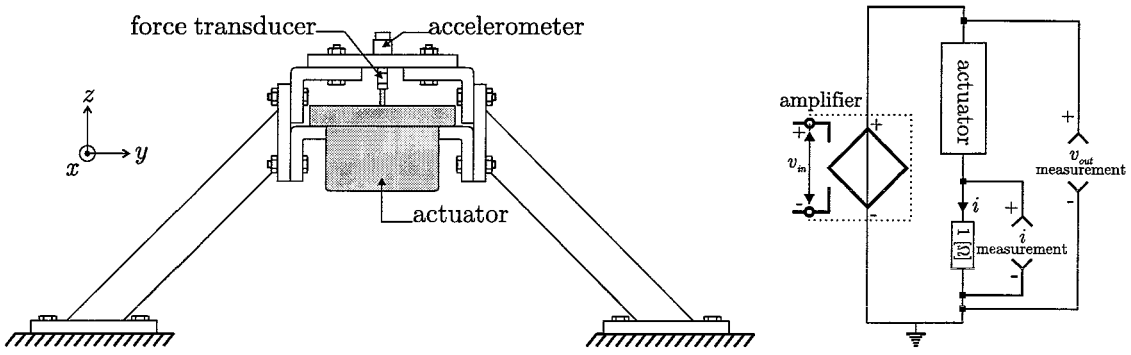

(a) physical design and construction of the set-up.

(b) measurement set-up for electrical quantities.

Figure 3.3: experimental set-up for the determination of amplifier/actuator dynamics.

over the measurement-resistor is *not* negligible. One needs to take this into account when determining a model structure. The reason that this method of measuring the current i is used anyway, is the fact that the measuring system `DIFA` can only measure voltages. Because the minus pole of each connector of `DIFA` is grounded, the current i through the actuator can only be measured on the grounded side. This is also the reason why the voltage drop over the actuator alone could not be determined directly: one will then have to measure both the voltage before the actuator, relative to the ground and the voltage after the actuator, relative to the ground, followed by a subtraction. In table 3.1 a summary of all measured quantities is shown.

channel	measurement	unit
1	F_{act}	[N]
2	$\ddot{z}_a$	[m/s^2]
3	v_{in}	[V]
4	v_{out}	[V]
5	i	[A]

Table 3.1: summary of the measurements.

In order to be able to determine the dynamic behaviour of the amplifier and the actuator, the described set-up has been used to acquire measurements in three load cases. The reason for using three load cases is that some parameters can be estimated only in specific load cases. The used load cases are:

1. Actuator connected to the 'fixed world'.
2. Actuator connected to a mass m_{x_1} of 664.4 [g].
3. Actuator connected to a mass m_{x_2} of 1003.6 [g].

The masses include a mass of 14.0 [g] for the accelerometer. The influence on the dynamics of part of the mass of both the force transducer and the wiring has been presumed to be negligible.

With the help of the measuring system DIFA a zero mean white noise (ZMWN) signal has been provided to the system as an input voltage v_{in}. By means of this signal, transfer functions have been determined under the following circumstances:

- The input voltage v_{in} (channel 3) has been used as a reference signal.
  - The reference voltage of 1 [V], internally generated by the D-TAC 200 (DIFA), is internally amplified with -5 [dB], resulting in the required input voltage v_{in}. The reason why this level has been chosen is that the (small) measurement-resistor (literally) goes up in smoke or at least the resistance value of the resistor fluctuates too much as a result of temperature fluctuations when larger amplification factors are used, as the measurement-resistor can consume only approximately 1 [W].
  - For the measurements with the small mass m_{x_1} and with the large mass m_{x_2} a voltage offset of respectively -0,2 [V] and -0,3 [V] has been added to the input signal v_{in} in order to keep the actuator core from reaching its movement limits under the influence of gravity.
  - The upper limit of the frequency spectrum of the generated ZMWN has been set to the sample frequency f_s during each experiment.
- Only alternating current (AC) components have been measured.
- The frequency response functions (FRFs) have been determined with the help of DIFA's H_1 estimator, i.e. $H_{yx}(f) = \frac{\hat{S}_{xy}(f)}{\hat{S}_{xx}(f)} = \frac{\frac{1}{NT}\sum_{k=1}^{N} \overline{X}_k(T,f)Y_k(T,f)}{\frac{1}{NT}\sum_{k=1}^{N} \overline{X}_k(T,f)X_k(T,f)}$, see [15].
  In the FRF plots in this chapter, the index y in $H_{yx}(f)$ indicates the output channel number. The index x indicates the input channel number.
- 64 realizations of 16384 samples each have been used for the estimation of the transfer functions.
- For the determination of the FFTs *no* use has been made of windows.
- Measurements have been carried out twice: at sample frequencies f_s of 3.2 [kHz] and of 25.6 [kHz].
- The accelerometer has been screwed on a small plate which in turn has been glued to the frame, as a magnetic fixation had proved to be unreliable when the system is excited with frequencies higher than approximately 1 [kHz].

3.3 Dynamics

In this section, models for the dynamics of respectively the amplifier and the actuator will be discussed and their parameters will be estimated.

3.3.1 The amplifier

In the past [24, 19] it has always been assumed that the used amplifier (TPO 25, manufactured by Ling Dynamic Systems) can be regarded as a so-called voltage-current transactor. That is a controlled current source together with its controller, regarded as one component (see [20]). An example of such a transactor is a voltage-current amplifier. The magnitude

of the current i that is generated by the current source then depends on the input voltage v_{in} only. For an ideal voltage-current amplifier, the current i that is to be generated at the output side, can be prescribed regardless of the load and regardless of the frequency spectrum of the input signal v_{in}. The transfer between the input voltage v_{in} on the input side and the current i on the output side can then be described by a constant. Behaviour of the amplifier like a voltage-current amplifier is desirable when a linear relation exists between the generated actuator force F_{act} and the current i through the coil of the actuator.

Concerning the transfer H_{43} between the input voltage v_{in} and the output voltage v_{out} and the transfer H_{53} between the input voltage v_{in} and the current i through the actuator, experiments lead to comparable results in different realizations. In figure 3.4 the transfers H_{43} and H_{53} are shown for the three different load cases. The experiments have been carried out using a sample frequency f_s of 3.2 [kHz].

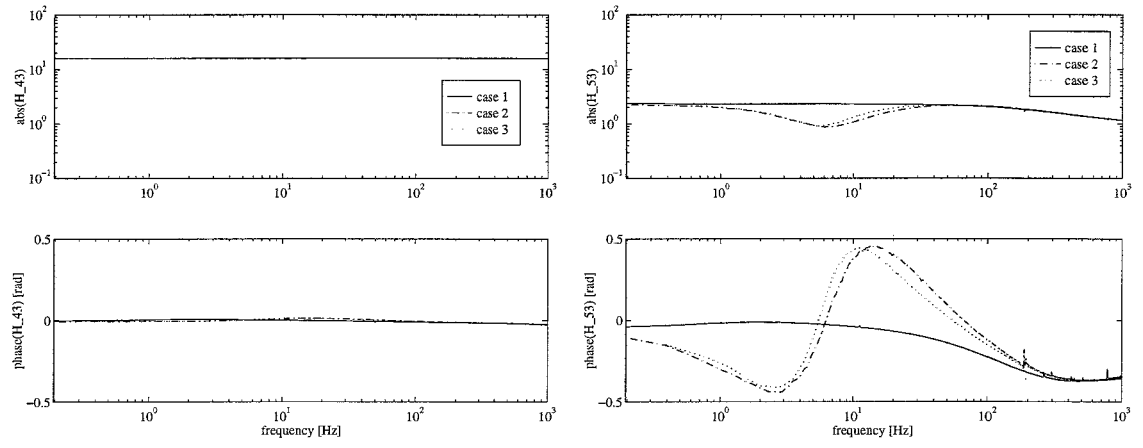

(a) transfer H_{43}, i.e. from v_{in} to v_{out}.

(b) transfer H_{53}, i.e. from v_{in} to i.

Figure 3.4: transfers from input voltage v_{in} to respectively output voltage v_{out} and current i.

Figure 3.4 shows that the transfer H_{53} between the input voltage v_{in} of the amplifier and the actuator current i is quite frequency dependent and therefore load dependent, whereas the transfer H_{43} to the output voltage v_{out} of the amplifier is nearly constant. Also, in the voltage-current transfer the influence of the mechanical dynamics can be clearly noticed: in load cases 2 and 3 a dip in the response occurs in the neighbourhood of 7 [Hz], apparently as a result of the unsuppressed movements of the actuator core, as this dip does not occur in load case 1. The influence of these movements appears in the nett current i through the back EMF[1]. This means that the amplifier should rather be considered to be a voltage-voltage amplifier than a voltage-current amplifier.

As a consequence of the fact that the amplifier should be regarded as a voltage-voltage amplifier, the actuator force F_{act} is *not* proportional to the input voltage v_{in}, even if the force would be proportional to the current i. This is part of the explanation for the poor resemblance between the actuator force F_{act} and the desired control effort u in the experiments that have been carried out in the past. A model of sufficient quality will therefore have to be determined in order to adequately describe the voltage-current transfer of the

[1]EMF = Electro Motorial Force.

actuator. Only then, the input voltage v_{in} can be made proportional to the actuator force F_{act}. As the output voltage v_{out} is sufficiently close to proportional to the input voltage v_{in}, the total transfer between the input voltage v_{in} and the resulting actuator force F_{act} will then be proportional as well.
As appears in figure 3.4(a), the voltage-voltage amplifier is *not* ideal. Therefore, based on the transfer for load case 1, a frequency averaged amplification factor H_{amp} has been determined. This factor H_{amp} is approximately 15.94 [-].

3.3.2 The actuator

The actuator used is a shaker, an electro-mechanical device that generates a force F_{act} as a result of a current i through the actuator. The generated force is the Lorentz force, caused by the current i through a coil, that has been winded on the actuator core and resides in a permanent magnetic field, caused by a permanent magnet with magnetic induction B [T]. In order to apply the resulting actuator force F_{act} to the load, the core is connected to the load as shown in figure 1.3. To restrict the freedom of movement of the core, it is hung up in a package of springs (see [24]). The influence on the generated actuator force F_{act} of the mass of the core and the springs can *not* be neglected. A model for the actuator can therefore be divided into an electrical submodel and a mechanical submodel. These are discussed below.

Electrical submodel

A consequence of the use of a voltage-voltage amplifier is that the electrical components of the actuator determine which model is to be used to describe the current i through the actuator. In the past a model has been proposed (see [24]), represented by equation 3.1. As, at that time, the amplifier had been presumed to be a voltage-current amplifier, the quality of the model has not been evaluated. Therefore, the suitability of this model for the description of the electrical part of the actuator dynamics is tested here.

$$v_{out} = iR_{tot} + L\frac{\mathrm{d}i}{\mathrm{d}t} - Bl\dot{z}_a, \tag{3.1}$$

$$R_{tot} = R_{act} + R_{meas.}. \tag{3.2}$$

The first term of equation 3.1 accounts for the resistive part of the impedance of the actuator R_{act} as well as for the measurement-resistor $R_{meas.}$. The second term accounts for the electrical behaviour of the actuator coil. L [H] represents the self-induction of the coil. The third term accounts for the influence of the back EMF. B [T] is the magnetic induction of the permanent magnetic field, l [m] is the effective length of the coil windings. $\dot{z}_a$ is the speed at which the coil on the core (and therefore the core itself) moves through the magnetic field. The minus sign in front of the term is a result of the orientation of the coil windings in the magnetic field.

To suppress the influence of the back EMF, a transfer function is determined for load case 1, i.e. with the actuator fixed to the 'world'. There is hardly any influence of the back EMF, as the connection between the actuator and the world eliminates the possibility for movement as much as possible. The transfer function has been determined by dividing the data representing the complex transfer functions respectively of the current i through the actuator as a result of the input voltage v_{in} and the output voltage v_{out} as a result of

the input voltage v_{in}:

$$H_{54}(f) = \frac{H_{53}(f)}{H_{43}(f)}.$$

In figure 3.5 the transfer H_{54} between the output voltage v_{out} and the current i through the actuator is represented by a solid line. The sample frequency f_s has been set to 12.8 [kHz] during this experiment.

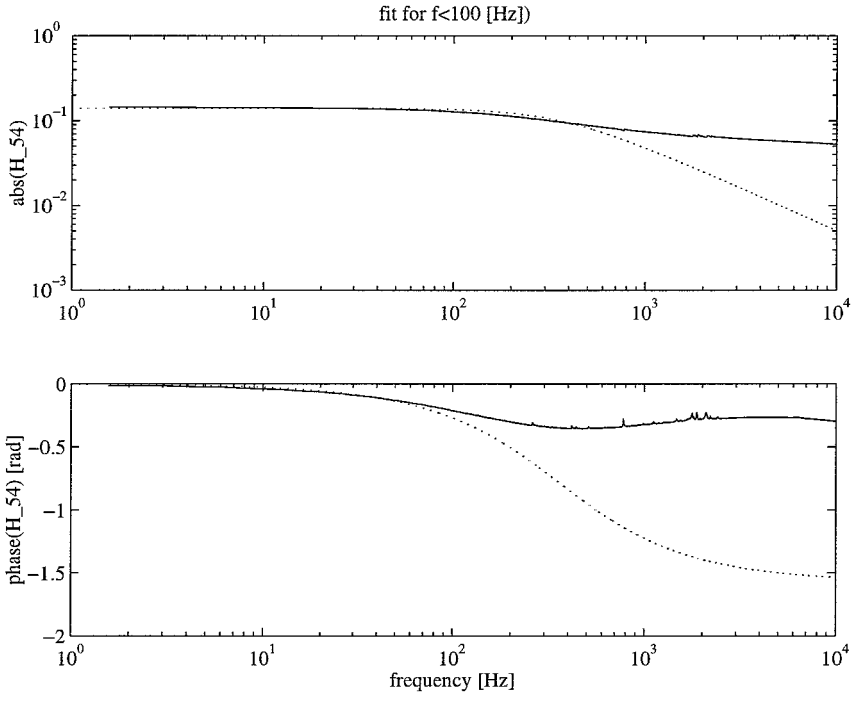

Figure 3.5: transfer from output voltage v_{out} to current i, actuator fixed to the 'world'.

After Laplace transformation of equation 3.1 without the term representing the back EMF, the following 1^{st} order model is found:

$$H_{v_{out}\rightarrow i} = \frac{I(s)}{V_{out}(s)} = \frac{1}{R_{tot} + Ls}. \tag{3.3}$$

In figure 3.5 a dotted line represents an attempt to fit this model to the data for frequencies up to 100 [Hz], as it appeared that a reasonable fit to this 1^{st} order model is possible for frequencies of up to approximately 200 [Hz].
For the fitting procedure, the MATLAB-function `invfreqs` has been used. The used routine, based on this function, can be found in appendix E.2.3. For this fit, quadratic weighting has been used with the minimum weight set at 100 [Hz]. The fit resulted in the following values for the model parameters: R_{tot}=7.1 [Ω] and $L = 3.1 \cdot 10^{-3}$ [H].
A measurement of the resistive part of the impedance R_{act} of the actuator has indicated that this value is approximately 6.4 [Ω], whereas the value is 6.1 [Ω] according to the fit procedure, as $R_{meas.} = 1$ [Ω].

Because of this difference and because the assumed 1^{st} order behaviour of the electrical part of the actuator has not become apparent in the data representing the 'measured' transfer function, the quality of the chosen model should be considered to be insufficient

for frequencies above 200 [Hz]. The model structure itself is the main cause for this: it appears to provide a physically incorrect description of the electro-dynamics. The transfer function shown in figure 3.5, is comparable to figure 3.4(b), as the difference between v_{in} and v_{out} is just the constant factor H_{amp}. When this comparison is made with the transfer functions produced by load cases 2 and 3 where the fixation has been replaced by a known mass, it shows that the approximation of the fixation to the world using the steel profiles is adequate. Therefore, that is *not* to be considered the cause of this behaviour.
Anyway, up to frequencies of approximately 200 [Hz], the description of the dynamics, using this model, can be considered sufficient. However, if the model is accepted, it should be viewed as a 1^{st} order black-box model: the values of the parameters are influenced by unmodelled (electro-)dynamics and apparently do *not* just represent the electrical components defined in the model.

Four ways to deal with the modelling problem are:

1. Replace the voltage-voltage amplifier by a high performance voltage-current amplifier. When such an amplifier is used, the use of a (more) complicated model becomes superfluous. This, however, would be an expensive work-around.

2. Ignore the influence of the back EMF and the influence of the coil and use only the resistive part of the impedance of the actuator to determine a transfer factor instead of a dynamic transfer function. As a matter of fact, that's what has happened so far by assuming that the amplifier is a voltage-current amplifier.

3. Accept the physical incorrectness of the model that provides a good description for frequencies up to 200 [Hz] and use it as a black-box model. Of course, that is expected to limit the adequate description of the dynamic behaviour of the *total* transfer to a frequency of approximately 200 [Hz] at most.

4. Fit a higher order black-box model. When using this approach, the parameters for such a model can not be attributed to properties of physical components. As a result, it will be difficult to devise a suitable parameter identification experiment, because compensation for operating conditions, such as for example the influence of an identification mass m_{x_i}, will be non-trivial.

Mechanical submodel

The actuator force F_{act} should be proportional to the actuator current i under ideal circumstances. In that case, the actuator force is also known, if the model that translates the input voltage v_{in} to the current i through the actuator is adequate. However, as indicated before, the effects of the mechanical components on the realized actuator force F_{act} can not be neglected when using *this* actuator. Therefore, the following mechanical model is used, as proposed by De Vries [24]:

$$F_{act} = -iBl - m_a\ddot{z}_a - b_a\dot{z}_a - k_a z_a. \tag{3.4}$$

The minus sign in front of the first term is a result of the orientation in the magnetic field of the current i through the coil windings. In equation 3.4, m_a, b_a and k_a account for respectively the effective mass, the mechanical damping and the mechanical stiffness of the actuator. z_a is the displacement of the actuator core, i.e. of the connection between the mass and the actuator. The reader should note that, when used in conjunction with the beam with one-sided spring, the displacements are in the y-direction, as the actuator

then is oriented differently.

In order to determine the value of the product Bl, load case 1 is used again. In equation 3.4 the terms in $\dot{z}_a$ and $\ddot{z}_a$ can be neglected, i.e. z_a is a constant, if the amplitude of the input signal is not too high, resulting in:

$$F_{act} \simeq -iBl - k_a z_a. \tag{3.5}$$

The term $k_a z_a$ itself does introduce a static offset, but this offset does not influence the estimation of the product Bl, as only AC components have been measured. Figure 3.6 shows the transfer between the current i through the actuator and the actuator force F_{act}. The data-set has been produced using a sample frequency f_s of 3.2 [kHz]. The figure also shows an unweighted 0^{th} order fit, based on the frequency transfer function data up to 100 [Hz]. The fit is represented by means of a dotted line.

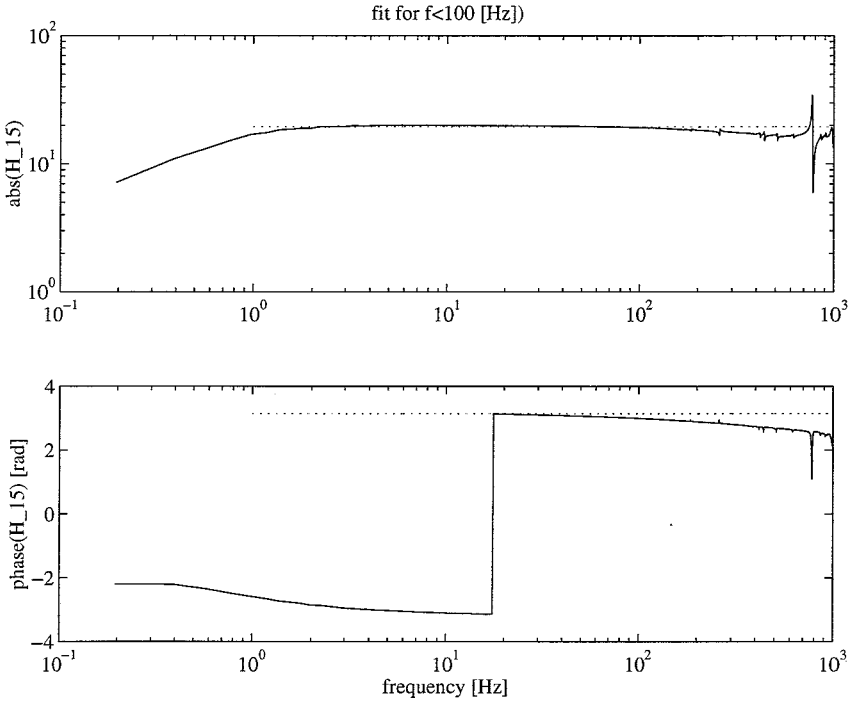

Figure 3.6: transfer from i to F_{act}, actuator fixed to the 'world'.

This behaviour appears to match the behaviour described by equation 3.5 very well. The value of the product Bl is estimated at 19.5 [N/A].

For the determination of the parameters m_a, b_a and k_a the fixation to the world is replaced by a connection to a known mass m_{x_i}, so that $F_{act} = m_{x_i}\ddot{z}_a$, as shown in figure 3.7. Substitution of $F_{act} = m_{x_i}\ddot{z}_a$ in equation 3.4, followed by Laplace transformation, results in the following description for the transfer between the current i through the actuator and the position z_a:

$$H_{i \to z_a} = \frac{Z_a(s)}{I(s)} = \frac{-Bl}{(m_a + m_{x_i})s^2 + b_a s + k_a}. \tag{3.6}$$

However, the acceleration $\ddot{z}_a$ is measured, not the position z_a. Then applies:

$$H_{i \to \ddot{z}_a} = \frac{s^2 Z_a(s)}{I(s)} = \frac{-Bls^2}{(m_a + m_{x_i})s^2 + b_a s + k_a}. \tag{3.7}$$

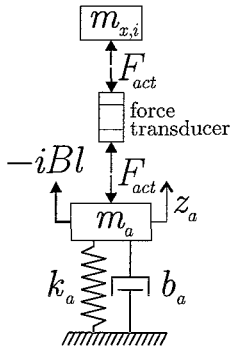

Figure 3.7: representation of the mechanical submodel for load cases 2 and 3.

Thus, the $H_{i\to\ddot{z}_a}$ data that have been acquired with `DIFA` can be transformed to $H_{i\to z_a}$ by dividing the data of $H_{i\to\ddot{z}_a}$ by s^2. In principle, this operation is desirable, because the used fit procedure `invfreqs` does not allow to fit polynomials with constraints for the values of certain coefficients, e.g. a polynomial of degree 2 with its 0^{th} and 1^{st} coefficient set to zero.

By using the measurements for load cases 2 and 3, i.e. with a connection to a known additional mass m_{x_1}, m_{x_2} respectively, the (other) model parameters can be estimated. This can be done in two ways:

1. The value of the product Bl is known already, based on load case 1. If this value is used, the other parameters can be estimated directly, based on the data of *either* load case 2 *or* load case 3. Fits based on these data sets should produce similar parameter values.

2. Based on the data of both load cases 2 and 3. Once measurements have been acquired using the 2 different known masses, the mass m_a and the product Bl can be estimated. Then, b_a and k_a are also known. Of course, the value of the product Bl that is found using these measurements, should equal the value that has been determined using load case 1.

Both methods have been applied in the following. In order to determine the model parameters, a fit has been made in two ways:

1. Fit a numerator polynomial of degree 0, i.e. n_0, together with a denominator polynomial of degree 2, i.e. $d_0s^2 + d_1s + d_2$:

$$H_{fit} = \frac{Z_a(s)}{I(s)} = \frac{n_0}{d_0s^2 + d_1s + d_2}. \tag{3.8}$$

   In the fit procedure, d_0 is scaled to 1, which results in:

$$\frac{Bl}{m_a + m_{x_i}} = \left(\frac{n_0}{d_0}\right)_i \Rightarrow m_a = \frac{Bl}{n_{0_i}} - m_{x_i}. \tag{3.9}$$

2. Fit a numerator polynomial of degree 2, i.e. $n_0s^2 + n_1s + n_2$, together with a denominator polynomial of degree 2, i.e. $d_0s^2 + d_1s + d_2$, to the original transfer function and set coefficients n_1 en n_2 to 0 afterwards:

$$H_{fit} = \frac{Z_a(s)}{I(s)} = \frac{n_0s^2 + n_1s + n_2}{d_0s^2 + d_1s + d_2}. \tag{3.10}$$

In the fit procedure, d_0 is scaled to 1, which results in:

$$\frac{Bl}{m_a + m_{x_i}} = \left(\frac{n_0}{d_0}\right)_i \Rightarrow m_a = \frac{(m_x n_0)_2 - (m_x n_0)_1}{n_{0_1} - n_{0_2}}. \tag{3.11}$$

The minus sign that is present in equation 3.7, has been omitted in these models. This is allowed as the accelerometer indicates an acceleration in positive z-direction as a negative acceleration if the accelerometer is oriented as indicated in figure 3.3(a).

In table 3.2 the values of the coefficients n_0 are indicated for the fits with the different data sets. The data describing the transfer function up to a frequency of 100 [Hz] are used. Lower frequencies have been weighted quadratically higher than the higher frequencies with the minimum weight set at 100 [Hz]. In the first column, the load case and the sample frequency f_s have been indicated. The second column shows the value of n_0 for the originally determined transfer $H_{i\to\ddot{z}_a}$. The third column shows the value of n_0 based on $H_{i\to z_a}$.

data set	$H_{i\to\ddot{z}_a}$	$H_{i\to z_a}$
m_{x_1}, 3k2	25.3007	18.7735
m_{x_1}, 25k	25.2575	27.1383
m_{x_2}, 3k2	17.2716	16.5310
m_{x_2}, 25k	17.2351	19.9437

Table 3.2: values of fitted n_0 for untransformed and transformed transfer.

It needs to be remarked that the coefficients found on the basis of the transformed transfer (3^{rd} column) are very sensitive to the various settings, like for instance the sample frequency. Most likely, the small amplitude of the vibrations is the cause for this behaviour. Therefore, the second method to determine the *polynomial* coefficients was selected, i.e. to fit a transfer function with both the numerator and the denominator polynomials of degree 2 to the original data for $H_{i\to\ddot{z}_a}$, ignoring the results for the values of n_1 and n_2 afterwards.

If we use the previously found value of the product Bl (method 1), then the different data sets yield different values for the effective mass m_a of the actuator: 0.107 and 0.127 [kg]. This suggests that the previously determined value of Bl is not correct. If we use both sets to estimate all parameters (method 2), the following model parameters are found:

parameter	**value**	**unit**
Bl	18.4	[N/A]
m_a	0.065	[kg]
b_a	35	[Ns/m]
k_a	$1.35 \cdot 10^3$	[N/m]

Table 3.3: found parameter values for the mechanical submodel.

Thus, the undamped eigenfrequency of the mechanical submodel of the actuator is approximately 23 [Hz]. It's remarkable that the value for Bl indeed is different than the one determined before. However, it needs to be said that the parameters are very sensitive to small variations in the fitting procedure and the quantity of data to be fitted.

Figures 3.8(a) and 3.8(b) show both the transfer functions $H_{i\to\ddot{z}_a}$ based on the measurements and the fitted transfer functions for respectively load case 2 and load case 3. It can

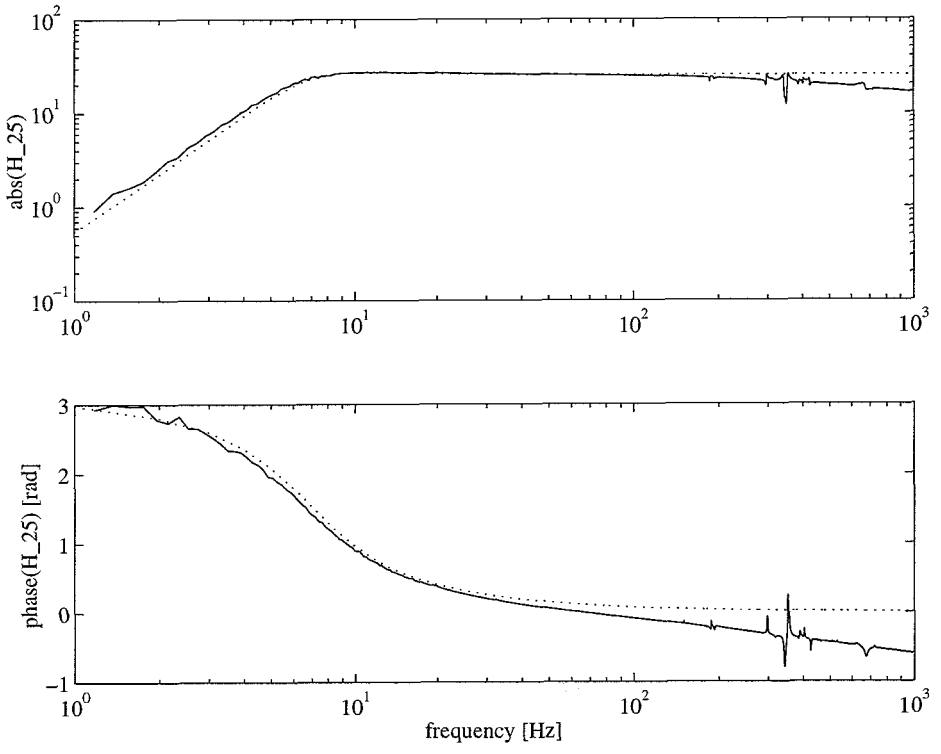

(a) connection with mass m_{x_1}.

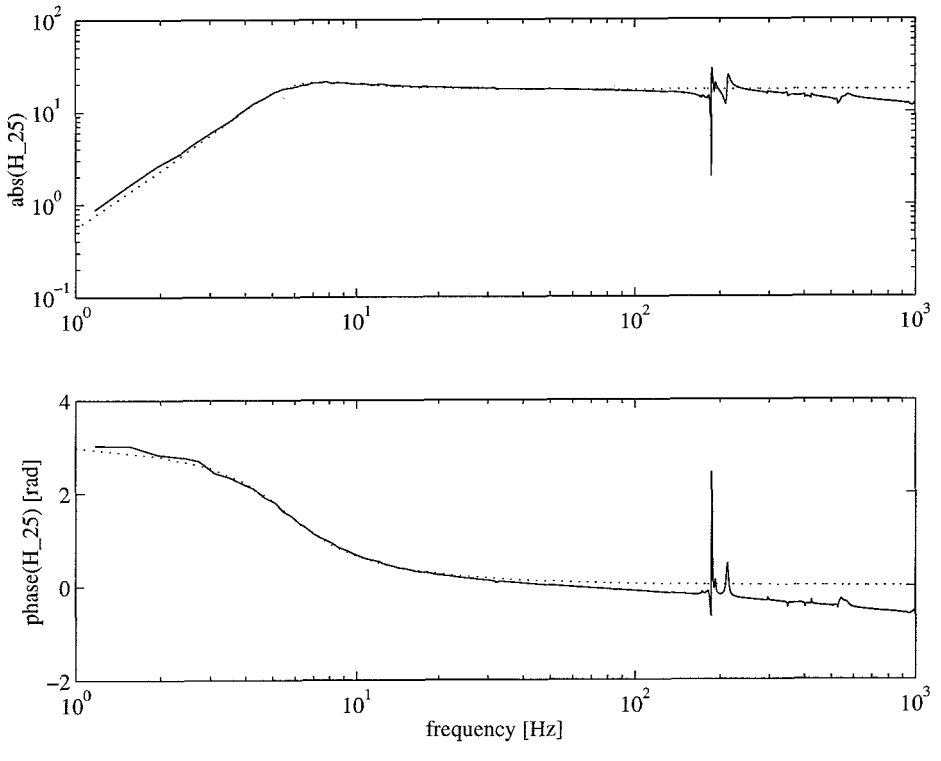

(b) connection with mass m_{x_2}.

Figure 3.8: transfers from i to $\ddot{z}_a$ (solid) and the fitted models (dotted).

be concluded that with the values of the model parameters listed in table 3.3 a fit has been found that provides an adequate description for frequencies up to approximately 200 [Hz]. Ignoring coefficients n_1 and n_2 therefore seems reasonable and the parameters estimated with method 2 are acceptable.

3.3.3 Total transfer function

Now that the parameters for both submodels have been estimated, we can determine the performance of the electrical submodel and the mechanical submodel combined. Substitution of the transfer function describing the transfer between the output voltage v_{out} of the amplifier and the current i through the actuator, given by equation 3.1, in equation 3.4 yields after some reorganization:

$$\xrightarrow[Z_a(s)]{V_{out}(s)} \boxed{F_{act}(s) = \frac{-Bl}{R_{tot}+sL}V_{out}(s) - \left(m_a s^2 + (b_a + \frac{B^2l^2}{R_{tot}+sL})s + k_a\right) Z_a(s)} \xrightarrow{F_{act}(s)}$$

The damping has become frequency dependent. This is caused by the back EMF.

If we look at the situation that the actuator is connected to the known mass m_{x_i} and remember that $H_{amp} = v_{out}/v_{in}$ defines the amplification factor of the amplifier, the total transfer function can be described by the following 3^{rd} order model:

$$H_{v_{in}\to\ddot{z}_a} = \frac{s^2 Z_a(s)}{V_{in}(s)} = \frac{-BlH_{amp}s^2}{(R_{tot}+sL)\left((m_a+m_{x_i})s^2 + (b_a + \frac{B^2l^2}{R_{tot}+sL})s + k_a\right)}. \tag{3.12}$$

Figures 3.9(a) and 3.10(a) show the transfer functions between the input voltage v_{in} and the acceleration $\ddot{z}_a$ for respectively load case 2 and load case 3, i.e. the situation that the force transducer has been connected with respectively a mass m_{x_1} or a mass m_{x_2}. The description provided by the models is even adequate up to frequencies of approximately 500 [Hz] and is still quite acceptable for higher frequencies. The resonance peaks above 1000 [Hz] were caused by the eigenfrequencies of the screw-thread connections, e.g. the connection between the mass and the force transducer.

Thus, it is possible to find a fairly reasonable description for the dynamics of the amplifier/actuator combination. However, in comparison with the previously used description, this description requires additional calculations as a result of the influence of the coil and of the back EMF.

In figure 3.9(b) and 3.10(b) is displayed what the transfer $H_{v_{in}\to\ddot{z}_a}$ looks like if the influence of the back EMF is *not* accounted for, for respectively load case 2 and load case 3. In that case, only the resistor and the coil are modelled. If these figures are compared with figure 3.9(a) and 3.10(a), it becomes apparent that the influence of the back EMF should not be ignored. As expected, it improves the transfer description in the low frequency range.

In figure 3.9(c) and 3.10(c) is indicated what the transfer $H_{v_{in}\to\ddot{z}_a}$ looks like if the entire electro-dynamics are left out, for respectively load case 2 and load case 3. In that case, only the value of the resistor is used. This is what has happened in the past by assuming that the amplifier was a voltage-current amplifier. As has been observed in practice, this description is not adequate. If these figures are compared with figure 3.9(b) and 3.10(b), it becomes apparent that the coil improves the transfer description in the higher frequency range.

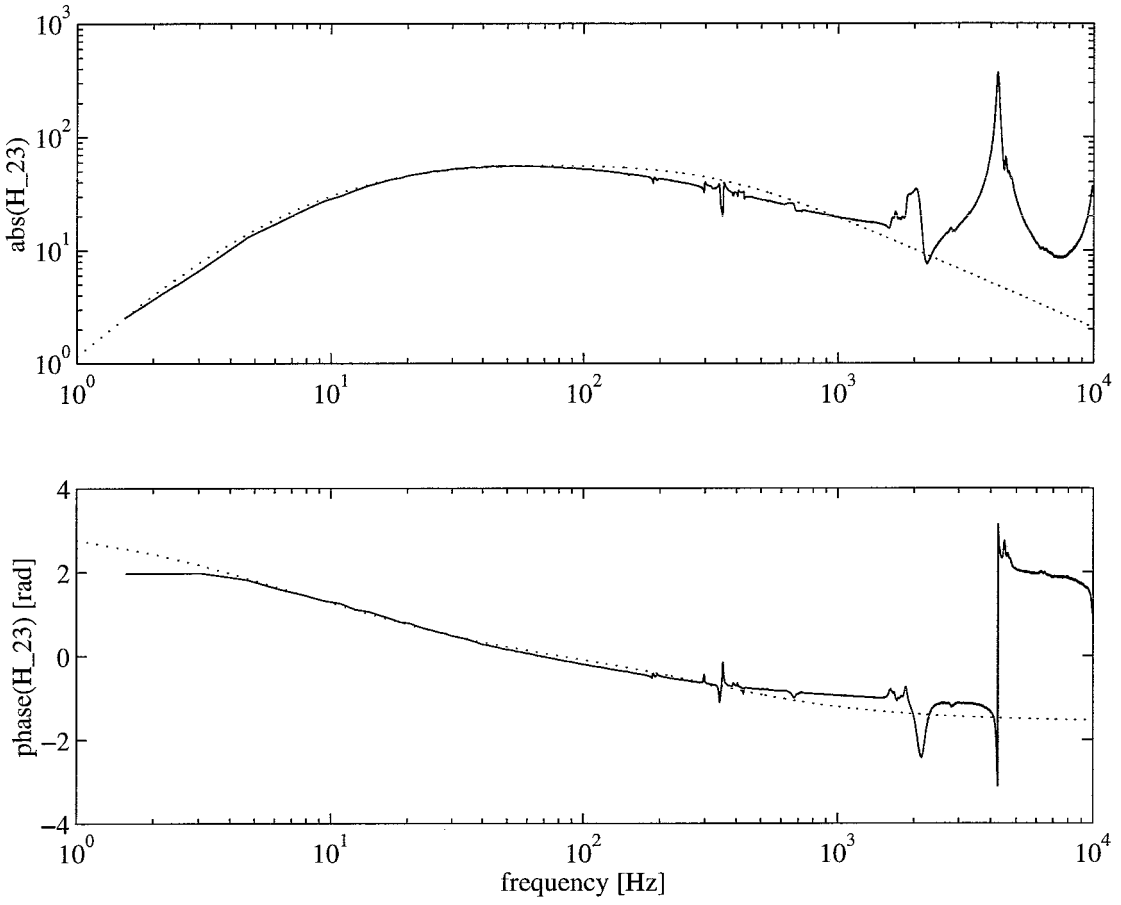

(a) fit using both the mechanical submodel and the complete electrical submodel.

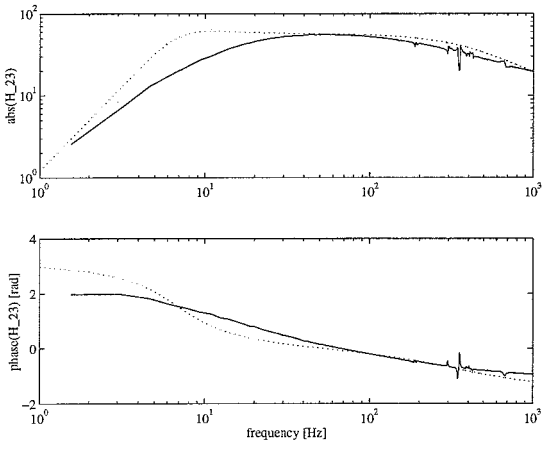

(b) same, but without the back EMF.

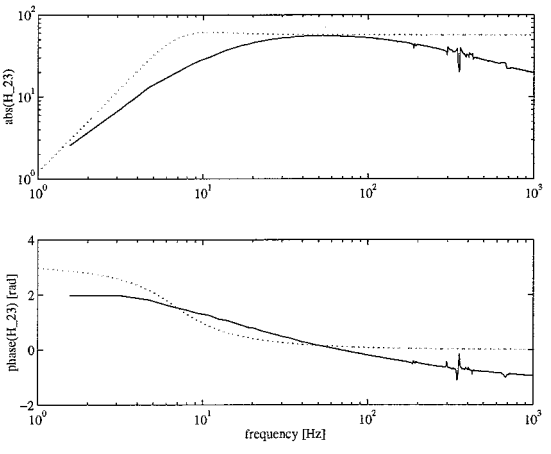

(c) no electro *dynamics* (resistor only).

Figure 3.9: total transfer from v_{in} to $\ddot{z}_a$; connection with mass m_{x_1} (load case 2). (fit=dotted)

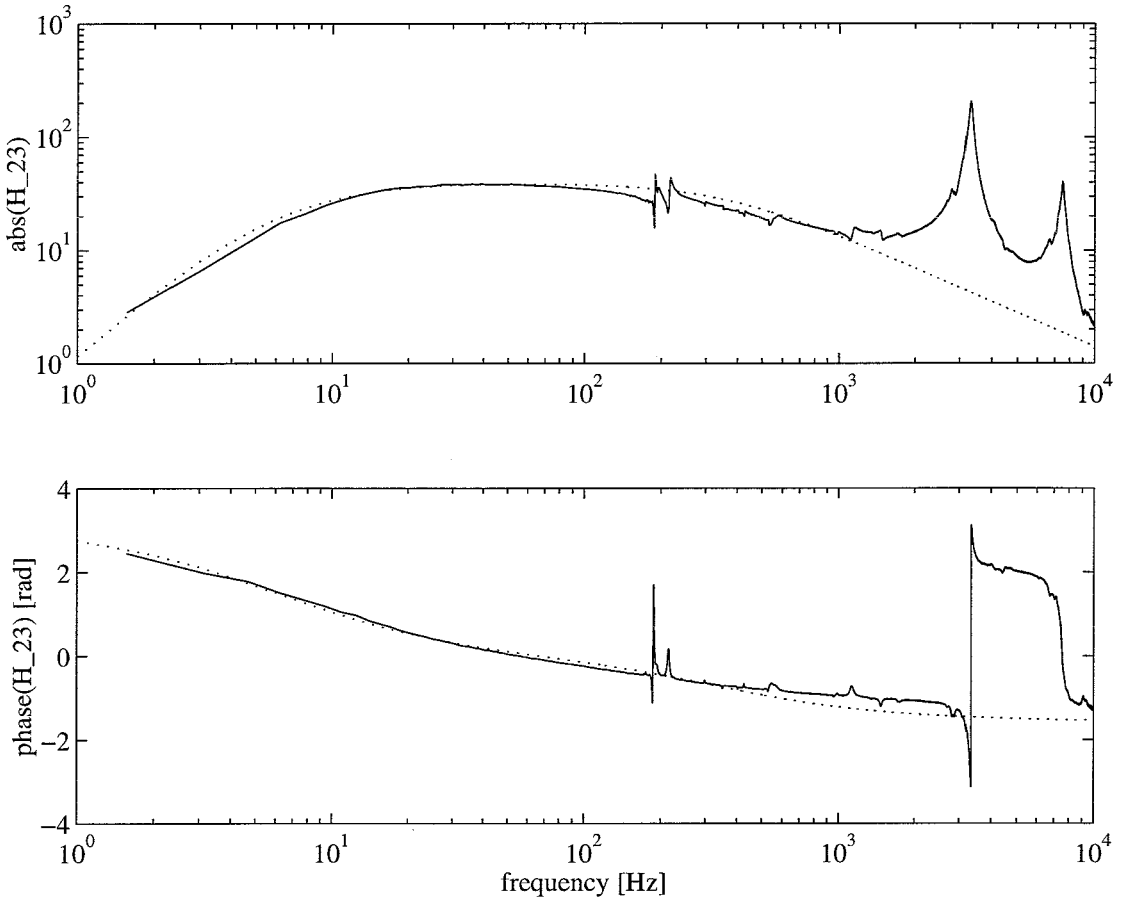

(a) fit using both the mechanical submodel and the complete electrical submodel.

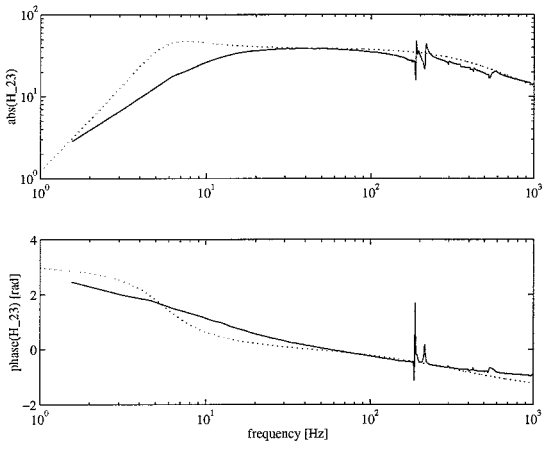

(b) same, but without the back EMF.

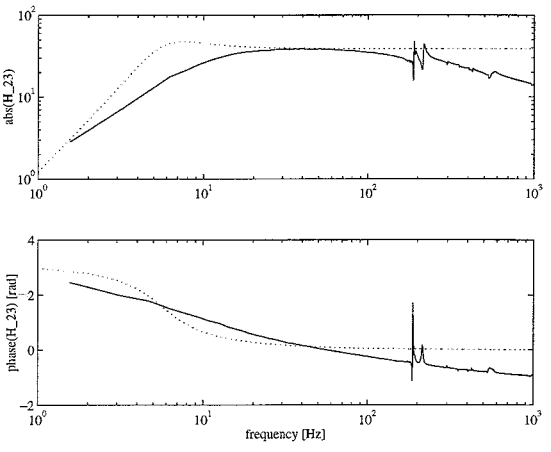

(c) no electro *dynamics* (resistor only).

Figure 3.10: total transfer from v_{in} to $\ddot{z}_a$; connection with mass m_{x_2} (load case 3). (fit=dotted)

3.4 Implementation for the beam with one-sided spring

The discussed model, together with its parameters, has been implemented in the experimental environment of the beam with one-sided spring.

The PC is used to calculate the desired control effort u. Using the inverse of the total transfer function, the desired control effort u is compensated for the combined amplifier/actuator dynamics. This results in a compensated control effort u_{comp} which is sent to the DAC instead of the desired control effort u itself. Figure 3.11 shows the same block diagram as figure 3.1 with some of the transfer factors substituted.

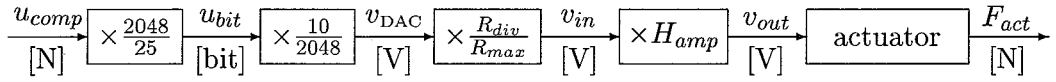

Figure 3.11: block-diagram of the generation of the actuator force; some transfers substituted.

The factor R_{div}/R_{max} requires some additional explanation. This factor is introduced by the voltage divider which is based on a 10 [kΩ] potentiometer. Therefore, $R_{max} = 10$ [kΩ]. By means of the resistance R_{div} the user can change the part of the voltage drop that is supplied to the amplifier as input voltage v_{in}.

As we want the actuator force F_{act} to match the desired control effort u, it follows that:

$$F_{act} = u = -iBl - (m_a\ddot{y}_a + b_a\dot{y}_a + k_a y_a). \tag{3.13}$$

The current i through the actuator required for this actuator force is therefore:

$$i = -\frac{u + m_a\ddot{y}_a + b_a\dot{y}_a + k_a y_a}{Bl}. \tag{3.14}$$

Substitution in equation 3.1 yields the following 3^{rd} order model for the required output voltage v_{out}:

$$v_{out} = -\frac{u + m_a\ddot{y}_a + b_a\dot{y}_a + k_a y_a}{Bl}R + L\frac{d}{dt}\left(-\frac{u + m_a\ddot{y}_a + b_a\dot{y}_a + k_a y_a}{Bl}\right) - Bl\dot{y}_a. \tag{3.15}$$

From the block diagram described by figure 3.11 it follows that F_{act} equals the desired control effort u if the control effort u is compensated to u_{comp} as follows:

$$u_{comp} = v_{out} \times \frac{1}{H_{amp}} \times \frac{R_{max}}{R_{div}} \times \frac{2048}{10} \times \frac{25}{2048} \text{ [N]}. \tag{3.16}$$

This result has been implemented in the C^{++} code for the beam controller using a simple Euler differentiation scheme to perform the differentiation, required for the evaluation of equation 3.15.

The value for R_{div} that must be used during experiments, follows from substitution of the parameter values in the block diagram shown in figure 3.11. If a *constant* control effort u is to be applied, the dynamics can be left out, provided that the actuator core does not move. In that case (apart from the sign) the control effort u should equal u_{comp} due to the absence of dynamics that would otherwise require compensation, resulting in:

$$R_{div} = \frac{R}{Bl} \times \frac{1}{H_{amp}} \times R_{max} \times \frac{2048}{10} \times \frac{25}{2048} = 520 \text{ [Ω]}.$$

3.4.1 Experimental results

The performance of the model and its parameters has been tested by means of two tests.

Experiment with a sine shaped test signal

In this test the one-sided spring has been removed from the beam system and the sample frequency f_s has been set at 2000 [Hz]. The signal that the actuator should produce, was arbitrarily chosen to be a sine shaped actuator force F_{act} with an amplitude of 10 [N] and a frequency of 37 [Hz]. Using respectively the compensation model without (left graph) electro dynamics and with (right graph) electro dynamics, the results displayed in figure 3.12 have been produced. In both cases the new model parameters have been used.

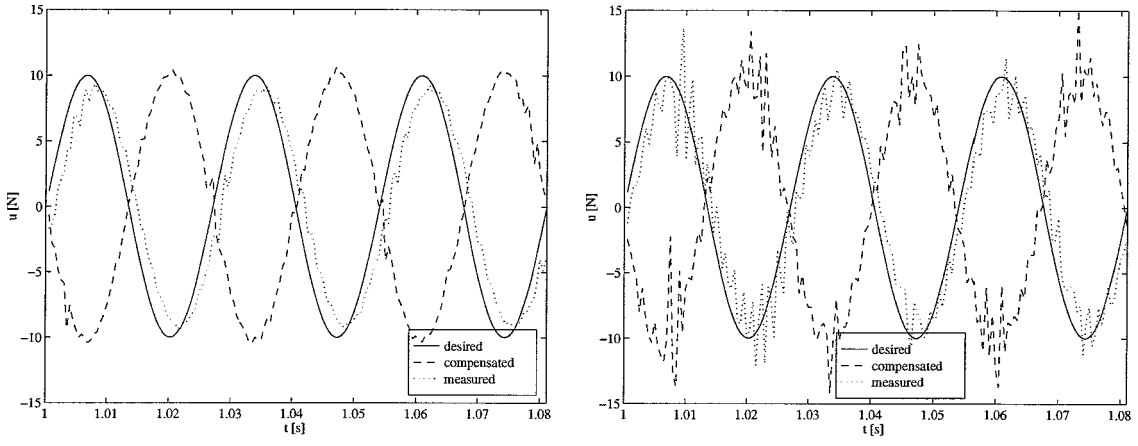

(a) without compensation for electro dynamics.

(b) complete model with Euler scheme.

Figure 3.12: quality of the generation of $u = 10\sin(2\pi f_e t)$, $f_e = 37$ [Hz].

The figures shows the calculated desired force u, the force u_{comp} that has been compensated for actuator/amplifier dynamics and the measured resulting force F_{act}. While there is some improvement in amplitude and phase of the generated force F_{act}, a disturbing noise distorts the generated actuator force F_{act} when the electro dynamics are accounted for. The noise is caused by differentiation, required as a result of the 3^{rd} order compensation model. Apparently the Euler scheme is insufficient to perform adequate numerical differentiation here. Especially the acceleration signals are responsible for this noisy behaviour.

A controller experiment

This experiment has been carried out using the controller discussed in section 2.3. To prevent the noise in the generated actuator force F_{act} when using the complete new model from possibly destabilizing the system, the model without compensation for the electro dynamics has been selected for this experiment instead. The source code (including two new synchronization routines) has been included in appendix E.1.
In the beam model that has been used in this experiment, the linear damper used by [14] (again) has been omitted. A modal damping ratio of 0.05 for each mode has been used to represent the internal damping of the system. Like in the past, the actuator was located at node 34. After synchronizing the desired trajectory for the actuator DOF y_a with the

excitation force F_{ex} the measurements were started. The controller was started after an additional second had elapsed. Figure 3.13 shows the results of the controller experiment.

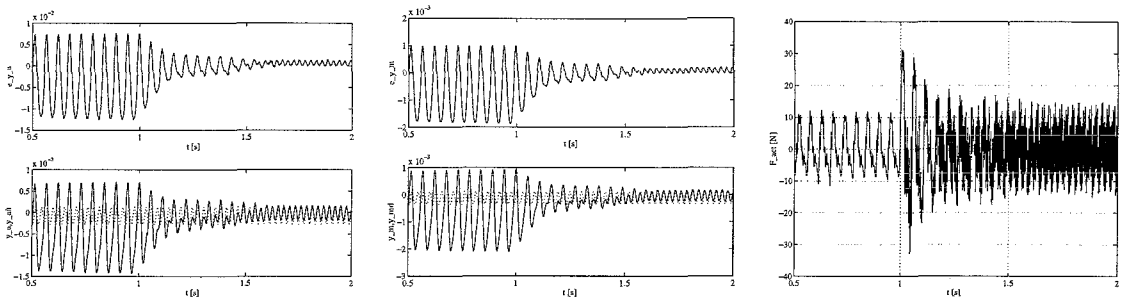

(a) response of 1^{st} DOF, y_a. (b) response of 2^{nd} DOF, y_m. (c) measured actuator force.

Figure 3.13: results of a controller experiment, $f_s = 500$ [Hz].

Figures 3.13(a) and 3.13(b) show that the controller adequately forces the beam system from the $\frac{1}{2}$ subharmonic solution into the harmonic solution. The top graphs show the course of the tracking errors of the interface DOFs. The lower graphs show both the response of the DOF (solid) and their corresponding desired trajectories (dotted).
The required control effort shown in figure 3.13(c) becomes smaller, but quite some effort remains required as a result of several disturbance sources, such as measuring errors, time discretization errors, quantization errors and model errors.
During the 1^{st} second of the experiment, i.e. before the controller is started, the actuator only compensates for its own influence on the beam dynamics. As can be seen in figure 3.13(c) the compensation based on the model without compensation for the electro dynamics is not ideal, as the resulting measured actuator force is not 0 [N].

3.5 Conclusions

- Using a 2^{nd} order model, it is possible to provide an adequate description of the mechanical part of the transfer of the actuator for frequencies up to approximately 200 [Hz].
- Using a resistor-coil-back-EMF model for the transfer between voltage and current in combination with a standard 2^{nd} order mass-spring-damper model for the transfer between the current i and the actuator force F_{act}, the total transfer can be adequately described for frequencies up to approximately 500 [Hz].
- So far, it has not been possible to find a physically interpretable model of the behaviour of the electrical part of the actuator.
- The 3^{rd} order model requires some additional CPU power to perform numerical differentiation in a real-time environment. The 133 [MHz] Pentium based PC can handle this adequately. However, the Euler differentiation scheme, used to perform numerical differentiation in the real-time environment, has proved to be unable to perform the required differentiation adequately.
- Using the new model parameters and synchronization routines, the performance of the controller experiment improves significantly.

Chapter 4

Concluding remarks and recommendations

Concluding this report, it is appropriate to evaluate the results and the research itself.

Conclusions:

Regarding the actuator positioning issue:

- The optimality of an actuator position for the beam with one-sided spring is dominated by the behaviour of the zero dynamics. Therefore, the stability of the zero dynamics can theoretically provide a good basis for an actuator positioning criterion.
- Quantification of this stability has proved to be rather difficult due to the non-linear nature of the considered system. As a measure to quantify the stability of the zero dynamics, an enveloping exponential function has proved to be too sensitive to operating conditions, such as sample frequency f_s and initial conditions. The occurrence of bifurcations and other non-linear effects in the behaviour of the zero dynamics, when excited with a (small) disturbance, further restricts the applicability of the measure.
- Considering the non-linear nature of the system, it is unlikely that an exact (preferably analytical) actuator positioning measure, independent of operating conditions such as initial state and sample frequency f_s, can be found at all.
- For the continuous time controller case, the research has not yielded a *consistent* optimal actuator position x_a with regard to the stability of the zero dynamics yet. For the discrete time controller case, the current actuator position (node 34) has turned out to be not such a bad choice after all, since it exhibits good damping behaviour of the uncontrolled DOFs. The best position would be node 58, but that position is not available as a result of the dimensions of the mass unbalance.
- The behaviour of the zero dynamics shown in this report indicates that the controller is *not* robust after all and contradicts the robustness of the controller claimed by Van De Vorst [23].

Regarding the performance of the amplifier/actuator combination:

- The combined actuator/amplifier model can theoretically provide an adequate description of the actuator/amplifier dynamics for frequencies up to 500 [Hz]. In practice the poor quality of some of the signals (especially the acceleration signals) significantly restrict the usability of the models.

- A new controller experiment has shown that the performance of the controller already benefits greatly from the new model parameters and synchronization routines, i.e. even without compensation for the electro-dynamics. Even though the actuator force F_{act} still does not disappear, it no longer keeps clipping to its minimum/maximum.

Furthermore, the following recommendations can be made:

Recommendations

- Research into the background of the performance improvement as a result of the filter effect, as caused by time discretization of the control effort u.
- Further research into the stability of the zero dynamics. The occurrence of bifurcations and other non-linear behaviour are research inviting features of the non-linear zero dynamics.
- Research into the benefit of multiple actuators. The system is expected to benefit greatly from the use of multiple actuators for two reasons:
  - More DOFs can be controlled towards their approximated desired trajectories $\hat{q}_i$, corresponding to the harmonic solution of the beam with one-sided spring. Thus the region of attraction of solutions of the zero dynamics other than $\underset{\sim}{0}$ is expected to be reduced.
  - The controller will have more influence on the spot in phase space where the zero dynamics will be 'reached'.
- Control performance is expected to benefit greatly from a better physical representation of the linear one-sided spring in the experimental set-up. Currently, the controller is especially (over-)sensitive to the setting of the bolt.
- It would be useful to replace the voltage-voltage amplifier of the experimental set-up with a real voltage-current amplifier. If a description, better than up to 500 [Hz] is required, it is recommendable to replace the entire amplifier/actuator combination by a combination that does not require modelling or can be modelled more easily.

Bibliography

[1] An-Chen, L., Song-Tsuen, C.: *Collocated sensor/actuator positioning and feedback design in the control of flexible structure systems*, Journal of vibration and acoustics, vol. 116, 1994.

[2] Assinck, F.A., *Experimentele verificatie van het steady-state gedrag van een opgelegde balk met een lokale niet-lineaire ondersteuning*, Eindhoven University of Technology, WFW report 93.093 (in Dutch), 1993.

[3] Balas, M.J., *Active control of flexible systems*, Journal of optimization theory and applications, vol. 25, no. 3, 1978.

[4] Barker, D.S., *Spillover minimization in the control of self-adjoint distributed parameter systems*, Journal of astronautical sciences, vol. 34, no. 2, 1986.

[5] Banens, J., *Documentation on TCE modules*, Eindhoven University of Technology, WFW Report 94.050, 1994.

[6] Banens, J., *TCE simulator tools*, Eindhoven University of Technology, WFW Report 94.139, 1994.

[7] Difa Measuring Systems B.V., *DSA 200 Getting started manual*, 1995.

[8] Fey, R.H.B., *Steady-state behaviour of reduced dynamic systems with local nonlinearities*, Ph.D.thesis, ISBN 90-9004680-1, 1991.

[9] Friedland, B., *Advanced Control System Design*, Prentice-Hall, New Jersey, ISBN 0-13-010653-4, 1996.

[10] Gawronski, W., *Balanced control of flexible structures*, Springer Verlag, ISBN 3-540-76017-2, 1996.

[11] Georges, D., *The use of observability and controllability gramians or functions for optimal sensor and actuator location in finite-dimensional systems*, Proceedings of the 34^{th} IEEE conference on decision and control, New Orleans, Lousiana, 1995.

[12] Goeij, M. de, *Experimenten met de vernieuwde meetopstelling voor de opgelegde balk met lokale niet-lineaire ondersteuning*, WFW Report 94.008, 1994.

[13] Jager, A.G. de, Lammerts, I., Veldpaus, F., *Course on Advanced control*, Eindhoven University of Technology, lecture notes 4708 (partially in Dutch).

[14] Kant, A.R., *Stabiliseren van instabiele periodieke oplossingen van niet-lineaire mechanische systemen*, TNO report 95-WEC-R0620 (in Dutch), 1995.

[15] Kraker, A. de, *Numeriek-Experimentele Analyse van Dynamische Systemen*, Eindhoven University of Technology, lecture notes 4668 (in Dutch).

[16] Lammerts, I.M.M., *Adaptive computed reference computed torque control of flexible manipulators*, Ph.D.thesis, Eindhoven University of Technology, ISBN 90-386-0332-0, 1993.

[17] Mucci, P.J., *Active vibration control of a beam subjected to AM or FM disturbances*, Noise control engineering journal, vol. 43, no. 5, 1995.

[18] Kondoh, S., *The positioning of sensors and actuators in the vibration control of flexible systems*, JSME International journal, series III, vol. 33, no. 2, 1990.

[19] Sanders, L.T.A., *Implementatie van een schakelvlakregeling op een balk met enkelzijdige veer*, Eindhoven University of Technology, WFW report 96.033 (in Dutch), 1996.

[20] Schot, J.A. et al., *Inleiding tot de elektrische aandrijftechniek*, Eindhoven University of Technology, lecture notes 5723 (in Dutch), 2^{nd} revised edition, 1989.

[21] Slotine, J.J. E. & Li, W., *Applied nonlinear control*, Prentice-Hall, New Jersey, ISBN 0-13-040890-5, 1991.

[22] Vidyasagar, M., *Nonlinear Systems Analysis*, Prentice-Hall, New Jersey, ISBN 0-13-623463-1, 2^{nd} edition, 1992.

[23] Vorst, E.L.B. van de, *Long term dynamics and stabilization of nonlinear mechanical systems*, Ph.D. thesis, Eindhoven University of Technology, ISBN 90-386-0177-8, 1996.

[24] Vries, A.F. de, *Trillingsregeling voor niet-lineaire mechanische systemen: een experimentele analyse*, Eindhoven University of Technology, WFW report: 95.052 (in Dutch), 1995.

Appendix A

Conditions for asymptotic stability of the zero dynamics

Consider the following linear, time-invariant system with the same number of inputs in $\underset{\sim}{u}$ as the number of outputs in $\underset{\sim}{y}$:

$$\begin{aligned} \dot{\underset{\sim}{x}} &= \underline{A}\underset{\sim}{x} + \underline{B}\underset{\sim}{u}, \\ \underset{\sim}{y} &= \underline{C}\underset{\sim}{x} + \underline{D}\underset{\sim}{u}. \end{aligned} \tag{A.1}$$

The transfer matrix $\underline{H}(j\omega)$ can be written as:

$$\underline{H}(j\omega) = \frac{\underset{\sim}{Y}(j\omega)}{\underset{\sim}{U}(j\omega)} = \underline{C}(j\omega\underline{I} - \underline{A})^{-1}\underline{B} + \underline{D}. \tag{A.2}$$

The Kalman-Yacubovitch theorem (see [9, 21, 22]) states that, under the assumptions that

- $\underline{H}(j\omega)$ is so-called positive real (i.e. even the real part of the smallest eigenvalue of Hermitian matrix $[\underline{H}(j\omega) + \overline{\underline{H}}(j\omega)]$ is positive),
- $\underline{A}$ is Hurwitz (i.e. has all its eigenvalues in the left half-plane),
- the pair $(\underline{A}, \underline{B})$ is controllable,
- the pair $(\underline{C}, \underline{A})$ is observable,

a symmetric positive definite matrix $\underline{P}$, matrices $\underline{Q}$ and $\underline{W}$ and a scalar $\epsilon > 0$ exist, satisfying (see [22]):

$$\begin{aligned} \underline{A}^T\underline{P} + \underline{P}\underline{A} &= -\epsilon\underline{P} - \underline{Q}^T\underline{Q}, \\ \underline{B}^T\underline{P} + \underline{W}^T\underline{Q} &= \underline{C}, \\ \underline{W}^T\underline{W} &= \underline{D} + \underline{D}^T. \end{aligned} \tag{A.3}$$

Assuming that there are $2n$ state equations (n DOFs) and $m < 2n$ inputs and outputs, the dimensions of $\underline{P}$, $\underline{Q}$ and $\underline{W}$ are respectively $2n \times 2n$, $m \times 2n$ and $m \times m$.

The usefulness of this theorem can be demonstrated using a non-linear SISO system. As displayed in figure A.1, the system's transfer function $H(j\omega)$ can be split into a positive real transfer function $F(j\omega)$ and a non-linearity ϕ with a transfer function $\phi()$, producing output value $\phi(y)$.

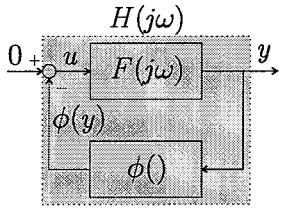

Figure A.1: split up non-linear system (Lur'e problem).

The SISO system can be described as

$$\begin{aligned} \dot{\underset{\sim}{x}} &= \underline{A}\underset{\sim}{x} + \underset{\sim}{b}u, \\ y &= \underset{\sim}{c}^T\underset{\sim}{x}, \\ u &= -\phi(y), \end{aligned} \tag{A.4}$$

where $\underline{A}$ is Hurwitz, $(\underline{A}, \underset{\sim}{b})$ is controllable and $(\underset{\sim}{c}^T, \underline{A})$ is observable.
The scalar transfer function $F(j\omega)$ is defined as:

$$F(j\omega) = \underset{\sim}{c}^T(j\omega\underline{I} - \underline{A})^{-1}\underset{\sim}{b}. \tag{A.5}$$

Application of the Kalman-Yacubovitch theorem yields the following conditions:

$$\underline{A}^T\underline{P} + \underline{P}\underline{A} = -\epsilon\underline{P} - \underset{\sim}{q}\underset{\sim}{q}^T, \ \epsilon > 0 \text{ and } \underset{\sim}{c} = \underline{P}\underset{\sim}{b}. \tag{A.6}$$

The non-linearity ϕ is supposed to be sector-bounded, which means that it lies in the first and third quadrants of the $(y, \phi(y))$ plot, or:

$$0 \leq \frac{\phi(y)}{y} \leq \infty. \tag{A.7}$$

Choosing as a candidate Lyapunov function

$$V = \underset{\sim}{x}^T\underline{P}\underset{\sim}{x}, \tag{A.8}$$

yields

$$\begin{aligned} \dot{V} &= \dot{\underset{\sim}{x}}^T\underline{P}\underset{\sim}{x} + \underset{\sim}{x}^T\underline{P}\dot{\underset{\sim}{x}} \\ &= (\underline{A}\underset{\sim}{x} - \underset{\sim}{b}\phi(y))^T\underline{P}\underset{\sim}{x} + \underset{\sim}{x}^T\underline{P}(\underline{A}\underset{\sim}{x} - \underset{\sim}{b}\phi(y)) \\ &= \underset{\sim}{x}^T(\underline{A}^T\underline{P} + \underline{P}\underline{A})\underset{\sim}{x} - 2\phi(y)\underset{\sim}{b}^T\underline{P}\underset{\sim}{x} \\ &= -\epsilon\underset{\sim}{x}^T\underline{P}\underset{\sim}{x} - \underset{\sim}{x}^T\underset{\sim}{q}\underset{\sim}{q}^T\underset{\sim}{x} - 2\phi(y)y. \end{aligned} \tag{A.9}$$

This means that for a non-linear system with a sector-bounded non-linearity and a positive-real transfer function, global asymptotic stability can be proved. However, systems with positive-real linear subsystems are seldom met in practice. In other words, the Nyquist diagram seldom remains to the right of the imaginary axis. However, it does often remain right of a vertical line located at $\Re[F(j\omega)] = -\frac{1}{k}$ in the left half-plane. If this is the case, a transformed positive-real transfer function $F_t(j\omega)$ can be created via a summation known as loop transformation:

$$F_t(j\omega) = F(j\omega) + \frac{1}{k}. \tag{A.10}$$

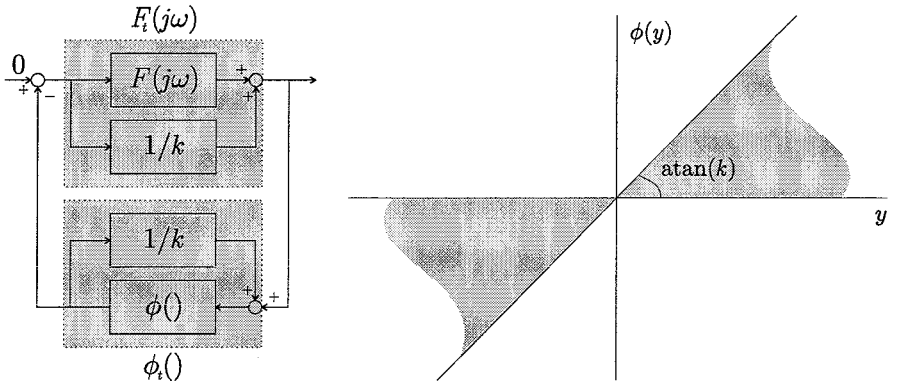

(a) block diagram. (b) resulting sector condition for $\phi(y)$.

Figure A.2: loop transformation.

The resulting transformed non-linearity ϕ_t again has to belong to the sector $[0, \infty)$. Figure A.2(a) shows that $\phi_t()$ can be written as

$$\phi_t() = \frac{\phi()}{1 - \frac{1}{k}\phi()}, \tag{A.11}$$

where the non-linearity ϕ has to satisfy the following sector condition, see figure A.2(b):

$$0 \leq \frac{\phi(y)}{y} \leq k. \tag{A.12}$$

Thus, a sufficient condition for the stability of the non-linear system is obtained when the Nyquist diagram of the linear part remains to the right of the vertical line through $(-\frac{1}{k}, 0)$. A drawback of this method is that its applicability is very limited, as it requires that the imaginary part of the complex transfer function is 0 at the frequency where the minimum real part occurs and this need not be the case. *Popov's criterion* can be used to overcome this problem. It states:

- Suppose $\underline{A}$ is Hurwitz,
- the pair ($\underline{A}$,$\underline{B}$) is controllable,
- the pair ($\underline{C}$,$\underline{A}$) is observable,
- the non-linearity ϕ belongs to the sector (0,∞),

then the system (equation A.4) is globally asymptotically stable if there exist a number $r > 0$ such that:

$$\forall \omega \geq 0,\ \Re[(1 + jr\omega)F(j\omega)] \geq \varepsilon,\ \varepsilon > 0. \tag{A.13}$$

The proof of this theorem can be obtained using the Kalman-Yacubovitch theorem, see also [22]. Equation A.13 can be written as:

$$\forall \omega \geq 0,\ \Re[G(j\omega)] \geq \varepsilon, \tag{A.14}$$

where:

$$\begin{aligned} G(j\omega) &= (1+jr\omega)F(j\omega) \\ &= (1+jr\omega)\underline{c}^T(j\omega\underline{I}-\underline{A})^{-1}\underline{b} \\ &= \underline{c}^T(j\omega\underline{I}-\underline{A})^{-1}\underline{b} + r\underline{c}^T(j\omega\underline{I}-\underline{A}+\underline{A})(j\omega\underline{I}-\underline{A})^{-1}\underline{b} \\ &= \underline{c}^T(j\omega\underline{I}-\underline{A})^{-1}\underline{b} + r\underline{c}^T(j\omega\underline{I}-\underline{A})(j\omega\underline{I}-\underline{A})^{-1}\underline{b} + r\underline{c}^T\underline{A}(j\omega\underline{I}-\underline{A})^{-1}\underline{b} \\ &= \underline{c}^T(j\omega\underline{I}-\underline{A})^{-1}\underline{b} + r\underline{c}^T\underline{b} + r\underline{c}^T\underline{A}(j\omega\underline{I}-\underline{A})^{-1}\underline{b} \\ &= r\underline{c}^T\underline{b} + \underline{c}^T(\underline{I}+r\underline{A})(j\omega\underline{I}-\underline{A})^{-1}\underline{b}. \end{aligned} \tag{A.15}$$

Applying the Kalman-Yacubovitch theorem for the transfer function $G(j\omega)$ yields:

$$\begin{aligned} \underline{A}^T\underline{P} + \underline{P}\underline{A} &= -\epsilon\underline{P} - \underline{q}\underline{q}^T, \\ \underline{b}^T\underline{P} + w\underline{q}^T &= \underline{c}^T(\underline{I}+r\underline{A}), \\ w^2 &= 2r\underline{c}^T\underline{b}. \end{aligned} \tag{A.16}$$

Choose the following candidate Lyapunov function:

$$V(\underline{x}) = \underline{x}^T\underline{P}\underline{x} + 2r\psi(y), \tag{A.17}$$

with:

$$\psi(y) = \int_0^y \phi(\sigma)d\sigma, \psi(y) \geq 0. \tag{A.18}$$

The derivative of $V(\underline{x})$ can then be written as:

$$\begin{aligned} \dot{V}(\underline{x}) &= \dot{\underline{x}}^T\underline{P}\underline{x} + \underline{x}^T\underline{P}\dot{\underline{x}} + 2r\phi(y)\dot{y} \\ &= (\underline{A}\underline{x} - \underline{b}\phi(y))^T\underline{P}\underline{x} + \underline{x}^T\underline{P}(\underline{A}\underline{x} - \underline{b}\phi(y)) + 2r\phi(y)\underline{c}^T(\underline{A}\underline{x} - \underline{b}\phi(y)) \\ &= \underline{x}^T(\underline{A}^T\underline{P} + \underline{P}\underline{A})\underline{x} - 2\phi(y)\underline{b}^T\underline{P}\underline{x} + 2r\phi(y)\underline{c}^T\underline{A}\underline{x} - 2r\underline{c}^T\underline{b}\phi^2(y) \\ &= -\epsilon\underline{x}^T\underline{P}\underline{x} - \underline{x}^T\underline{q}\underline{q}^T\underline{x} - 2\phi(y)(\underline{c}^T(\underline{I}+r\underline{A}) - w\underline{q}^T)\underline{x} + 2r\phi(y)\underline{c}^T\underline{A}\underline{x} - 2r\underline{c}^T\underline{b}\phi^2(y) \\ &= -\epsilon\underline{x}^T\underline{P}\underline{x} - \underline{x}^T\underline{q}\underline{q}^T\underline{x} + 2w\phi(y)\underline{q}^T\underline{x} - 2r\underline{c}^T\underline{b}\phi^2(y) - 2\phi(y)\underline{c}^T\underline{x} \\ &= -\epsilon\underline{x}^T\underline{P}\underline{x} - \underline{x}^T\underline{q}\underline{q}^T\underline{x} + 2w\phi(y)\underline{q}^T\underline{x} - w^2\phi(y)^2 - 2\phi(y)y \\ &= -\epsilon\underline{x}^T\underline{P}\underline{x} - (\underline{q}^T\underline{x} - w\phi(y))^2 - 2\phi(y)y, \end{aligned} \tag{A.19}$$

which is negative definite. A more constrained version of Popov's criterion for the usage of sector-bounded non-linearities with an upper-bound, can be given by:

$$\forall\omega \geq 0,\ \Re[(1+jr\omega)F(j\omega)] + \frac{1}{k} \geq \varepsilon,\ \varepsilon > 0, \tag{A.20}$$

where the non-linear element ϕ has to belong to the sector $(0,k)$. The proof for this criterion can be obtained in the same way as the proof obtained with the former version, described by equation A.13. This can be seen when equation A.20 is transformed by means of a loop transformation:

$$\forall\omega \geq 0,\ \Re[(1+jr\omega)F_t(j\omega)] \geq \varepsilon,\ \varepsilon > 0. \tag{A.21}$$

The non-linear element ϕ has to belong to the sector $(0,k)$, see equations A.10, A.11 and A.12. The graphical representation of Popov's criterion is known as the Popov plot, i.e. a plot in which the real part of $F(j\omega)$ versus ω times the imaginary part of $F(j\omega)$ is drawn. Equation A.20 implies that the plot should stay to the right of a straight line through the point $(-\frac{1}{k}, 0)$ with slope $\frac{1}{r}$.

Appendix B

Description of the new simulators

Three simulators have been developed in order to find a quantitative measure for the stability of the zero dynamics in a control experiment:

1. A discrete time controller simulator.
2. A continuous time controller simulator.
3. A zero dynamics simulator.

Each simulator has been implemented in C^{++} using the TCE toolbox (see [5] and [6]). This toolbox has been developed within the Systems and Control section and is used more and more, because of the following features:

- Simulations run faster in the C^{++} environment than in the native MATLAB V4.x environment.
- The toolbox provides extensive and fast matrix manipulations that can even be used in a real-time (experimental) environment.
- It can provide output in MATLAB format. This facilitates post processing of the data.
- If written properly, the discrete time simulator can be used in conjunction with the real-time interface without any additional programming.
- It has a very good built-in integration routine, based on the Runge Kutta integration scheme with variable stepsize and combined with a discontinuity handler. Needless to say that these features have been very useful for the beam with one-sided spring.
- It has been ported to ANSI (TCE $V1.2\beta$) for the occasion. As a result, it also runs on the (usually faster) Unix boxes and on Windows NT.

Using the previously developed simulator as a basis (see [19]), the three mentioned simulators have been developed. Technical details behind the development of the simulators are left out; only aspects that are directly relevant for the results will be discussed briefly.

The following adaptations have been made to the original simulator (see [19]):

- The simulators provide the full state of the system. One ought to realize that this is not possible in an experimental set-up, as virtual DOFs can not be measured. Even though it's possible to reconstruct the full system state, the state is exported

by the simulator to the controller as if it were possible to measure it, in order to eliminate the influence of reconstruction errors. As a result, the new simulators can *not* directly be used in the experimental set-up.

- The absolute value of the control effort u is no longer clipped to a maximum force of 20 [N].
- In the continuous time implementation the sample frequency f_s is used only to determine the points in time where the state, input, etcetera are to be reported. The controller force is evaluated as if an analog (i.e. continous time) controller has been used. The controller source code has therefore been moved to the simulator source code in the continuous time case.
- In the zero dynamics simulator the sample frequency f_s is used to determine the frequency range for the FFTs. The number of recorded samples determines the 'resolution' of the frequency axis of the FFTs. The state vector column $\underset{\sim}{x}$ is defined by the tracking errors $\underset{\sim}{e}$ and their time derivates instead of by the DOFs themselves. As follows from equation 2.20, the system exhibits two discontinuities in this case, one of which is state independent and depends only on the time t, as it is caused by the sign of the desired trajectory $y_{m,d}$.

In order to reduce the length of this report, the source code for the simulators has *not* been included.

B.1 Operating conditions

- Unless stated otherwise, the controller is started immediately, at $t = 0$ [s].
- When using the discrete time controller or the continuous time controller, the system starts from its resting position. This means that the initial conditions of the system are set to $\underset{\sim}{q}_0 = \dot{\underset{\sim}{q}}_0 = \underset{\sim}{0}$.
- When the discrete time controller is used, a sample frequency f_s is required. It has been set to $f_s = 9990$ [Hz], because $9990 = 270 \times f_e$. This allows the use of time series for the desired trajectories without additional interpolation.

Appendix C

Value tables of numerical results

C.1 Coefficients c_1 and c_2

node	c_1	c_2	node	c_1	c_2
3	5.01	0.4964	35	2.494	1.667
4	4.651	0.7783	36	2.548	1.707
5	4.313	0.8721	37	2.507	1.683
6	4.086	0.9436	38	2.575	1.727
7	3.883	0.9829	39	2.629	1.743
8	3.725	1.027	40	2.604	1.704
9	3.584	1.059	41	2.667	1.703
10	3.468	1.094	42	2.661	1.635
11	3.385	1.141	43	2.619	1.536
12	3.311	1.181	44	2.559	1.416
13	3.175	1.179	45	2.419	1.262
14	3.116	1.212	46	2.221	1.12
15	3.062	1.25	47	1.941	1.021
16	3.001	1.276	48	1.53	1.017
17	2.874	1.265	49	1.114	1.133
18	2.897	1.333	50	1.693	0.9998
19	2.869	1.37	51	2.084	1.071
20	2.712	1.339	52	2.369	1.241
21	2.728	1.392	53	2.581	1.475
22	2.719	1.433	54	2.711	1.718
23	2.653	1.441	55	2.72	1.892
24	2.686	1.502	56	2.699	2.021
25	2.686	1.539	57	2.606	2.07
26	2.596	1.521	58	2.513	2.081
27	2.625	1.57	59	2.399	2.061
28	2.62	1.6	60	2.301	2.037
29	2.602	1.614	61	2.145	1.966
30	2.591	1.637	62	2.089	1.918
31	2.58	1.655	63	1.945	1.793
32	2.562	1.658	64	1.642	1.549
33	2.53	1.663	65	1.156	1.218
34	2.498	1.661	66	0.7173	1.134

Table C.1: coefficients c_1 and c_2 for $k = 0$ [kN/m], *discrete* time controller.

node	c_1	c_2	node	c_1	c_2
3	4.953	0.09575	35	2.328	0.1957
4	4.454	0.108	36	2.294	0.1995
5	4.096	0.1119	37	2.245	0.2028
6	3.844	0.1148	38	2.208	0.2067
7	3.648	0.1171	39	2.157	0.2103
8	3.49	0.1192	40	2.101	0.2138
9	3.361	0.1214	41	2.041	0.2173
10	3.25	0.1234	42	1.971	0.2204
11	3.139	0.1247	43	1.889	0.2231
12	3.081	0.1281	44	1.801	0.2257
13	3.014	0.1305	45	1.694	0.2273
14	2.959	0.1331	46	1.566	0.2277
15	2.907	0.1356	47	1.415	0.227
16	2.863	0.1382	48	1.245	0.2251
17	2.817	0.1405	49	1.159	0.2277
18	2.779	0.1431	50	1.28	0.2423
19	2.746	0.1457	51	1.45	0.2596
20	2.714	0.1483	52	1.612	0.2758
21	2.687	0.1511	53	1.754	0.2907
22	2.651	0.1534	54	1.886	0.3048
23	2.637	0.1569	55	2.01	0.3188
24	2.611	0.1597	56	2.134	0.3328
25	2.587	0.1626	57	2.256	0.3473
26	2.565	0.1656	58	2.37	0.3622
27	2.543	0.1687	59	2.498	0.3791
28	2.521	0.1719	60	2.631	0.3967
29	2.498	0.1751	61	2.775	0.4157
30	2.475	0.1785	62	2.931	0.4353
31	2.446	0.1815	63	3.099	0.4532
32	2.418	0.185	64	3.268	0.4635
33	2.392	0.1887	65	3.337	0.4526
34	2.362	0.1922	66	3.349	0.4323

Table C.2: coefficients c_1 and c_2 for $k = 0$ [kN/m], *continuous* time controller.

node	c_1	c_2	node	c_1	c_2
3	6.606	1.057	35	4.405	1.048
4	6.029	0.0755	36	4.694	1.262
5	4.449	-0.3819	37	4.485	-0.5316
6	5.192	0.6852	38	4.388	-0.9179
7	5.088	0.9201	39	4.215	-0.6178
8	5.03	1.02	40	3.679	-0.3023
9	4.869	0.9759	41	4.059	1.114
10	4.69	1.045	42	3.904	1.037
11	4.751	1.079	43	3.945	1.124
12	4.781	1.096	44	3.871	1.11
13	4.848	1.099	45	3.766	1.05
14	4.627	-0.1015	46	3.705	1.083
15	4.422	-0.08793	47	3.501	0.999
16	4.999	1.438	48	3.509	1.104
17	5.633	1.442	49	3.38	1.083
18	5.331	1.561	50	3.306	1.109
19	4.902	1.505	51	3.208	1.117
20	4.901	1.356	52	3.233	1.255
21	4.611	1.417	53	3.313	1.235
22	4.559	1.422	54	3.392	1.588
23	4.537	1.413	55	3.231	1.543
24	4.634	1.46	56	3.087	1.555
25	4.624	1.494	57	2.972	1.618
26	4.636	1.545	58	2.924	1.748
27	4.619	1.611	59	2.562	1.551
28	4.719	1.634	60	2.4	1.536
29	4.73	1.619	61	2.078	1.411
30	4.768	1.618	62	1.255	1.108
31	5.056	1.723	63	1.628	1.276
32	5.021	1.384	64	1.15	0.9847
33	5.043	1.58	65	0.9375	0.8803
34	4.411	1.078	66	0.3	0.5679

Table C.3: coefficients c_1 and c_2 for $k = 165$ [kN/m], *discrete* time controller.

node	c_1	c_2	node	c_1	c_2
3	6.589	0.07422	35	4.389	0.1639
4	5.837	0.0002517	36	4.672	0.1712
5	5.15	0.002899	37	6.626	-0.006156
6	4.826	0.02368	38	5.598	0.002304
7	4.916	0.06341	39	4.972	0.000205
8	5.051	0.000704	40	4.137	0.1647
9	4.758	0.09754	41	3.939	0.1953
10	4.801	-0.0005021	42	3.894	0.199
11	4.725	0.1062	43	3.814	0.2011
12	4.899	0.1106	44	3.749	0.2038
13	4.814	0.001278	45	3.665	0.205
14	4.529	0.000366	46	3.54	0.2053
15	4.572	0.1342	47	3.379	0.2037
16	4.984	0.1511	48	3.245	0.2012
17	6.039	0.001503	49	3.059	0.1966
18	4.686	0.006734	50	2.871	0.1916
19	4.403	0.00648	51	2.575	0.1842
20	4.62	0.0006822	52	2.734	0.1883
21	4.607	0.1517	53	2.399	0.179
22	4.557	0.1569	54	1.734	0.1594
23	4.572	0.1636	55	2.107	0.1701
24	4.547	0.1736	56	1.93	0.1626
25	4.713	0.1715	57	1.791	0.1542
26	4.588	0.1953	58	1.683	0.1514
27	4.639	0.2046	59	1.571	0.1457
28	4.115	-0.001629	60	1.49	0.1421
29	4.678	0.2122	61	1.441	0.1374
30	4.707	0.2122	62	1.452	0.1359
31	4.896	0.2156	63	1.421	0.1352
32	5.358	0.04536	64	1.494	0.1385
33	4.792	0.2002	65	1.623	0.1447
34	3.863	0.04211	66	1.757	0.1508

Table C.4: coefficients c_1 and c_2 for $k = 165$ [kN/m], *continuous* time controller.

C.2 Eigenvalues of matrix $\underline{A}$

node	eigenvalues of $\underline{A}$		node	eigenvalues of $\underline{A}$	
3	$-0.09 \pm 118.95j$	$-0.80 \pm 803.30j$	35	$-0.16 \pm 204.17j$	$-0.66 \pm 703.79j$
4	$-0.10 \pm 129.46j$	$-0.77 \pm 776.03j$	36	$-0.16 \pm 207.76j$	$-0.67 \pm 711.14j$
5	$-0.10 \pm 133.16j$	$-0.75 \pm 763.20j$	37	$-0.17 \pm 211.49j$	$-0.68 \pm 719.11j$
6	$-0.10 \pm 135.49j$	$-0.74 \pm 754.61j$	38	$-0.17 \pm 215.35j$	$-0.69 \pm 727.63j$
7	$-0.10 \pm 137.41j$	$-0.73 \pm 747.40j$	39	$-0.18 \pm 219.36j$	$-0.71 \pm 736.58j$
8	$-0.11 \pm 139.20j$	$-0.73 \pm 740.74j$	40	$-0.18 \pm 223.54j$	$-0.72 \pm 745.85j$
9	$-0.11 \pm 140.94j$	$-0.72 \pm 734.34j$	41	$-0.18 \pm 227.88j$	$-0.73 \pm 755.25j$
10	$-0.11 \pm 142.68j$	$-0.71 \pm 728.12j$	42	$-0.19 \pm 232.40j$	$-0.75 \pm 764.59j$
11	$-0.11 \pm 144.44j$	$-0.70 \pm 722.06j$	43	$-0.19 \pm 237.12j$	$-0.76 \pm 773.64j$
12	$-0.11 \pm 146.23j$	$-0.69 \pm 716.15j$	44	$-0.20 \pm 242.05j$	$-0.77 \pm 782.11j$
13	$-0.11 \pm 148.05j$	$-0.69 \pm 710.43j$	45	$-0.20 \pm 247.20j$	$-0.78 \pm 789.71j$
14	$-0.11 \pm 149.92j$	$-0.68 \pm 704.94j$	46	$-0.21 \pm 252.58j$	$-0.79 \pm 796.11j$
15	$-0.11 \pm 151.83j$	$-0.67 \pm 699.70j$	47	$-0.21 \pm 258.23j$	$-0.80 \pm 800.96j$
16	$-0.12 \pm 153.80j$	$-0.67 \pm 694.77j$	48	$-0.22 \pm 264.15j$	$-0.80 \pm 803.95j$
17	$-0.12 \pm 155.81j$	$-0.66 \pm 690.17j$	49	$-0.23 \pm 270.37j$	$-0.80 \pm 804.78j$
18	$-0.12 \pm 157.88j$	$-0.65 \pm 685.95j$	50	$-0.23 \pm 276.91j$	$-0.80 \pm 803.19j$
19	$-0.12 \pm 160.01j$	$-0.65 \pm 682.15j$	51	$-0.24 \pm 283.80j$	$-0.80 \pm 799.03j$
20	$-0.12 \pm 162.20j$	$-0.64 \pm 678.81j$	52	$-0.25 \pm 291.06j$	$-0.79 \pm 792.22j$
21	$-0.12 \pm 164.45j$	$-0.64 \pm 675.96j$	53	$-0.26 \pm 298.72j$	$-0.77 \pm 782.78j$
22	$-0.13 \pm 166.76j$	$-0.64 \pm 673.64j$	54	$-0.27 \pm 306.81j$	$-0.75 \pm 770.85j$
23	$-0.13 \pm 169.15j$	$-0.63 \pm 671.88j$	55	$-0.27 \pm 315.37j$	$-0.73 \pm 756.65j$
24	$-0.13 \pm 171.60j$	$-0.63 \pm 670.71j$	56	$-0.28 \pm 324.42j$	$-0.71 \pm 740.49j$
25	$-0.13 \pm 174.12j$	$-0.63 \pm 670.17j$	57	$-0.29 \pm 334.02j$	$-0.68 \pm 722.71j$
26	$-0.13 \pm 176.72j$	$-0.63 \pm 670.28j$	58	$-0.31 \pm 344.18j$	$-0.65 \pm 703.72j$
27	$-0.14 \pm 179.40j$	$-0.63 \pm 671.08j$	59	$-0.32 \pm 354.95j$	$-0.62 \pm 683.89j$
28	$-0.14 \pm 182.16j$	$-0.63 \pm 672.58j$	60	$-0.33 \pm 366.34j$	$-0.59 \pm 663.65j$
29	$-0.14 \pm 185.01j$	$-0.63 \pm 674.80j$	61	$-0.35 \pm 378.35j$	$-0.56 \pm 643.38j$
30	$-0.15 \pm 187.95j$	$-0.63 \pm 677.76j$	62	$-0.36 \pm 390.93j$	$-0.54 \pm 623.50j$
31	$-0.15 \pm 190.98j$	$-0.64 \pm 681.47j$	63	$-0.38 \pm 403.96j$	$-0.51 \pm 604.49j$
32	$-0.15 \pm 194.11j$	$-0.64 \pm 685.93j$	64	$-0.40 \pm 417.13j$	$-0.48 \pm 586.96j$
33	$-0.15 \pm 197.35j$	$-0.65 \pm 691.15j$	65	$-0.42 \pm 429.75j$	$-0.45 \pm 571.86j$
34	$-0.16 \pm 200.70j$	$-0.66 \pm 697.11j$	66	$-0.44 \pm 440.48j$	$-0.43 \pm 560.81j$

Table C.5: node numbers and corresponding eigenvalues for matrix $\underline{A}$; $k = 165$ [kN/m].

C.3 Values of r

node	r	node	r
3	1.5435	35	0.3593
4	1.3229	36	0.3363
5	1.2493	37	0.3140
6	1.2041	38	0.2924
7	1.1680	39	0.2716
8	1.1349	40	0.2515
9	1.1031	41	0.2322
10	1.0724	42	0.2136
11	1.0418	43	0.1958
12	1.0114	44	0.1789
13	0.9811	45	0.1627
14	0.9507	46	0.1473
15	0.9204	47	0.1327
16	0.8901	48	0.1189
17	0.8600	49	0.1058
18	0.8298	50	0.0936
19	0.7997	51	0.0822
20	0.7696	52	0.0716
21	0.7399	53	0.0617
22	0.7102	54	0.0527
23	0.6808	55	0.0444
24	0.6516	56	0.0369
25	0.6227	57	0.0301
26	0.5942	58	0.0241
27	0.5660	59	0.0188
28	0.5383	60	0.0143
29	0.5110	61	0.0104
30	0.4843	62	0.0071
31	0.4581	63	0.0044
32	0.4324	64	0.0021
33	0.4074	65	0.0002
34	0.3830	66	0.0000

Table C.6: node numbers and corresponding values for r; $k = 165$ [kN/m].

Appendix D

Diana data file

```
:EXPERIMENT Balk met enkelzijdige veer
UNITS: N, m, kg
'COORDI'
   1   -1.50000E-02   0.00000E+00   0.00000E+00
   2    0.00000E+00   0.00000E+00   0.00000E+00
   3    1.00000E-02   0.00000E+00   0.00000E+00
   4    2.00000E-02   0.00000E+00   0.00000E+00
   5    3.00000E-02   0.00000E+00   0.00000E+00
   6    4.00000E-02   0.00000E+00   0.00000E+00
   7    5.00000E-02   0.00000E+00   0.00000E+00
   8    6.00000E-02   0.00000E+00   0.00000E+00
   9    7.00000E-02   0.00000E+00   0.00000E+00
  10    8.00000E-02   0.00000E+00   0.00000E+00
  11    9.00000E-02   0.00000E+00   0.00000E+00
  12    1.00000E-01   0.00000E+00   0.00000E+00
  13    1.10000E-01   0.00000E+00   0.00000E+00
  14    1.20000E-01   0.00000E+00   0.00000E+00
  15    1.30000E-01   0.00000E+00   0.00000E+00
  16    1.40000E-01   0.00000E+00   0.00000E+00
  17    1.50000E-01   0.00000E+00   0.00000E+00
  18    1.60000E-01   0.00000E+00   0.00000E+00
  19    1.70000E-01   0.00000E+00   0.00000E+00
  20    1.80000E-01   0.00000E+00   0.00000E+00
  21    1.90000E-01   0.00000E+00   0.00000E+00
  22    2.00000E-01   0.00000E+00   0.00000E+00
  23    2.10000E-01   0.00000E+00   0.00000E+00
  24    2.20000E-01   0.00000E+00   0.00000E+00
  25    2.30000E-01   0.00000E+00   0.00000E+00
  26    2.40000E-01   0.00000E+00   0.00000E+00
  27    2.50000E-01   0.00000E+00   0.00000E+00
  28    2.60000E-01   0.00000E+00   0.00000E+00
  29    2.70000E-01   0.00000E+00   0.00000E+00
  30    2.80000E-01   0.00000E+00   0.00000E+00
  31    2.90000E-01   0.00000E+00   0.00000E+00
  32    3.00000E-01   0.00000E+00   0.00000E+00
  33    3.10000E-01   0.00000E+00   0.00000E+00
  34    3.20000E-01   0.00000E+00   0.00000E+00
  35    3.30000E-01   0.00000E+00   0.00000E+00
  36    3.40000E-01   0.00000E+00   0.00000E+00
  37    3.50000E-01   0.00000E+00   0.00000E+00
  38    3.60000E-01   0.00000E+00   0.00000E+00
  39    3.70000E-01   0.00000E+00   0.00000E+00
  40    3.80000E-01   0.00000E+00   0.00000E+00
  41    3.90000E-01   0.00000E+00   0.00000E+00
  42    4.00000E-01   0.00000E+00   0.00000E+00
  43    4.10000E-01   0.00000E+00   0.00000E+00
  44    4.20000E-01   0.00000E+00   0.00000E+00
  45    4.30000E-01   0.00000E+00   0.00000E+00
  46    4.40000E-01   0.00000E+00   0.00000E+00
  47    4.50000E-01   0.00000E+00   0.00000E+00
  48    4.60000E-01   0.00000E+00   0.00000E+00
  49    4.70000E-01   0.00000E+00   0.00000E+00
  50    4.80000E-01   0.00000E+00   0.00000E+00
  51    4.90000E-01   0.00000E+00   0.00000E+00
  52    5.00000E-01   0.00000E+00   0.00000E+00
  53    5.10000E-01   0.00000E+00   0.00000E+00
  54    5.20000E-01   0.00000E+00   0.00000E+00
  55    5.30000E-01   0.00000E+00   0.00000E+00
  56    5.40000E-01   0.00000E+00   0.00000E+00
  57    5.50000E-01   0.00000E+00   0.00000E+00
  58    5.60000E-01   0.00000E+00   0.00000E+00
  59    5.70000E-01   0.00000E+00   0.00000E+00
  60    5.80000E-01   0.00000E+00   0.00000E+00
  61    5.90000E-01   0.00000E+00   0.00000E+00
  62    6.00000E-01   0.00000E+00   0.00000E+00
  63    6.10000E-01   0.00000E+00   0.00000E+00
  64    6.20000E-01   0.00000E+00   0.00000E+00
  65    6.30000E-01   0.00000E+00   0.00000E+00
  66    6.40000E-01   0.00000E+00   0.00000E+00
  67    6.50000E-01   0.00000E+00   0.00000E+00
  68    6.60000E-01   0.00000E+00   0.00000E+00
  69    6.70000E-01   0.00000E+00   0.00000E+00
  70    6.80000E-01   0.00000E+00   0.00000E+00
  71    6.90000E-01   0.00000E+00   0.00000E+00
  72    7.00000E-01   0.00000E+00   0.00000E+00
  73    7.10000E-01   0.00000E+00   0.00000E+00
  74    7.20000E-01   0.00000E+00   0.00000E+00
  75    7.30000E-01   0.00000E+00   0.00000E+00
  76    7.40000E-01   0.00000E+00   0.00000E+00
  77    7.50000E-01   0.00000E+00   0.00000E+00
  78    7.60000E-01   0.00000E+00   0.00000E+00
  79    7.70000E-01   0.00000E+00   0.00000E+00
  80    7.80000E-01   0.00000E+00   0.00000E+00
  81    7.90000E-01   0.00000E+00   0.00000E+00
  82    8.00000E-01   0.00000E+00   0.00000E+00
  83    8.10000E-01   0.00000E+00   0.00000E+00
  84    8.20000E-01   0.00000E+00   0.00000E+00
  85    8.30000E-01   0.00000E+00   0.00000E+00
  86    8.40000E-01   0.00000E+00   0.00000E+00
  87    8.50000E-01   0.00000E+00   0.00000E+00
  88    8.60000E-01   0.00000E+00   0.00000E+00
  89    8.70000E-01   0.00000E+00   0.00000E+00
  90    8.80000E-01   0.00000E+00   0.00000E+00
  91    8.90000E-01   0.00000E+00   0.00000E+00
  92    9.00000E-01   0.00000E+00   0.00000E+00
  93    9.10000E-01   0.00000E+00   0.00000E+00
  94    9.20000E-01   0.00000E+00   0.00000E+00
  95    9.30000E-01   0.00000E+00   0.00000E+00
  96    9.40000E-01   0.00000E+00   0.00000E+00
  97    9.50000E-01   0.00000E+00   0.00000E+00
  98    9.60000E-01   0.00000E+00   0.00000E+00
  99    9.70000E-01   0.00000E+00   0.00000E+00
 100    9.80000E-01   0.00000E+00   0.00000E+00
 101    9.90000E-01   0.00000E+00   0.00000E+00
 102    1.00000E+00   0.00000E+00   0.00000E+00
 103    1.01000E+00   0.00000E+00   0.00000E+00
 104    1.02000E+00   0.00000E+00   0.00000E+00
 105    1.03000E+00   0.00000E+00   0.00000E+00
 106    1.04000E+00   0.00000E+00   0.00000E+00
 107    1.05000E+00   0.00000E+00   0.00000E+00
 108    1.06000E+00   0.00000E+00   0.00000E+00
 109    1.07000E+00   0.00000E+00   0.00000E+00
 110    1.08000E+00   0.00000E+00   0.00000E+00
 111    1.09000E+00   0.00000E+00   0.00000E+00
 112    1.10000E+00   0.00000E+00   0.00000E+00
 113    1.11000E+00   0.00000E+00   0.00000E+00
 114    1.12000E+00   0.00000E+00   0.00000E+00
 115    1.13000E+00   0.00000E+00   0.00000E+00
 116    1.14000E+00   0.00000E+00   0.00000E+00
 117    1.15000E+00   0.00000E+00   0.00000E+00
 118    1.16000E+00   0.00000E+00   0.00000E+00
 119    1.17000E+00   0.00000E+00   0.00000E+00
 120    1.18000E+00   0.00000E+00   0.00000E+00
 121    1.19000E+00   0.00000E+00   0.00000E+00
 122    1.20000E+00   0.00000E+00   0.00000E+00
 123    1.21000E+00   0.00000E+00   0.00000E+00
 124    1.22000E+00   0.00000E+00   0.00000E+00
 125    1.23000E+00   0.00000E+00   0.00000E+00
 126    1.24000E+00   0.00000E+00   0.00000E+00
 127    1.25000E+00   0.00000E+00   0.00000E+00
 128    1.26000E+00   0.00000E+00   0.00000E+00
 129    1.27000E+00   0.00000E+00   0.00000E+00
 130    1.28000E+00   0.00000E+00   0.00000E+00
 131    1.29000E+00   0.00000E+00   0.00000E+00
 132    1.30000E+00   0.00000E+00   0.00000E+00
 133    1.31500E+00   0.00000E+00   0.00000E+00
 134    6.50000E-01  -1.00000E+00   0.00000E+00
 135    0.00000E+00   1.00000E-02   0.00000E+00
```

```
136    0.00000E+00   2.00000E-02   0.00000E+00
137    0.00000E+00   3.00000E-02   0.00000E+00
138    0.00000E+00   4.00000E-02   0.00000E+00
139    0.00000E+00   5.00000E-02   0.00000E+00
140    0.00000E+00   6.00000E-02   0.00000E+00
141    0.00000E+00   7.00000E-02   0.00000E+00
142    0.00000E+00   8.00000E-02   0.00000E+00
143    0.00000E+00   9.20000E-02   0.00000E+00
144    1.30000E+00   1.00000E-01   0.00000E+00
145    1.30000E+00   2.00000E-02   0.00000E+00
146    1.30000E+00   3.00000E-02   0.00000E+00
147    1.30000E+00   4.00000E-02   0.00000E+00
148    1.30000E+00   5.00000E-02   0.00000E+00
149    1.30000E+00   6.00000E-02   0.00000E+00
150    1.30000E+00   7.00000E-02   0.00000E+00
151    1.30000E+00   8.00000E-02   0.00000E+00
152    1.30000E+00   9.20000E-02   0.00000E+00
153    3.20000E-01  -1.00000E+00   0.00000E+00
'ELEMEN'
CONNEC
 1     L6BEN   1  2
 2     L6BEN   2  3
 3     L6BEN   3  4
 4     L6BEN   4  5
 5     L6BEN   5  6
 6     L6BEN   6  7
 7     L6BEN   7  8
 8     L6BEN   8  9
 9     L6BEN   9  10
 10    L6BEN   10  11
 11    L6BEN   11  12
 12    L6BEN   12  13
 13    L6BEN   13  14
 14    L6BEN   14  15
 15    L6BEN   15  16
 16    L6BEN   16  17
 17    L6BEN   17  18
 18    L6BEN   18  19
 19    L6BEN   19  20
 20    L6BEN   20  21
 21    L6BEN   21  22
 22    L6BEN   22  23
 23    L6BEN   23  24
 24    L6BEN   24  25
 25    L6BEN   25  26
 26    L6BEN   26  27
 27    L6BEN   27  28
 28    L6BEN   28  29
 29    L6BEN   29  30
 30    L6BEN   30  31
 31    L6BEN   31  32
 32    L6BEN   32  33
 33    L6BEN   33  34
 34    L6BEN   34  35
 35    L6BEN   35  36
 36    L6BEN   36  37
 37    L6BEN   37  38
 38    L6BEN   38  39
 39    L6BEN   39  40
 40    L6BEN   40  41
 41    L6BEN   41  42
 42    L6BEN   42  43
 43    L6BEN   43  44
 44    L6BEN   44  45
 45    L6BEN   45  46
 46    L6BEN   46  47
 47    L6BEN   47  48
 48    L6BEN   48  49
 49    L6BEN   49  50
 50    L6BEN   50  51
 51    L6BEN   51  52
 52    L6BEN   52  53
 53    L6BEN   53  54
 54    L6BEN   54  55
 55    L6BEN   55  56
 56    L6BEN   56  57
 57    L6BEN   57  58
 58    L6BEN   58  59
 59    L6BEN   59  60
 60    L6BEN   60  61
 61    L6BEN   61  62
 62    L6BEN   62  63
 63    L6BEN   63  64
 64    L6BEN   64  65
 65    L6BEN   65  66
 66    L6BEN   66  67
 67    L6BEN   67  68
 68    L6BEN   68  69
 69    L6BEN   69  70
 70    L6BEN   70  71
 71    L6BEN   71  72
 72    L6BEN   72  73
 73    L6BEN   73  74
 74    L6BEN   74  75
 75    L6BEN   75  76
 76    L6BEN   76  77
 77    L6BEN   77  78
 78    L6BEN   78  79
 79    L6BEN   79  80
 80    L6BEN   80  81
 81    L6BEN   81  82
 82    L6BEN   82  83
 83    L6BEN   83  84
 84    L6BEN   84  85
 85    L6BEN   85  86
 86    L6BEN   86  87
 87    L6BEN   87  88
 88    L6BEN   88  89
 89    L6BEN   89  90
 90    L6BEN   90  91
 91    L6BEN   91  92
 92    L6BEN   92  93
 93    L6BEN   93  94
 94    L6BEN   94  95
 95    L6BEN   95  96
 96    L6BEN   96  97
 97    L6BEN   97  98
 98    L6BEN   98  99
 99    L6BEN   99  100
100    L6BEN   100  101
101    L6BEN   101  102
102    L6BEN   102  103
103    L6BEN   103  104
104    L6BEN   104  105
105    L6BEN   105  106
106    L6BEN   106  107
107    L6BEN   107  108
108    L6BEN   108  109
109    L6BEN   109  110
110    L6BEN   110  111
111    L6BEN   111  112
112    L6BEN   112  113
113    L6BEN   113  114
114    L6BEN   114  115
115    L6BEN   115  116
116    L6BEN   116  117
117    L6BEN   117  118
118    L6BEN   118  119
119    L6BEN   119  120
120    L6BEN   120  121
121    L6BEN   121  122
122    L6BEN   122  123
123    L6BEN   123  124
124    L6BEN   124  125
125    L6BEN   125  126
126    L6BEN   126  127
127    L6BEN   127  128
128    L6BEN   128  129
129    L6BEN   129  130
130    L6BEN   130  131
131    L6BEN   131  132
132    L6BEN   132  133
133    sp2tr   67  134
134    sp2tr   134  67
135    L6BEN   2  135
136    L6BEN   135  136
137    L6BEN   136  137
138    L6BEN   137  138
139    L6BEN   138  139
140    L6BEN   139  140
141    L6BEN   140  141
142    L6BEN   141  142
143    L6BEN   142  143
144    L6BEN   132  144
145    L6BEN   144  145
146    L6BEN   145  146
147    L6BEN   146  147
148    L6BEN   147  148
149    L6BEN   148  149
150    L6BEN   149  150
151    L6BEN   150  151
152    L6BEN   151  152
153    pt3t   67
154    pt3t   34
155    sp2tr   34  153
MATERI
 / 1-132 / 1
 / 135-152 / 2
  153       5
  154       6
  155       7
  133       8
  134       9
GEOMET
 / 1-132 /  1
 / 135-152 / 2
'MATERI'
 1     densit      7746.3
       young       2.1e11
       poison      0.3
```

```
 2      densit      7713.3
        young       2.1e11
        poison      0.3
 5      mass        0.446
 6      mass        0.0
 7      damp        0.0
        spring      0.0
 8      damp        0.0
:                   11.6250 ('eenzijdige demping !!')
        spring      0.0
 9      spring      0.0
'design'
:eenzijdige veerstijfheid
  3     165e3
  2     37
  5     0.984e-3
  8     1.e16
 10     1.0
 21      1e-4
 22      150.0
 23      37
 24      0.984e-3
 25      0.1
 30      0.0
 31      200.0
 32      0.0
 33      200.0
 34      0.0
 35      200.0
 36      0.0
 37      0.0
 38      0.0
 39      0.
 40      0.
 41      100.0
 42      1.0
 43      50.0
 44      5.e-1
 45      1.e2
 46      1.e1
 47      1.e1
 48      0.0
 49      1.e3
 50      1.0e0
 51      0.e-0
 52      1.e-5
 53      0.00
 54      2.0
 56      1.0
 57      0.0
 81      1.0
 82      100.0
 83      0.5
 84      100.0
 85      1.0
 86      20.0
 87      200.0
 88      200.0
 89      20000.0
 90      1.0
 97      0.0
100      0.0
101     10.0
102     10.0
103     10.0
104     10.0
105     10.0
106     10.0
107     10.0
108     10.0
109     10.0
110     10.0
111     0.1
112     0.0
113     0.0
114     0.0
115     0.0
116     0.0
117     0.0
118     0.0
119     0.0
120     0.0
121     1.0
122     0.0
123     5.0
124     4.0
125     0.0
126     0.0
127     1.0
128     1.e-12
140     0.0
141     0.0
'geomet'
:afmetingen balk
 1      zaxis       0.0 0.0 1.0
        crosse      9.0E-4
        inerti      7.5E-9
 2      zaxis       0.0 0.0 1.0
        crosse      7.5E-5
        inerti      6.25E-12
'directions'
 1      1.0 0.0 0.0
 2      0.0 1.0 0.0
 3      0.0 0.0 1.0
'supports'
/ 1-133 /   tr 1 tr 3 ro 1 ro 2
/ 143 152 /  tr 1 tr 2 tr 3 ro 1 ro 2 ro 3
/ 134 153 /  tr 1 tr 2 tr 3 ro 1 ro 2
'loads'
 case 1
 nodal
  67      f  2 1.0
'inivar'
 displa 1
  67     t 2    0.0
 veloci 1
  67     t 2    0.0
'genelm'
 1      type        balkzonderactuator
        elemen      1-132 135-143 144-152 153 154 155
        ifcnod     / 31 67 / tr 2
        cms         NOFLEX
        frequb      350.0
'end'
```

Appendix E

Source code

E.1 New C^{++} source for the control experiment

E.1.1 Main program

```
/* beam_act.cpp
=============

This is an adapted version of beam.cpp. It compensates
for the influence of the actuator/amplifier dynamics.

Optional use of a data-set for desired trajectories
(instead of destra) has also been added
(enable through a define "destra_from_mat").

Expects file BEAM_IN.MAT with:
(1*1) sf - sample frequency  [Hz]
(1*1) n - number of samples to go [-]
(1*1)   n_start - number of samples before start
(1*1) f_e - excitation frequency [Hz]
(1*1) lambda - sliding mode parameter [Hz]
(1*1) eta - sliding mode parameter [m/s^2]
(1*1) sigma - sliding mode parameter [m/s]
(3*3)   M - mass matrix
(21*1) C - truncated Fourier series (desired trajectory)
     OR (1*3) xd - desired trajectory (requires define and sf/f_e samples)
(3*3) K - stifness matrix
(3*3) B - damping matrix
(6*4) G - (stationary) optimal Kalman filter (4 measurements)
(1*1) k - spring stifness [N/m]
(1*1) me - lumped excenter mass [kg]
(1*1) re - lumped mass radial distance [m]
(1*1) fco_z2 - cut-off frequency ya_ddot     [Hz]
(1*1) fco_z3 - cut-off frequency ym_ddot     [Hz]
(1*1) control_node - node number of actuator DOF [-]

Creates MATLAB Result file BEAM_OUT.MAT:
name size meaning
---------------
z n*exp_nz_max measurements
u n*exp_nu commands as applied
wait 3*1 wait count info vector

Remark: exp_nz_max is defined for the specific experiment.
Remark: when running a real experiment, wait will hold
minimum wait count
maximum wait count
average wait count
in function exp_get; see exp.doc for details;
when running a simulator, wait will hold
Total clock time used
# integrator steps with progression
```

```
# integrator steps without progression
see sim.doc for details.
*/

#include <tce.h>
#include <conio.h>
#include <stdio.h>
#include <stdlib.h>
#include <math.h>
#include <exp_b.def>
#define sgn(x) ((x>0)?1:((x<0)?-1:0))
#define dmin(x,y) ((x<y)?x:y)
#define dmax(x,y) ((x>y)?x:y)

#define nu_max 1
#define nz_max 7

int n,/* Number of cycles to run */
n_start,/* Samples before start */
j,/* Current sample */
nu = nu_max,/* Actual number of commands */
nz = nz_max,/* Actual number of measurements */
control_node; /* Node number of actuator DOF */
double sf; /* Sample frequency [Hz] */

double t [1],/* Time */
u [nu_max],/* Commands (as requested) */
z [nz_max],/* Measurements */
wait[3];

ivec sub1,sub2;
double dt;
double saturation,lambda,s,sigma,eta,f_e,w,edot,e,k,me,re;
mat M,M_inv,K,B,G(6,4),A(6,6),fos(3,3),Fex(6,1),xdot(6,1);
double xd[3],C[21],z_previous[7];
double z_filtered[2],fco_z2,fco_z3,m_unbalance=0.446;
double  H_versterker=15.94,R=6.1,Bl=18.4,v_uit,R_sp=522,R_tot=10.06e3;
double didt_desired,i_desired,i_previous,phase,ud[1];
double L=3.1e-3,m_a=0.065,b_a=35,k_a=1.35e3;
//double L=0,m_a=0,b_a=0,k_a=0;
//double m_a=0.15,b_a=95,k_a=1200,L=0;
mat xhat(6,1);

#include "compensa.cpp"
#include "syncs.cpp"
#include "calib.cpp"

void epilog(void) {
printf("\nSaving data in MAT-file...\n");
ml_open("beam_out",1);
ts_save_all(1);
ml_put_scalar(phase,"phase_shift");
ml_put_vec(wait,3,"wait");
printf("Finished...\n");
}

void prolog(void) {
exp_dim(&nu,&nz); /* Ask actual nu and nz */

ml_open("beam_in",0);
#ifdef destra_from_mat
printf("Desired trajectory 'xd' will NOT be approximated...\n");
ts_load0(xd,3,"xd");
#else
if (ml_get_vec(C,21,"C")==0) tce_error("not available in inputfile");
#endif
sf = ml_get_scalar("sf",0);
n  = (int)ml_get_scalar("n",0);
n_start  = (int)ml_get_scalar("n_start",0);
f_e  = ml_get_scalar("f_e",0);
```

```
sigma  = ml_get_scalar("sigma",0);
eta  = ml_get_scalar("eta",0);
lambda  = ml_get_scalar("lambda",0);
k = ml_get_scalar("k",0);
me = ml_get_scalar("me",0);
re = ml_get_scalar("re",0);
fco_z2 = ml_get_scalar("fco_z2",0);
fco_z3 = ml_get_scalar("fco_z3",0);
control_node = (int)ml_get_scalar("control_node",0);
if ( sf<=0 ) tce_error("sf must be >0");
if ( (me==0)||(re==0)||(f_e==0)||(n==0)||(sigma==0)||(lambda==0)||
(eta==0)||(control_node==0) )
tce_error("one or more parameters invalid!");
if (k==0) printf("WARNING: one-sided spring disabled (k=0)!\n");
M= ml_get_mat("M");
K= ml_get_mat("K");
B= ml_get_mat("B");
// G= ml_get_mat("G");
M_inv=inv(M);
w=2*M_PI*f_e;
printf("Matlab parameters have been loaded succesfully...\n");
printf("Actuator positioned at node %i...\n",control_node);
calibration_check();
if ( !n_start==0 ) {printf("Controller starts after %d samples!\n",n_start);}
printf("Sample frequency: %f [Hz]\n",sf);
printf("Samples to record: %d\n",n);
sub1=ilist(1,3);
sub2=ilist(4,3);
A.ssa(sub1,sub2,eye(3));
A.ssa(sub2,sub2,-M_inv*B);
/*
The statement for xhat is nasty, but nevertheless it seems to work:
matrix xhat is interpreted as an array of doubles which is required
for this function to work properly.
*/
// ts_init0(xd,3,n,"xd"); /* Initialize time series for xd */
// ts_init0(t,1,n,"t"); /* Initialize time series for t */
ts_init0(z,nz,n,"z"); /* Initialize time series for z */
ts_init0(ud,nu,n,"ud"); /* Initialize time series for ud */
ts_init0(u,nu,n,"u"); /* Initialize time series for u */
}

void new_destra(int calc_dofs,int order) {
/*
This function 'destra' has been adapted so that it provides desired
trajectories for a requested number of DOFs. These trajectories are
sorted by DOF number (inner) and then by derivative order (outer)
for maximum state sorting compatibility
*/
int i,j,k,harmonics=10;
// printf("Controller excitation force phase: %f [rad]\n-\n",w*t[0]+phase-
... floor((w*t[0]+phase)/2/M_PI)*2*M_PI);
for (i=0;i<=order;i++) {
  for (j=0;j<calc_dofs;j++) {
    xd[j+i*calc_dofs]=((i==0)?C[j*(2*harmonics+1)]:0.0);
    for (k=1;k<=harmonics;k++) {
      xd[j+i*calc_dofs]+=pow(k*w,i)*(
      cos(k*(w*t[0]+phase)+M_PI/2*i)*C[k+j*(2*harmonics+1)]+
      sin(k*(w*t[0]+phase)+M_PI/2*i)*C[k+harmonics+j*(2*harmonics+1)]);
    }
  }
}
}

void simple_state_reconstruction(void)
{
xhat.p[0]=z[0];
xhat.p[1]=z[1];
z_filtered[0]=(z_previous[2]+2*M_PI*fco_z2/sf*z[2])/(1+2*M_PI*fco_z2/sf);
z_filtered[1]=(z_previous[3]+2*M_PI*fco_z3/sf*z[3])/(1+2*M_PI*fco_z3/sf);
```

```
xhat.p[3]=(z[0]-z_previous[0])*sf+z_previous[2]/2/sf;
xhat.p[4]=(z[1]-z_previous[1])*sf+z_previous[3]/2/sf;
fos.ssa(2,2,k*floor(sgn(xhat.p[1])+1)/2);
A.ssa(sub2,sub1,-M_inv*(K+fos));
Fex.p[3]=u[0];
Fex.p[4]=z[4]+m_unbalance*z[3];
Fex.p[5]=0;
Fex.ssa(sub2,1,M_inv*Fex(sub2,1));

/* berekening schatting yv (3 dof model)
Voorbeeld van wijze waarop een matrix-index in C++ is gedefinieerd:

    1  2  3  4  5  6
1 [ 0  6 12 18 24 30 ]
2 [ 1  7 13 19 25 31 ]
3 [ 2  8 14 20 26 32 ]
4 [ 3  9 15 21 27 33 ]
5 [ 4 10 16 22 28 34 ]
6 [ 5 11 17 23 29 35 ]
*/

xhat.p[2]=1/(A.p[15]/A.p[33]-A.p[16]/A.p[34])*
  (
  (z[2]-Fex.p[3]-(A.p[3]*z[0]+A.p[9]*z[1]+A.p[21]*xhat.p[3]+A.p[27]*xhat.p[4]))/A.p[33]-
  (z[3]-Fex.p[4]-(A.p[4]*z[0]+A.p[10]*z[1]+A.p[22]*xhat.p[3]+A.p[28]*xhat.p[4]))/A.p[34]
  );
xhat.p[5]=1/(A.p[33]/A.p[15]-A.p[34]/A.p[16])*
  (
  (z[2]-Fex.p[3]-(A.p[3]*z[0]+A.p[9]*z[1]+A.p[21]*xhat.p[3]+A.p[27]*xhat.p[4]))/A.p[15]-
  (z[3]-Fex.p[4]-(A.p[4]*z[0]+A.p[10]*z[1]+A.p[22]*xhat.p[3]+A.p[28]*xhat.p[4]))/A.p[16]
  );
z_previous[0]=z[0];
z_previous[1]=z[1];
z_previous[2]=z_filtered[0];
z_previous[3]=z_filtered[1];
}

double sweep(void) // linear frequency sweep
{ double f_sweep,f_max_sweep=100;
f_sweep=f_max_sweep*t[0]/(n/sf);
printf("f_sweep=%f [Hz]\r",f_sweep);
return 10*sin(2*M_PI*f_sweep*t[0]);
}


void control(void)
{
/* First "reconstruct" the full state of the system */
simple_state_reconstruction();

/* Then calculate the control-force, based on the estimated state */
fos.ssa(2,2,k*floor(sgn(xhat.p[1])+1)/2);
A.ssa(sub2,sub1,-M_inv*(K+fos));
Fex.p[3]=0;
Fex.p[4]=z[4]+m_unbalance*z[3];
Fex.p[5]=0;
Fex.ssa(sub2,1,M_inv*Fex(sub2,1));
xdot=A*xhat+Fex; //needs full state.
// printf("t=%f, xd=%f, %f, %f (diana)\n",t[0],xd[0],xd[1],xd[2]);
#ifndef destra_from_mat
new_destra(1,2);
// printf("t=%f, xd=%f, %f, %f (destra)\n",t[0],xd[0],xd[1],xd[2]);
#endif
e=xhat.p[0]-xd[0];
edot=xhat.p[3]-xd[1];
s=lambda*e+edot;
if (fabs(s/sigma)>=1.0)
{
saturation=sgn(s/sigma);
}
```

```
else
{
saturation=s/sigma;
}
if (j>=n_start)
{
//      PD-regeling: (CTC+PD)
ud[0]=(-xdot.p[3]+xd[2]-(eta+lambda)*edot-eta*lambda*e)/M_inv.p[0];
//      Schakelvlakregeling: SCTC
// ud[0]=(-xdot.p[3]+xd[2]-lambda*edot-eta*saturation)/M_inv.p[0];
}
else
{
ud[0]=0;
}
// ud[0]=10*sin(2*M_PI*37*t[0]);
// ud[0]=sweep();
ud[0]=0;
// xhat.p[3]=0;
u[0]=compensate_act2();
// u[0]=compensate_act1();
u[0]=sgn(u[0])*dmin(fabs(u[0]),25);

}


void run(void) {
/*
Timing for data in the time series, in MATLAB notation, is:
- z(k,:) contains the measurements at time t = (k-1)*dT, where
  dT = 1/sf; so the first sample is at time t = 0.
- u(k,:) are the commands issued at time t = (k-1)*dT; with
  Zero Order Hold characteristic they apply between time
  t = (k-1)*dT and k*dT. So, measurements z(k,:) do not
  depend on commands u(k,:).
*/
t[0]=0.0;
dt=1.0/sf;
exp_init(z,nz,u,dt,wait);
phase=sync3();
j=1;
// printf("*** Start run\n");
while ( j<=n ) {
#ifdef destra_from_mat
ts_get_all(); // fetch desired trajectory+derivatives
#endif
control();
exp_put(); // apply actuator-force
ts_put_all(); // dump current data to buffer
exp_get(); // fetch new measurements
t[0]+=dt;
j++;
}
printf("*** End run\n");
exp_fini();
}

void main(void){
     printf("Initializing beam controller...\n");
printf("\nSpecific features:\n==================\n");
printf("- Simple state reconstruction\n");
printf("- Compensation for actuator dynamics\n\n");
prolog();
run();
epilog();
}

/* end of beam.cpp */
```

E.1.2 Calibration check

```
int calibration_check(void) {
printf("You may check the calibration now (switch off exciter)...\n");
printf("Press any key to end calibration check...\n");

int i,j,m = 1;
int refresh_rate=2;
extern int ana_buf[16];
double sum_z[nz_max];
long sum_ana[nz_max];

while ( m*refresh_rate<100 ) m *= 2;

exp_init(z,nz,u,1.0/(m*refresh_rate),wait);
printf(" ya [mm] ym [mm],  bit values\n");

while ( 1 ) {

for ( j=0; j<nz; j++ ) {
sum_z[j] = 0;
sum_ana[j] = 0;
}

for ( i=0; i<m; i++ ) {
exp_get();
for ( j=0; j<nz; j++ ) {
sum_z[j] += z[j];
sum_ana[j] += ana_buf[j];
}}

for ( j=0; j<nz; j++ ) {
sum_z[j] /= m;
sum_ana[j] /= m;
}

printf( "%7.4lf %7.4lf, %5ld %5ld\r",
1000*sum_z[0],1000*sum_z[1],
sum_ana[0],sum_ana[1]);
if ( kbhit() ) break;
}

exp_fini();

getch();
printf("\n");
printf("(Re)start exciter. Press any key to start experiment...\n");
while ( kbhit() );
getch();
return 0;
}
```

E.1.3 Actuator dynamics

```
double compensate_act1(void) {
return -(ud[0]+m_a*xdot.p[3]+b_a*xhat.p[3]+k_a*xhat.p[0]);
}

double compensate_act2(void) {
double u_compensated;
i_desired=-(ud[0]+m_a*xdot.p[3]+b_a*xhat.p[3]+k_a*xhat.p[0])/Bl;
didt_desired=(i_desired-i_previous)*sf;// Simple euler differentiation
i_previous=i_desired;
u_compensated=(i_desired*R+L*didt_desired-Bl*xhat.p[3]) // alle model kennis
// u_compensated=(i_desired*R+L*didt_desired) //geen tegen EMK compensatie
// u_compensated=(i_desired*R-Bl*xhat.p[3]) // geen spoel
// u_compensated=i_desired*R //oude model
/H_versterker/(R_sp/R_tot)*2048/10*exp_u0_res;
return u_compensated;
}
```

E.1.4 Synchronization functions

The controller can only function adequately if the quality of the synchronization of the desired trajectories and the excitation force F_{ex} is appropriate. Three different synchronization functions are implemented:

1. External trigger signal on channel 7. This signal can only be used for $f_s = 500$ [Hz] and has been used in the past (see [19]).

2. This function determines the phase shift by means of the argument of the sine shaped excitation force F_{ex}:

$$\texttt{phase\_shift} = \arccos\left(\frac{F_{ex}}{|F_{ex}|}\right), \; |F_{ex}| \simeq m_e r_e \omega^2. \tag{E.1}$$

   To achieve adequate accuracy in the determination of the required phase shift, it is essential that the amplitude of the excitation force is correct. Therefore, rather than using the value of $m_e r_e \omega^2$ used for the models, the value is determined by numerical real-time integration (using the trapezium rule) of the absolute value $|F_{ex}|$ of the measured excitation force during p (`sync_periods` in the source code) excitation periods:

$$\underbrace{m_e r_e \omega^2 \int_0^{\frac{p}{f_e}} |\cos(\omega t)| dt}_{\text{calculated}} = p|F_{ex}|\frac{2}{\pi f_e} \text{ [N]}. \tag{E.2}$$

3. Locates the zero transition of the excitation force F_{ex}. To prevent a fake transition as a result of (measurement) noise to be selected, a candidate transition is monitored for a number of samples `horizon`. Accordingly, the required phase shift is returned through the variable `phase_shift`.

Note that functions 2 and 3 require that the excitation force measurement is compensated for the inertia of the mass-unbalance.

```
double sync1(void) {
/*

Begin van de synchronisatie tussen de gemeten en de gesimuleerde
excitatiekracht

*/
// printf("Synchronizing...\n");
while ( z[6] <= 0.45 ) {
exp_get(); // fetch new measurements
}
return 0;
}

double sync2(void) {
/*
Synchronisatie tussen de gemeten excitatiekracht en de gewenste
trajectorie. Meet werkelijke F_ex gedurende \'e\'en periode en
bepaalt vervolgens de amplitude en de fase van de kracht ten
opzichte van de referentie F_ex. Hiermee wordt de fase van
de gewenste trajectorie aangepast aan de werkelijke fase van
de excitatiekracht. De gemeten kracht moet uiteraard in de
berekeningen worden gebruikt, niet de referentie F_ex.
*/
double phase_shift=0,sync_int=0,amp_estimate=0,
```

```
      F_ex_final,dt_final;
int i,useful=0,sync_periods=200,max_to_be_used=200,
     sync_size=(int)floor(sync_periods*sf/f_e)+1;
// printf("sync_size=%i\n",sync_size);
mat ref_set(sync_size,1),sync_set(sync_size,1);
// printf("Synchronizing during %i excitation periods...\n",sync_periods);
for ( i=0;i<sync_size-1;i++ ) { // sync_size-1 steps
ref_set.p[i]=cos(w*(i+1)/sf);
exp_get(); // fetch new measurements
sync_set.p[i]=z[4]+m_unbalance*z[3];
// printf("measured=%f, reference=%f\n",sync_set.p[i]/me/re/pow(w,2),ref_set.p[i]);
// Calculate the area here in order to reduce peak CPU load:
sync_int+=fabs(sync_set.p[i])*dt;
// printf("%i Integral=%f, current=%f\n",i+1,sync_int,sync_set.p[i]);
}
/*
Compensate for the over-estimated contribution of the first
interval and the but last interval
(i has become equal to sync_size-1, so there's only one element
left to fill)
*/
sync_int-=fabs(sync_set.p[0])/2*dt+fabs(sync_set.p[i-1])/2*dt;
/*
Add the contribution of the final interval:
*/
ref_set.p[i]=1; //
exp_get(); // fetch new measurements
sync_set.p[i]=z[4]-m_unbalance*z[3];
F_ex_final=sync_set.p[i-1]+(sync_set.p[i]-sync_set.p[i-1])*(sync_periods*sf/f_e-i);
dt_final=(sync_periods*sf/f_e-i)*dt;
// printf("F_ex_final=%f,dt_final=%f\n",F_ex_final,dt_final);
sync_int+=(fabs(sync_set.p[i-1])+fabs(F_ex_final))/2*dt_final;
/*
Scale the synchronization data to amplitude 1, using a numerical
area calculation based on the synchronization data. The area
defined by the time integral is:
int(abs(A*cos(w*t)),t=0..w/2/pi*sync_periods)=2/Pi/f_e*A*sync_periods.
Thus the amplitude A can be estimated using the numerical
approximation of this area. A reasonable (1st order) estimate
of the area is (calculated above):
1/sf*(F_0+F_n+2*sum(F_i,i=1...n-1))/2=(....).
Therefore, a reasonable estimate for the amplitude A is:
A=Pi*f_e/2*(....)/sync_periods.
*/
amp_estimate=M_PI*f_e/2*sync_int/sync_periods;
// amp_estimate=me*re*pow(w,2);
printf("Estimated amplitude F_ex: %f [N]\n",amp_estimate);
sync_set=sync_set/amp_estimate;
/*
Determine average phase shift based on subset of data
subset used to avoid negative effects of phase transitions
(when the sign changes; when this occurs, the product of
 the two derivatives is negative):
*/
for ( i=1;i<sync_size;i++ ) {
if ( ((ref_set.p[i]-ref_set.p[i-1])*
      (sync_set.p[i]-sync_set.p[i-1])>0) &
     (fabs(sync_set.p[i])<1) &
     (useful<max_to_be_used) ) {
useful+=1;
// printf("i=%i, arg1=%f, arg2=%f, difference=%f\n",i,acos(sync_set.p[i]),
... acos(ref_set.p[i]),acos(sync_set.p[i])-acos(ref_set.p[i]));
phase_shift=(phase_shift*(useful-1)+
fabs(acos(sync_set.p[i])-acos(ref_set.p[i])))
/useful;
}
}
if (useful<=1) phase_shift=M_PI;

// printf("Estimated required phase shift: %f [rad] (based on %i useful samples)\n",
```

```
// phase_shift,useful);
// printf("Starting experiment...\n");
return phase_shift;
}

double sync3(void) {
/*
Synchronisatie tussen de gemeten excitatiekracht en de gewenste
trajectorie. Meet nuldoorgangen van positief naar negatief
van F_ex en bepaalt op basis hiervan de fase van de
excitatiekracht tijdens de huidige run. Na een nuldoorgang
wordt gedurende 'tests' samples bekeken of de candidaat
nuldoorgang betrouwbaar is door te kijken of de functie
monotoon daalt gedurende de testperiode.
*/
double phase_shift=0,F_exc;
// double di;
int i=0,horizon=(int)floor(sf/f_e/8),candidate=0,tests=horizon;
// printf("Synchronizing...\n");
while ( tests ) {
i+=1;
// printf("tests=%i, candidate=%i\n",tests,candidate);
exp_get(); // fetch new measurements
F_exc=z[4]+m_unbalance*z[3];
if ( candidate ) {
if ( F_exc>z_previous[4] )
{candidate=0;} // candidate dismissed
else
{tests-=1;} // candidate still valid
}
else {
if ( (F_exc<=0) & (z_previous[4]>=0) ) {
/* di=-z_previous[4]/(F_exc-z_previous[4]);
printf("di=%f\n",di);
printf("F_ex=%f\n",F_exc);
printf("z_previous[4]=%f\n",z_previous[4]);
*/
candidate=1;
tests=horizon;
}
}
z_previous[4]=F_exc;
}
phase_shift=M_PI/2+w/sf*horizon;
// printf("Estimated required phase shift: %f [rad]\n",
// phase_shift);
// printf("Starting experiment...\n");
return phase_shift;
}
```

E.2 MATLAB files

E.2.1 Routine for the determination of r (Popov's criterion)

```
function results=det_r(calc_nodes)
%Procedure:
%----------
%1) locate a value of Re{F} where Re{F}<-1/k on the outer "loop",
%   e.g. min(Re{F})
%2) locate a value on the outer "loop" of Re{F} where Re{F}>-1/k
%3) find a dRe{}/d{Im} so that Re{F}+dRe{}/dIm{}*Im{F}=-1/k
%stiffness='165k';
stiffness='82k5';
mod_damp='0.001';
%data_path=['/users/sg3/borre/cpp/data/' stiffness];
data_path=['d:\borre\cpp\data\' mod_damp '\' stiffness];
tex_path=['./tex/' stiffness];
plots=1;
if ~exist('calc_nodes')
```

```
   disp('USAGE: det_r([nodes])');
else
   results=[];
   for j=1:length(calc_nodes)
      close all
      disp(['Initializing run with actuator at node ' num2str(calc_nodes(j)) '...'])
      return_path=pwd;
      cd (data_path)
      filename=['node_' num2str(calc_nodes(j))];
      if ~exist([filename '.m'])
         disp(['No system data available for actuator '...
         'positioned at node ' num2str(calc_nodes(j)) '!'])
         cd (return_path)
      else
         eval(filename)
         cd (return_path)
         A=[zeros(2,2) eye(2,2);-inv(M(2:3,2:3))*K(2:3,2:3) -inv(M(2:3,2:3))*B(2:3,2:3)];
         b=[[0 0]';inv(M(2:3,2:3))*[1 0]'];
         c=eye(4,1);
% step 1:
         clear w x y
         counter=1;
         w(counter)=0;
         F=c'*inv(1i*w(counter)*eye(size(A))-A)*b;
         x(counter)=real(F);y(counter)=w(counter)*imag(F);
         counter=counter+1;
         w(counter)=w(counter-1)+0.1;
         F=c'*inv(1i*w(counter)*eye(size(A))-A)*b;
         x(counter)=real(F);y(counter)=w(counter)*imag(F);
         while ~( x(counter)>x(counter-1) & y(counter)>y(counter-1) )
            counter=counter+1;
            reduction=0;
            w(counter)=w(counter-1)*2^(1/(2^reduction));
            F=c'*inv(1i*w(counter)*eye(size(A))-A)*b;
            x(counter)=real(F);y(counter)=w(counter)*imag(F);
            % Adjust 'w' if |dy/dx| too large in one step:
            while ( sqrt((x(counter)-x(counter-1))^2+ ...
                        (y(counter)-y(counter-1))^2)>1e-7 & ...
                    reduction<12 )
               reduction=reduction+1;
               w(counter)=w(counter-1)*2^(1/(2^reduction));
               F=c'*inv(1i*w(counter)*eye(size(A))-A)*b;
               x(counter)=real(F);y(counter)=w(counter)*imag(F);
            end
         end
         if (plots)
            figure
            plot(x(1:max(size(x))-1),y(1:max(size(y))-1),x(counter-1),y(counter-1),'*',-1/k,0,'r*');
            set(gca,'FontName','Times')
            title(['Partial Popov plot, actuator at node ' num2str(control_node)], ...
                  'FontName','Times')
            xlabel('Re(F)','Fontname','Times');
            ylabel('w*Im(F)','FontName','Times')
            hold on
         end
         w_lower=w(counter-1)
% step 2:
         clear w x y;
         counter=1;
         w(counter)=w_lower;
         F=c'*inv(1i*w(counter)*eye(size(A))-A)*b;
         x(counter)=real(F);y(counter)=w(counter)*imag(F);
         while ( x(counter)<-1/k )
            counter=counter+1;
            reduction=0;
            w(counter)=w(counter-1)*2^(1/(2^reduction));
            F=c'*inv(1i*w(counter)*eye(size(A))-A)*b;
            x(counter)=real(F);y(counter)=w(counter)*imag(F);
            % Adjust 'w' if |dy/dx| too large in one step:
            while ( sqrt((x(counter)-x(counter-1))^2+ ...
```

```
                    (y(counter)-y(counter-1))^2)>1e-8 & ...
                reduction<16 )
            reduction=reduction+1;
            w(counter)=w(counter-1)*2^(1/(2^reduction));
            F=c'*inv(1i*w(counter)*eye(size(A))-A)*b;
            x(counter)=real(F);y(counter)=w(counter)*imag(F);
         end
      end
      if ( plots )
         w_addon=logspace(log10(w(counter)),5,500);
         for counter2=1:max(size(w_addon))
            F=c'*inv(1i*w_addon(counter2)*eye(size(A))-A)*b;
            x(counter+counter2)=real(F);y(counter+counter2)=w_addon(counter2)*imag(F);
         end
         plot(x,y);
      end
      w_upper=w(counter)
% step 3:
      if (w_upper==w_lower)
         dxdy=0;
         x_test=x(counter);
      else
         counter=2;
         dxdy=(x(counter)-x(counter-1))/(y(counter)-y(counter-1));
         x_test=x(counter)+dxdy*(0-y(counter));
      end
      while ( (x_test<-1/k)&(counter<length(w)) )
         counter=counter+1;
         dxdy=(x(counter)-x(counter-1))/(y(counter)-y(counter-1));
         x_test=x(counter)+dxdy*(0-y(counter));
      end
      if ( plots )
         axis([min(-1/k,1.1*x(counter)) -1.1*x(counter) 1.1*y(counter) 0])
         plot([x_test x(counter)+y(counter)*dxdy]',[0 2*y(counter)]','g')
         hold off
         print popov.eps -deps
         eval(['!mv popov.eps ' tex_path '/popov_' num2str(calc_nodes(j)) '.eps']);
      end
      results=[results;control_node dxdy w(counter) abs(x_test*k+1)];
      % Note: r=dx/dy, w(counter)=w where dxdy occurs!
      % abs((x_test*k+1)) is an indication for the relative error of the linear approximation
      eval(['save r_' stiffness ' results'])
   end
  end
end
```

E.2.2 Routine for envelope determination

This routine is used to determine the coefficients c_1 and c_2, as defined in equation 2.26.

After the maxima of the absolute value of the control effort u have been selected from the data past the point that the first part of the control objective has been satisfied, a horizon of 4 samples is used to filter the maxima in order to prevent local maxima from reducing the quality of the fit. The control effort u has not been windowed/clipped. The resulting envelope has been determined using an unweighted least squares fit.

Discrete time controller

```
global C f_e
ffts=0;
clip_force=0;
load beam_in
load beam_out
offset=0;
%offset=sf*3
error_flag=0;
```

```
close all
if ~exist('horizon') horizon=4, end;
if ( clip_force )
   if ~exist('min_force') min_force=-80, end;
   if ~exist('max_force') max_force=80, end;
end
useful_samples=[];
t=[0:1/sf:(length(u)-1)/sf]';
if exist('xd') xd_cpp=xd; clear xd; end;
xd=destra(3,1,t);
error=z(:,1)-xd(:,1);
zero_candidates=find(abs(error)<=1e-5);
%Found that 1e-5 provides reasonable results

%First time that the error matches the criterium:
%-------------------------------------------------------
% Welcome to the zero dynamics, part I
%-------------------------------------------------------
if ~(isempty(zero_candidates))
   zerodyn_start=zero_candidates(1);

   %Convergence test: abs(edot)<1e-7 for reasonable results
   %1e-7 changed to 5e-7 (november 1996)
   zero_candidate2=zero_candidates(find(abs(z(zero_candidates,4)...
                  -xd(zero_candidates,4))<5e-7));
end
%-------------------------------------------------------
% Welcome to the zero dynamics, part II
%-------------------------------------------------------
if (isempty(zero_candidate2)|isempty(zero_candidates))
   disp('WARNING: Unable to locate valid subset for zerodynamics analysis...')
   disp(['         Skipping analysis for actuator at node ' ...
         num2str(control_node) '!'])
else
   zerodyn_start=zero_candidates(zero_candidate2(1))
if ( clip_force )
   subset=find(u>min_force&u<max_force);
else
   subset=1:length(u);
end
   subset2=find(subset>zerodyn_start);
   subset=subset(subset2);
clear zero_candidates zero_candidate2 subset2
%The relevant dataset has now been extracted from the original data.
%We want to find the maxima within a certain horizon now...
uabs=abs(u);
for i=2:length(subset)-1
   if uabs(subset(i+1))-uabs(subset(i))<0&uabs(subset(i))-uabs(subset(i-1))>=0
      % This is a (local) maximum:
      useful_samples=[useful_samples;subset(i)];
   end;
end;
% useful_samples now contains all maxima of abs(u).
% The largest value within each horizon is assumed to be a useful datapoint.
% So let's find these maxima within each horizon:
subset=[];
for i=1:1:floor(length(useful_samples)/horizon)
   local_max=max(uabs(useful_samples(horizon*(i-1)+[1:horizon])));
   subset=[subset;find(abs(uabs-local_max)<=1e-14)];
end
useful_samples=subset;
% useful_samples now contains all maxima of abs(u) within each horizon.
clear subset
A=[ones(length(useful_samples),1) -t(useful_samples)];
b=log(uabs(useful_samples));
parameters=A\b
figure
subplot(211),
plot(t,u,'w')
set(gca,'FontName','Times')
```

```
hold on
plot(t(zerodyn_start+offset:length(t)), ...
exp(parameters(1))*exp(-parameters(2)*t(zerodyn_start:length(t))),'r')
%plot(t(useful_samples),uabs(useful_samples),'b+')
plot(t(zerodyn_start+offset:length(t)), ...
-exp(parameters(1))*exp(-parameters(2)*t(zerodyn_start:length(t))),'r')
ylabel('u [N]'),title(['actuator at node ' num2str(control_node) ', damping=' ...
  num2str(parameters(2))],'FontName','Times')
if ( clip_force )
   axis([0 n/sf min_force max_force]);
end
hold off
grid
subplot(212),
plot(t,error)
hold on
% A green mark for zerodyn_start:
plot(t(zerodyn_start),error(zerodyn_start),'*g')
hold off
grid
xlabel('t [sec]','Fontname','Times');
ylabel('e_y_a [m]','FontName','Times')
set(gca,'FontName','Times')
print force.eps -deps
%figure
%subplot(111)
%plot(t(useful_samples),uabs(useful_samples))
%hold on
%plot(t(useful_samples(1):length(t)),u(useful_samples(1):length(t)),'r')
%hold off
fft_size=2^floor(log(length(z)-zerodyn_start-offset)/log(2));
if ffts==1
   disp(['Calculating FFTs based on ' num2str(fft_size) ' samples'])
   max_freq=sf;
   max_freq=150;
   max_sample=floor(fft_size*max_freq/sf);
   freq_domain=sf/fft_size*[0:max_sample-1];
   t_domain=offset+zerodyn_start+[0:fft_size-1];
   fft_e_0=fft(z(t_domain,2)-xd(t_domain,2));
   fft_e_xi=fft(z(t_domain,3)-xd(t_domain,3));
   figure
   semilogy(freq_domain,abs(fft_e_0(1:max_sample)))
   set(gca,'FontName','Times')
   title(['actuator at node ' num2str(control_node) ', ' ...
     num2str(sf/fft_size) ' [Hz/sample]'],'FontName','Times')
   xlabel('f [Hz]','Fontname','Times');
   ylabel('fft(e_y_m)','FontName','Times')
   print fft1.eps -deps
   semilogy(freq_domain(1:max_sample), ...
               abs(fft_e_xi(1:max_sample)))
   set(gca,'FontName','Times')
   title(['actuator at node ' num2str(control_node) ', ' ...
     num2str(sf/fft_size) ' [Hz/sample]'],'FontName','Times')
   xlabel('f [Hz]','Fontname','Times');
   ylabel('fft(e_y_xi)','FontName','Times')
   print fft2.eps -deps
   clear freq_domain ffts
end
end
```

Continuous time controller

```
global C f_e
ffts=0;
clip_force=0;
load beam_in
load beam_out
offset=sf*3
error_flag=0;
close all
```

```
if ~exist('horizon') horizon=4, end;
if ( clip_force )
   if ~exist('min_force') min_force=-100, end;
   if ~exist('max_force') max_force=100, end;
end
useful_samples=[];
t=[0:1/sf:(length(z(:,7))-1)/sf]';
if exist('xd') xd_cpp=xd; clear xd; end;
xd=destra(3,1,t);
error=z(:,1)-xd(:,1);
zero_candidates=find(abs(error)<=1e-10);
%Found that 1e-10 provides reasonable results

%First time that the error matches the criterium:
%-------------------------------------------------------------
% Welcome to the zero dynamics, part I
%-------------------------------------------------------------
if ~(isempty(zero_candidates))
   zerodyn_start=zero_candidates(1);

   %Convergence test: abs(edot)<1e-10 for reasonable results
   zero_candidate2=zero_candidates(find(abs(z(zero_candidates,4)...
                   -xd(zero_candidates,4))<1e-10));
end
%-------------------------------------------------------------
% Welcome to the zero dynamics, part II
%-------------------------------------------------------------
if (isempty(zero_candidate2)|isempty(zero_candidates))
   disp('WARNING: Unable to locate valid subset for zerodynamics analysis...')
   disp(['         Skipping analysis for actuator at node ' ...
         num2str(control_node) '!'])
else
   zerodyn_start=zero_candidates(zero_candidate2(1))
if ( clip_force )
   subset=find(z(:,7)>min_force&z(:,7)<max_force);
else
   subset=1:length(z);
end
   subset2=find(subset>zerodyn_start+offset);
   subset=subset(subset2);
clear zero_candidates zero_candidate2 subset2
%The relevant dataset has now been extracted from the original data.
%We want to find the maxima within a certain horizon now...
uabs=abs(z(:,7));
for i=2:length(subset)-1
   if uabs(subset(i+1))-uabs(subset(i))<0&uabs(subset(i))-uabs(subset(i-1))>=0
      % This is a (local) maximum:
      useful_samples=[useful_samples;subset(i)];
   end;
end;
% useful_samples now contains all maxima of abs(u).
% The largest value within each horizon is assumed to be a useful datapoint.
% So let's find these maxima within each horizon:
subset=[];
for i=1:1:floor(length(useful_samples)/horizon)
   local_max=max(uabs(useful_samples(horizon*(i-1)+[1:horizon])));
   subset=[subset;find(abs(uabs-local_max)<=1e-14)];
end
useful_samples=subset;
% useful_samples now contains all maxima of abs(u) within each horizon.
clear subset
A=[ones(length(useful_samples),1) -t(useful_samples)];
b=log(uabs(useful_samples));
parameters=A\b
figure
subplot(211),
plot(t,z(:,7),'w')
set(gca,'FontName','Times')
hold on
plot(t(zerodyn_start+offset:length(t)), ...
```

```
exp(parameters(1))*exp(-parameters(2)*t(zerodyn_start+offset:length(t))),'r')
%plot(t(useful_samples),uabs(useful_samples),'b+')
plot(t(zerodyn_start+offset:length(t)), ...
-exp(parameters(1))*exp(-parameters(2)*t(zerodyn_start+offset:length(t))),'r')
ylabel('u [N]'),title(['actuator at node ' num2str(control_node) ', damping=' ...
num2str(parameters(2))],'FontName','Times')
if ( clip_force )
   axis([0 n/sf min_force max_force]);
end
hold off
grid
subplot(212),
plot(t,error)
hold on
% A green mark for zerodyn_start:
plot(t(zerodyn_start),error(zerodyn_start),'*g')
hold off
grid
xlabel('t [sec]','Fontname','Times');
ylabel('e_y_a [m]','FontName','Times')
set(gca,'FontName','Times')
print force.eps -deps
figure
subplot(211),
plot(t,z(:,2)-xd(:,2))
hold on
% A green mark for zerodyn_start:
plot(t(zerodyn_start),z(zerodyn_start,2)-xd(zerodyn_start,2),'*g')
hold off
grid
ylabel('e_y_m [m]','FontName','Times')
set(gca,'FontName','Times')
subplot(212),
plot(t,z(:,3)-xd(:,3))
hold on
% A green mark for zerodyn_start:
plot(t(zerodyn_start),z(zerodyn_start,3)-xd(zerodyn_start,3),'*g')
hold off
grid
xlabel('t [sec]','Fontname','Times');
ylabel('e_xi [m]','FontName','Times')
set(gca,'FontName','Times')
print errors.eps -deps
%figure
%subplot(111)
%plot(t(useful_samples),uabs(useful_samples))
%hold on
%plot(t(useful_samples(1):length(t)),z(useful_samples(1):length(t),7),'r')
%hold off
fft_size=2^floor(log(length(z)-zerodyn_start-offset)/log(2));
if ffts==1
   disp(['Calculating FFTs based on ' num2str(fft_size) ' samples'])
   max_freq=sf;
   max_freq=150;
   max_sample=floor(fft_size*max_freq/sf);
   freq_domain=sf/fft_size*[0:max_sample-1];
   t_domain=offset+zerodyn_start+[0:fft_size-1];
   fft_e_0=fft(z(t_domain,2)-xd(t_domain,2));
   fft_e_xi=fft(z(t_domain,3)-xd(t_domain,3));
   figure
   semilogy(freq_domain,abs(fft_e_0(1:max_sample)))
   set(gca,'FontName','Times')
   title(['actuator at node ' num2str(control_node) ', ' ...
   num2str(sf/fft_size) ' [Hz/sample]'],'FontName','Times')
   xlabel('f [Hz]','Fontname','Times');
   ylabel('fft(e_y_m)','FontName','Times')
   print fft1.eps -deps
   semilogy(freq_domain(1:max_sample), ...
                abs(fft_e_xi(1:max_sample)))
   set(gca,'FontName','Times')
```

```
   title(['actuator at node ' num2str(control_node) ', ' ...
   num2str(sf/fft_size) ' [Hz/sample]'],'FontName','Times')
   xlabel('f [Hz]','Fontname','Times');
   ylabel('fft(e_y_xi)','FontName','Times')
   print fft2.eps -deps
   clear freq_domain ffts
end
end
```

E.2.3 Routine for FRF-fit

```
% frf_fit
%========================
%     F [N]      (kanaal 1)
%     a [m/s^2]  (kanaal 2)
%  v_in [V]      (kanaal 3)
% v_uit [V]      (kanaal 4)
% i_act [A]      (kanaal 5)

%load frf_800
%close all
global channel2
f_max_data=ceil(frf_indep(length(frf_indep)));
%if ~strcmp(channel2,'adapted')
%  frf_h1(2:length(frf_indep),2)=frf_h1(2:length(frf_indep),2)./ ...
(2i*pi.*frf_indep(2:length(frf_indep))).^2;
%  channel2='adapted';
%  disp('NOTIFICATION: changed FRF of channel 2 to F/x_a !')
%end
clear H freqdomain
f_max=input(['Afbreekfrequentie f_max (<=' num2str(ceil(frf_indep(length(frf_indep)))) ') [Hz]? ']);
if isempty(f_max),f_max=ceil(frf_indep(length(frf_indep))),end;
min_weeg=input(['frequentie minimale weging (default=none)? ']);
disp('     F [N]      (kanaal 1)')
if strcmp(channel2,'adapted')
  disp('     x [m]      (kanaal 2) (getransformeerde versnelling)')
else
  disp('     a [m/s^2] (kanaal 2)')
end
disp('  v_in [V]      (kanaal 3)')
disp(' v_uit [V]      (kanaal 4)')
disp(' i_act [A]      (kanaal 5)')
ch_in=input(['Input kanaal (default=3)? ']);
if isempty(ch_in);ch_in=3;end;
ch_out=input(['Output kanaal (default=1)? ']);
if isempty(ch_out);ch_out=1;end;
o_num=input('Graad teller (default=2)? ');
if isempty(o_num);o_num=2;end;
o_den=input('Graad noemer (default=2)? ');
if isempty(o_den);o_den=2;end;
subset=find(frf_indep<=f_max);
subset=subset(2:length(subset));
if f_max>frf_indep(subset(length(subset)))+1
   f_max=ceil(frf_indep(subset(length(subset))));
   disp(['WARNING: changed f_max to ' num2str(f_max) ' [Hz]...'])
end
if isempty(min_weeg)
  [num,den]=invfreqs(frf_h1(subset,ch_out)./ ...
  frf_h1(subset,ch_in),frf_indep(subset)*2*pi,o_num,o_den,[],16,1e-6);
else
  if min_weeg>f_max;
    min_weeg=f_max;
    disp(['WARNING: changed min_weeg to ' num2str(min_weeg) ' [Hz]...'])
  end
  [num,den]=invfreqs(frf_h1(subset,ch_out)./frf_h1(subset,ch_in),frf_indep(subset)*2*pi, ...
o_num,o_den,abs(min_weeg-frf_indep(subset)).^2,16,1e-6);
end
%--- nette methode: ---
max_size=max(o_num,o_den)+1;
for i=1:max_size;
```

```
  freqdomain(:,i)=(2i*pi*([1:f_max_data]')).^(max_size-i);
end;
H=(freqdomain(:,max_size-o_num:max_size)*num').'./...
  (freqdomain(:,max_size-o_den:max_size)*den').';
clear freqdomain
figure
subplot(211),
loglog(1:f_max,abs(H(1:f_max)),frf_indep(subset),abs(frf_h1(subset,ch_out)./frf_h1(subset,ch_in)))
set(gca,'FontName','Times')
ylabel(['abs(H_' num2str(ch_out) num2str(ch_in) ')'],'FontName','Times'),
%title(['overdrachtfunctie H_' num2str(ch_out) num2str(ch_in) '(f) (gefit voor f<' ...
num2str(f_max) ' [Hz])'],'FontName','Times')
subplot(212),
semilogx(1:f_max,angle(H(1:f_max)),frf_indep(subset),angle(frf_h1(subset,ch_out).' ...
  ./frf_h1(subset,ch_in).'))
set(gca,'FontName','Times')
xlabel('frequency [Hz]','FontName','Times'),
ylabel(['phase(H_' num2str(ch_out) num2str(ch_in) ') [rad]'],'FontName','Times')

%use data to match decades:
f_max_decade=10^floor(log10(f_max_data))
decade_set=find(frf_indep>=1&frf_indep<=f_max_decade);

figure
subplot(211),
loglog(1:f_max_decade,abs(H(1:f_max_decade)),':w',frf_indep(decade_set), ...
  abs(frf_h1(decade_set,ch_out)./frf_h1(decade_set,ch_in)),'-w')
set(gca,'FontName','Times')
ylabel(['abs(H_' num2str(ch_out) num2str(ch_in) ')'],'FontName','Times'),
title(['fit for f<' num2str(f_max) ' [Hz])'],'FontName','Times')
subplot(212),
semilogx(1:f_max_decade,angle(H(1:f_max_decade)),':w',frf_indep(decade_set), ...
  angle(frf_h1(decade_set,ch_out).'./frf_h1(decade_set,ch_in).'),'-w')
set(gca,'FontName','Times')
xlabel('frequency [Hz]','FontName','Times'),
ylabel(['phase(H_' num2str(ch_out) num2str(ch_in) ') [rad]'],'FontName','Times')
max_index=find(abs(max(abs(frf_h1(:,ch_out)./frf_h1(:,ch_in)))-abs(frf_h1(:,ch_out)./ ...
  frf_h1(:,ch_in)))<1e-12);
f_Hmax=frf_indep(max_index)
Hmax=frf_h1(max_index,ch_out)./frf_h1(max_index,ch_in)
```

Appendix F

Hardware specifications

F.1 Sensors

channel	quantity	unit	sensor	serial number	sensitivity
0	y_a	[m]	LVDT Lucas-Schaevitz DC-E250	11886	0.6047 [mm/V]
1	y_m	[m]	LVDT Lucas-Schaevitz DC-E250	11747	0.6074 [mm/V]
2	$\ddot{y}_a$	[m/s^2]	Bruel-Kjaer 4367	1074096	2.45 [pCs^2/m]
3	$\ddot{y}_m$	[m/s^2]	Bruel-Kjaer 4367	805972	2.00 [pCs^2/m]
4	F_{ex}	[N]	Kiag Swiss 9311A	100817	3.93 [pC/N]
5	F_{act}	[N]	Kiag Swiss 9301A	132296	3.64 [pC/N]

Table F.1: specifications of the used sensors.

F.2 Amplifiers

channel	quantity	unit	amplifier	serial number	cut-off frequency	conversion factor
0	y_a	[m]	-	-	-	-
1	y_m	[m]	-	-	-	-
2	$\ddot{y}_a$	[m/s^2]	Kistler 5007	265826	[1 kHz]	50 [m/s^2/V]
3	$\ddot{y}_m$	[m/s^2]	Kistler 5007	43578	[1 kHz]	20 [m/s^2/V]
4	F_{ex}	[N]	Kistler 5007	52901	180 [kHz]	50 [N/V]
5	F_{act}	[N]	Kistler 5007	52900	180 [kHz]	20 [N/V]
out	-	[V]	TPO 25 ([V]→[V])	745	-	max

Table F.2: specifications of the used amplifiers.